ADVANCED MOBILE RECEIVERS AND DOWNLINK CHANNEL ESTIMATION FOR 3G UMTS-FDD WCDMA SYSTEMS

THÈSE NUMÉRO 2574 (2002)

PRÉSENTÉE AU DÉPARTEMENT DE SYSTÈMES DE COMMUNICATIONS

ÉCOLE POLYTECHNIQUE FÉDÉRALE DE LAUSANNE

POUR L'OBTENTION DU GRADE DE DOCTEUR ÈS SCIENCES

PAR

MASSIMILIANO LENARDI

Ingénieur en Electronique et Télécommunications,
Università degli Studi di Trieste, Italie

Composition du Jury:

Prof. Bixio Rimoldi, président du Jury
Prof. Dirk T.M. Slock, directeur de Thèse
Prof. Emre Telatar, corapporteur
Prof. Raymond Knopp, corapporteur
Prof. Pierre Comon, corapporteur
Prof. Marco Luise, corapporteur

Lausanne, EPFL
May, 2002

To my wife Daniela and my Family

Aknowledgements

This work represents my research activity during the last 3 years at Eurécom Institute. It is the result of a collaboration with my Thesis supervisor Professor Dirk T.M. Slock, who's invaluable contribution supported and helped me. I am grateful to him for his technical insights, constructive criticism and friendship. It was a challenge for me to restart research and study activities after having started to work since few months in a completely different area like networking can be. And I feel very glad and lucky for the chance Prof. Slock and Eurécom gave to me.

I would like to thank also EPFL, firstly because LTS laboratory accepted my collaboration for developing my M.Sc. final project in 1996/97 and secondly because DSC department gave me the possibility to attend the Doctoral School in Communications Systems in 1997/98, allowing me afterwards to proceed to a Ph.D. program at Eurécom as EPFL Student.

An important role has been played by the Réseaux Nationale de Recherche en Télécommunications (RNRT) which, through the project AUBE (Nouvelles Architectures UMTS en vue de l'integration sur silicium des functions Bande de basE du terminal) in collaboration with France Télécom - CNET, KURTOSIS, LIS, ST Microelectronics and Thomson CSF Communications (now Thales), financed part of my Ph.D.

A special thank goes to my colleagues and/or friends Chris, Daniela, Alessandro, Beppe & Maria Luisa, Jussi, David, Kader, Albert, Cristina, Irfan, Sergio, Giuseppe, Remy, Celine, Delphine, France & Sylvain, Catherine ... and many more who shared with me this adventure and personal/professional experience.

Thanks a lot also to the other Jury members, Professors Bixio Rimoldi, Emre Telatar, Raymond Knopp, Pierre Comon and Marco Luise, for having accepted to evaluate my work.

The last but not least thank goes to my wife Daniela, so patient with my "engineering" character, and our Families, always supporting us.

Advanced Mobile Receivers and Downlink Channel Estimation

for 3G UMTS-FDD WCDMA Systems

Massimiliano Lenardi

Abstract

The explosive growth of the mobile Internet is a major driver of wireless telecommunications market today. In future years, the number of online wireless users will exhibit strong progression in every geographic region and devices will tend to support multimedia applications which need big transmission data rates and high quality. Third generation telecommunication systems, like UMTS in Europe, aim at rates approaching 2 Mbits/s in particular cellular environments, but they will initially be deployed in coexistence with second generation systems, like GSM, which were conceived to support voice traffic, but are evolving to higher-data-rates versions like GPRS. These hybrid systems have the target to support globally data rates at least of 144 kbits/s and locally of 2 Mbits/s.

This thesis makes several contributions to the area of mobile advanced receivers and downlink channel estimation in the context of the physical layer of UMTS-FDD Wideband DS-CDMA systems. Advanced signal processing techniques are applied to increase performance of the terminal receiver by mitigating the distortion caused by the radio propagation channel and the interference introduced by the multiple access to the wireless system, as well as to improve the downlink channel estimation and/or approximation.

The conventional receiver for DS-CDMA communications is the RAKE receiver, which is a filter matched to the operations of spreading, pulse shape filtering and channel filtering. Such a Matched Filter (MF) maximizes the Signal-to-Interference-plus-Noise Ratio (SINR) at its output if the interference plus noise is white, but this is not the case in the synchronous downlink with cell-dependent scrambling, orthogonal codes and a common channel. A Zero-Forcing (ZF) equalizer is capable of improving SINR performance at high input Signal-to-Noise Ratio (SNR), but due to the noise enhancement its performance gets degraded at low input SNR. A natural solution in between the RAKE and the ZF receivers is a time invariant Minimum Mean Square Error (MMSE) receiver. An MMSE design is well-defined in the downlink since the received signal is cyclostationary with chip period due to the cell-dependent scrambling (in case on no beamforming).

We propose a restricted class of linear receivers for the downlink, exhibiting a lim-

ited or no complexity increase with respect to the RAKE receiver. These receivers have the same structure as a RAKE receiver, but the channel matched filter gets replaced by an equalizer filter that is designed to maximize the SINR at the output of the receiver. It turns out that the max-SINR equalizer is an unbiased MMSE for the desired user's chip sequence. The complexity of the max-SINR receiver is variable and can possibly be taken to be as low as in the RAKE receiver (same structure as the channel matched filter), while its adaptation guarantees improved performance with respect to the RAKE receiver. Various implementation strategies are considered and compared in simulations, in particular those max-SINR structures that exploit the nature of the overall channel seen by the receiver, i.e. the convolution between the radio propagation channel and the pulse shaping filter. When a mobile terminal is equipped with multiple sensors, a two dimensions (2D) RAKE receiver, i.e. a spatio-temporal channel MF, is traditionally implemented, but also in this case a max-SINR receiver is conceivable and becomes a spatio-temporal MMSE equalizer. Furthermore, a 2D max-SINR receiver allows better suppression of similarly structured intercell interference.

Third generation CDMA-based wireless systems foresee a loading fraction that is smaller than one, i.e. the number of users per cell is scheduled to be significantly less than the spreading factor to attain an acceptable performance. This means that a base station can set apart a subset of the codes, the excess codes, that it will not use. The existence of excess codes implies the existence of a noise subspace, which can be used to cancel the interference coming from a neighboring base station. In the case of aperiodic codes (such as in the FDD mode of UMTS), the noise subspace is time-varying due to the scrambling. This motivated us to introduce structured receivers that combine scrambling and descrambling operations with projections on code subspaces and linear time-invariant filters for equalization, interference cancellation and multipath combining. So the time-varying part of these receivers is limited to (de-)scrambling operations. Application of polynomial expansion at symbol or at chip rate is also developed and leads to receiver structures with Intercell Interference Cancellation branches.

The UMTS norm for 3rd generation wireless systems specifies, for the FDD downlink, that the use of Transmission Diversity (TD) techniques is optional at the base station, while it is mandatory for the mobile station. Multiple transmitting antennas at the base station can improve receiver performance due to increase in diversity and some schemes have been proposed for open loop systems (no knowledge of the downlink channel at the transmitter). We analyse the use of three TD techniques, Orthogonal TD (OTD), Space-Time TD (STTD), and Delay TD (DTD). All of them are compared for the two receiver structures, RAKE and max-SINR receivers.

Channel estimation and approximation play an important role, this being a critical

issue in achieving accurate user-of-interest detection. The RAKE receiver assumes a sparse/pathwise channel model so that the channel matched filtering gets done pathwise, with delay adjustment and decorrelation per path and maximum-ratio combining of path contributions at the symbol rate. Original RAKE receivers work with continuous delays, which are tracked by an Early-Late scheme. This requires signal interpolation and leads to suboptimal treatment of diffuse portions in the channel impulse response. These disadvantages can be avoided by a discrete-time RAKE, operating at a certain oversampled rate. Proper sparse modelling of the channel is an approximation problem that requires exploitation of the limited bandwidth of the pulse shape. We propose and simulate a number of sparse channel approximation algorithms along the lines of Matching Pursuit, of which the Recursive Early-Late (REL) approach appears most promising. We also analyse and simulate the effect of channel estimation on the RAKE output SINR.

Pilot-assisted channel estimation operates generally on a slot-by-slot basis, without exploiting the temporal correlation of the channel coefficients of adjacent slots. So we consider the estimation of mobile channels that are modelled as autoregressive processes with a bandwidth commensurate with the Doppler spread. Brute pilot-based FIR channel estimates are then refined by Wiener filtering across slots that performs the optimal compromise between temporal decorrelation due to Doppler spread and slot-wise estimation error. We furthermore propose adaptive filtering techniques to implement the optimal filtering before path extraction. Finally, we introduce polynomial expansion extensions, one at chip rate to improve the MMSE equalization performance of the structured chip rate equalizer, and one at symbol rate to bring the structured receiver performance closer to that of the global time-varying LMMSE receiver.

Advanced Mobile Receivers and Downlink Channel Estimation

for 3G UMTS-FDD WCDMA Systems

Massimiliano Lenardi

Sintesi

Lo sviluppo esplosivo dell'Internet mobile è oggi il fattore portante del mercato delle telecomunicazioni cellulari. Durante i prossimi anni, il numero di utenti in linea sarà sempre più grande in ogni regione geografica ed i dispositivi tenderanno a supportare applicazioni multimediali che richiederanno alte velocità di trasmissione con migliore qualità. I sistemi di telecomunicazioni di terza generazione, come l'UMTS in Europa, puntano a velocità di trasmissione vicine ai 2 Mbits/s in particolari situazioni, ma inizialmente saranno sviluppati in coesistenza con i sistemi di seconda generazione, come il GSM, che sono stati concepiti per sostenere traffico vocale, ma si stanno evolvendo a versioni a più alta velocità di trasmissione come il GPRS. Questi sistemi ibridi hanno l'obiettivo di permettere trasferimenti dati di almeno di 144 kbits/s in modo globale e di 2 Mbits/s localmente.

Questa tesi presenta vari contributi nell'area dei ricevitori mobili avanzati e della stima del canale radio del *downlink* (dalla stazione di base verso il terminale mobile) nel contesto del livello fisico dei sistemi *UMTS-FDD DS-CDMA* a banda larga. Tecniche avanzate di elaborazione dei segnali sono applicate per aumentare le prestazioni del ricevitore mobile attenuando le distorsioni causate dal canale di propagazione e dall'interferenza introdotta dall' accesso multiplo al sistema, cos come per migliorare la stima del canale di propagazione.

Il ricevitore convenzionale per le comunicazioni a divisione di codice è il *RAKE*, che è un filtro adattato al canale di propagazione, al codice della stazione di base (*scrambling*) ed al codice dell'utente (*spreading*). Tale ricevitore massimizza il rapporto Segnale-su-Interferenza-più-Rumore (*SINR*) in uscita se la somma interferenza più rumore è bianca, ma questo non è il caso nel downlink, con i segnali degli utenti sincroni fra loro, con lo scrambling proprio della stazione di base, con codici ortogonali e con un canale di propagazione comune. Un equalizzatore di canale *Zero-Forcing* (ZF) è capace di migliorare nettamente le prestazioni in termini di SINR se il rapporto Segnale-su-Rumore (*SNR*) in ingresso è alto, ma le sue prestazioni peggiorano rispetto al ricevitore RAKE a basso SNR in ingresso a causa dell'aumento del rumore stesso. Una soluzione naturale fra il RAKE ed il ZF è un ricevitore tempo-invariante ad errore

quadrato medio minimo (*MMSE*). Questo ricevitore è ben definito nel downlink poiché il segnale ricevuto è ciclostazionario con periodo uguale alla durata di un chip a causa dello scrambling (nel caso non sia implementato il beamforming).

Noi proponiamo una categoria di ricevitori lineari per il downlink, che non esibiscono maggiore complessità (o limitatamente maggiore) rispetto al ricevitore RAKE. Questi ricevitori hanno la stessa struttura del RAKE, ma il filtro adattato al canale di propagazione viene sostituito da un equalizzatore concepito per massimizzare l'SINR all'uscita del ricevitore. Risulta poi che l'equalizzatore *max-SINR* è un equalizzatore MMSE senza *bias* per la sequenza chip dell'utente voluto. La complessità del max-SINR è variabile e pu possibilmente essere tanto bassa quanto quella del RAKE (stessa struttura del filtro adattato al canale), mentre il relativo adattamento garantisce prestazioni SINR migliori rispetto al RAKE. Vengono considerate svariate strategie di implementazione (e confrontate in simulazioni), in particolare quelle strutture max-SINR che sfruttano la natura del canale totale visto dal ricevitore, cioè la convoluzione del canale di propagazione e del filtro di modulazione d'impulso (*pulse shaping filter*). Quando un terminale mobile è munito di più sensori (antenne), i ricevitori RAKE a due dimensioni (2D), cioè filtri adattati spazio-temporali, sono tradizionalmente usati, ma anche in questo caso è possibile concepire ricevitori max-SINR che risultano equalizzatori MMSE spazio-temporali. Inoltre, un ricevitore max-SINR permette una migliore cancellazione di interferenze strutturate in modo simile, ma provenienti da altre stazioni di base (*Intercell Interference*).

I sistemi wireless di terza generazione a divisione di codice prevedono un rapporto di carico del sistema minore di uno per raggiungere prestazioni accettabili, cioè il numero di utenti per cellula è previsto significativamente minore del fattore di espansione (*spreading factor*). Ci significa che una stazione di base pu fissare un sottoinsieme di codici spreading, *excess codes*, che non userà. L'esistenza di tale sottoinsieme implica l'esistenza di un sottospazio dovuto al rumore nel segnale ricevuto, che pu essere usato per annullare l'interferenza proveniente da una stazione di base vicina. Nel caso di codici totali aperiodici (quale nel modo di FDD di UMTS), il sottospazio dovuto al rumore è tempo-variabile a causa dello scrambling. Ci ci ha motivati nell'introdurre dei ricevitori strutturati che uniscono le operazioni di scrambling e descrambling a proiezioni nei sottospazi di codice spreading ed a filtri lineari tempo-invarianti per l'equalizzazione, la cancellazione d'interferenza e la ricombinazione dei cammini multipli del canale di propagazione. Cos la parte tempo-variante di questi ricevitori è limitata alle operazioni di (de)scrambling. L'applicazione dell'espansione polinomiale a livello di simbolo od a livello di chip è egualmente sviluppata e conduce a strutture di ricevitore con rami di annullamento di interferenza intercellulare.

Lo standard UMTS per i sistemi di terza generazione specifica, per il downlink del modo FDD, che l'uso delle tecniche di Diversità in Trasmissione (TD) è facoltativo alla stazione di base, mentre è obbligatorio per il terminale mobile. La presenza di antenne multiple nella stazione di base permette di migliorare le prestazioni del ricevitore mobile a causa dell'aumento della diversità; proponiamo nella tesi alcuni schemi per i sistemi open-loop (nessuna conoscenza del canale di propagazione da parte del trasmettitore). Analizziamo l'uso di tre tecniche TD, TD Ortogonale (OTD), TD Spazio-Temporale (STTD) ed TD a ritardo (DTD), tutte confrontate per due strutture di ricevitore, RAKE e max-SINR.

La stima del canale di propagazione o la sua approssimazione giocano un ruolo importante, critico per la decodifica esatta dei simboli dell'utente desiderato. Il RAKE presuppone un modello di canale di propagazione di tipo sparso (cammini multipli), in modo che il filtraggio adattatato venga fatto per cammino, con aggiustamento di ritardo e decorrelazione, per poi sommarne i vari contributi (maximum-ratio combining) a livello di simbolo. I ricevitori RAKE tradizionali funzionano con ritardi continui, stimati da uno schema cosiddetto Early-Late. Esso richiede l'interpolazione del segnale, che non è ottima nel caso di canali di propgazione diffusi o con ritardi molto vicini tra loro. Questi svantaggi possono essere evitati da un RAKE a tempo discreto, funzionante ad un tasso di campionamento maggiore rispetto alla frequenza di chip. La modellizzazione di tipo sparso del canale di propagazione è un problema di approssimazione che richiede lo sfruttamento della larghezza di banda limitata del filtro di modulazione di impulso. Proponiamo e simuliamo un certo numero di procedure di approssimazione sparsa del canale seguendo lo stile della ricerca di corrispondenza (Matching Pursuit), di cui il metodo Recursive Early-Late (REL) sembra il migliore. Inoltre, analizziamo e simuliamo l'effetto della stima di canale sull'SINR in uscita del RAKE.

La stima di canale basata sulla trasmissione di simboli pilota noti al ricevitore funziona generalmente su un periodo di slot, senza sfruttare la correlazione temporale dei coefficenti del canale di propagazione da una slot all'altra. Cos consideriamo la stima di canali radiomobili che sono modellizzati come processi autoregressivi con una larghezza di banda proporzionata alla larghezza di banda Doppler del canale stesso. Le stime FIR di canale basate sui simboli pilota (canale totale, non solo di propagazione) vengono raffinate da un filtro causale ottimo di Wiener che effettua un compromesso ottimale fra la decorrelatione temporale dovuta all'effetto Doppler e l'errore di stima del canale su base di tempo slot. Ancora, proponiamo una versione adattativa del filtraggio ottimo di Wiener prima dell'applicazione delle tecniche di estrazione dei cammini tipo REL. Per concludere, suggeriamo delle estensioni dell'espansione poli-

nomiale, una a livello di chip per migliorare le prestazioni di equalizzazione a MMSE del filtro strutturato ed una a livello di simbolo per avvicinare le prestazioni del ricevitore strutturato a quelle del ricevitore LMMSE tempo-variante globale.

Contents

List of Figures

Acronyms

2D	two dimensions
3GPP	3rd Generation Partnership Project
APWeq	Averaged Path-Wise Equalizer
AR(n)	Autoregressive Process of order n
AWGN	Additive White Gaussian Noise
AUBE	RNRT project: http://www.telecom.gouv.fr/rnrt/paube.htm
BER	Bit Error Rate
BPSK	Binary Phase Shift Keying
BS	Base Station
CDMA	Code Division Multiple Access
DFE	Decision Feedback Equalization or Decision Feedback Equalizer
DPCH	Dedicated Physical CHannel
DPP	Delay Power Profile
DS-CDMA	Direct Sequence - CDMA
DSP	Digital Signal Processor or Digital Signal Processing
DTD	Delay Transmit Diversity scheme
EPFL	École Politechnique Fédérale de Lausanne
ETSI	European Telecommunications Standards Institute
FDD	Frequency Division Duplex
FIR	Finite Impulse Response
GPRS	General Packet Radio Service
GSM	Global System for Mobile communications
IC	Interference Canceller
i.i.d.	Independent and identically distributed
ISI	Inter Symbol Interference
JIPWeq	Joint Iterative (alternating) Path-Wise Equalizer
JML	Joint Maximum Likelihood

LCMV	Linearly Constrained Minimum Variance (criterion)
LS	Least Squares
max-SINR	(or mSINR) SINR maximizing receiver
MAI	Multiple Access Interference
MF	Matched Filter or Matched Filtering
MIMO	Multiple Inputs Multiple Outputs
MIP	Multipath Intensity Profile (or Delay Power Profile)
MISO	Multiple Inputs Single Output
ML	Maximum Likelihood
(L)MMSE	(Linear) Minimum Mean Square Error
MOE	Minimum Output Energy
MPC	Multipath Propagation Channel
MS	Mobile Station
MSE	Mean Square Error
MUD	Multi User Detection
MUI	Multi User Interference
NMSE	Normalized Mean Square Error
PAPWeq	Per Antenna Path-Wise Equalizer
PDA	Personal Digital Assistant
PE	Polynomial Expansion
PIC	Parallel Interference Cancellation
PN	Pseudo Noise
PSD	Power Spectral Density
PWeq	Path-Wise Equalizer
OTD	Orthogonal Transmit Diversity scheme
OVSF	Orthogonal Variable Spreading Factor
QPSK	Quaternary Phase Shift Keying
RAKE	channel, scrambling and spreading matched filter receiver
REL	Recursive Early-Late
RF	Radio Frequency
RLS	Recursive Least-Squares (adaptive filtering)
RLSF	Recursive Least-Squares-Fitting (channel estimation technique)
RHS	Right Hand Side
RMSE	Root Mean Square Error
RNRT	Réseaux Nationale de Recherche en Télécommunications
RRC	Root Raised Cosine pulse shaping filter
SIC	Serial Interference Cancellation

SINR	Signal-to-Interference-plus-Noise Ratio
SISO	Soft Input Soft Output
STTD	Space-Time Transmit Diversity scheme
SVD	Singular Value Decomposition
TDMA	Time Division Multiple Access
TDD	Time Division Duplex
UMTS	Universal Mobile Telecommunication System
UTRA	UMTS Terrestrial Radio Access
WAP	Wireless Application Protocol
W-CDMA	Wideband Code Division Multiple Access
w.r.t.	with respect to
WSS-US	Wide Sense Stationary Uncorrelated Scattering
ZF	Zero-Forcing (equalizer or receiver)

List of Symbols

a	Constant scalar
$a(t)$	Continuous-time function of the variable t
$\boldsymbol{a}, A$	Constant vector
$a[n], a_n, A_n$	n^{th} element of the vector $\boldsymbol{a}$
$\boldsymbol{A}, \mathcal{A}$	Constant matrix (or vector when specified)
$A_{i,j}$	element of the matrix $\boldsymbol{A}$ in row i and column j
$\mathcal{T}(\boldsymbol{a})$	Block (if oversampling) Toeplitz convolution matrix with $\boldsymbol{a}$ (padded with zeroes) as first (block) row
P	Projection matrix on the columns of $\boldsymbol{P}^H$, $\mathsf{P} = \boldsymbol{P}\left(\boldsymbol{P}^H\boldsymbol{P}\right)^{-1}\boldsymbol{P}^H$
$\text{diag}\{\boldsymbol{a}\}$	diagonal matrix with vector $\boldsymbol{a}$ on the diagonal
$\text{blockdiag}\{[\boldsymbol{S}_i]\}$	block diagonal matrix with matrices $\boldsymbol{S}_i$ on the diagonal
$\overline{\text{diag}}\{\boldsymbol{A}\}$	diagonal matrix containing the diagonal of matrix $\boldsymbol{A}$
$\delta(t)$	Dirac delta in the variable t
$\delta[n]$	Discrete-time delta
$\boldsymbol{I}_N$	$N \times N$ Identity matrix
j	Imaginary unit
Γ_X	Signal-to-Interference-plus-Noise Ratio (SINR) of receiver X
$(\cdot)^*$	Complex conjugate operator
$(\cdot)^T$	Transpose operator
$(\cdot)^H$	Hermitian operator
$*$	Convolution operator
$\mathrm{E}_{a,b}[\cdot]$	Expectation operator over random variables a and b
$\otimes$	Kronecker product
$\odot$	Shur product
$\{S_{xx}\}^+$	(or just S_{xx}^+) Take causal part of the power spectral density of x

Chapter 1

Introduction

1.1 Issues in this Thesis

1.1.1 3^{rd} Generation Wireless Systems: Focus on the Downlink

Wireless communications are showing an unpredicted growth and the advent of 3^{rd} generation systems will open up the range of possible services and will significantly increase the available data rates and decrease the Bit Error Rate (BER). To achieve such data rates at such BERs, multiple access interference (the major impairment) cancellation will be required. 3^{rd} generation systems will use one form or another of Direct Sequence Code Division Multiple Access (DS-CDMA). This Thesis and Eurécom work in the context of RNRT project AUBE focus on the downlink mobile receiver physical-layer architecture (base station to mobile baseband signalling), on the detection of the user-of-interest signal within the users transmitting from a base station and on the estimation of the (common to all users) multipath propagation downlink channel.

1.1.2 RAKE Receiver and Discrete-Time Channel Representation

The RAKE receiver is certainly the reference receiver structure for comparisons with possible alternatives. It is a channel matched filter (MF), where the (total) channel is

the convolution of the spreading sequence (short/periodic), the scrambling sequence (long/aperiodic), the pulse shaping filter and the multipath propagation channel. The term RAKE refers to a sparse channel impulse response model in which the finite number of specular paths lead to fingers (contributions at various delays) in the channel impulse response.

As a first step we studied different implementations of the RAKE receiver, the classical one in which the propagation delays are taken from continuous time values and a discrete-time implementation which arises from the introduction of an oversampling factor with respect to the chip rate. In the latter version, because the Nyquist criterion is satisfied, the matched filtering for the propagation channel could be done in discrete-time domain, leading to a discrete-time representation of the channel impulse response.

The downlink transmission is synchronous (from an intracell point of view) and this synchronism encourages the use of orthogonal codes, which, anyway, due to the presence of multipath propagation, are not sufficient for a simple correlator to get rid of the intracell interference and to maximize the output SINR. RAKE receivers are able to combine the multipath contributions in order to maximize the output SNR, but they destroy the orthogonality between codes. So new alternative mobile receiver structures are required, such as Equalizers or Hybrid solutions (see next sections).

In the discrete-time RAKE, the estimation of the path delays becomes an issue of detecting at which sampling instants a finger should be put. This might be a simplification. A different advantage of the discrete time RAKE over the continuous-delay RAKE is that if the channel is diffuse, then the RAKE may have a problem in concentrating many paths around the same time instant. The approximation of the entire channel impulse response can be done by suboptimal iterative ML techniques or by Matching Pursuit techniques that exploit the structure of the channel itself (convolution of the radio propagation channel with the pulse shape filter).

1.1.3 Equalizer Receiver

If the base station does not use mobile-dependent beamforming, then the downlink channel towards a certain mobile is the same for the superposition of signals received by the mobile (even in the case of sectoring (non-ideal sectors), this reasoning could roughly be applied per sector). Hence, by first applying channel equalization at the receiver, the codes have again become orthogonal at the equalizer output.

Hence a correlator to get rid of all intracell (intrasector) interference can follow the equalizer. By using a fractionally-spaced equalizer, the excess bandwidth can be

used to cancel some of the intercell interference also. The problem with this approach is that a zero-forcing equalizer may produce quite a bit of noise enhancement. So in a given situation either the RAKE receiver or the equalizer receiver will perform better, depending on whether the intracell interference dominates the intercell interference plus noise or vice versa. Moreover, the equalizer approach is only applicable if no mobile-dependent beamforming is performed at the base station.

1.1.4 Hybrid Solutions

We investigated hybrid receiver structures combining the equalizer and RAKE components. The new structure consists of a RAKE preceded by an intracell interference canceller (IC). This IC has a desired signal suppression branch, which is build from a channel equalizer, followed by a projector that cancels the code of the signal of interest. This projector is then followed by re-filtering with the channel impulse response. At that point, the branch output contains the intracell interference in the same way as the received signal, and the signal of interest is removed. So by subtracting the branch output from the received signal, all intracell interference gets cancelled.

The new receiver structure acts similarly to the equalizer plus decorrelator receiver. However, noise plus intracell interference get treated differently and simulations show that the new receiver achieves improved performance. Further improvements can be obtained by replacing the refiltering coefficients by those resulting from a MMSE design.

1.1.5 Max-SINR Receiver

A natural solution to improve the ZF equalizer approach would be to replace a zero-forcing design by a MMSE design. Indeed, when cell-dependent scrambling is added to the orthogonal periodic spreading, then the received signal becomes cyclostationary with chip period (or hence stationary if sampled at chip rate) so that a time-invariant MMSE design becomes well-defined. Now, it may not be obvious a priori that such a MMSE equalizer leads to an optimal overall receiver. Due to the unique scrambler for the intracell users, the intracell interference after descrambling exhibits cyclostationarity with symbol period and hence is far from white noise. As a result, the SINR at the output of a RAKE receiver can be far from optimal in the sense that other linear receivers may perform much better.

In publication [1], we proposed a restricted class of linear receivers that have the same structure as a RAKE receiver, but the channel matched filter gets replaced by

an equalizer filter that is designed to maximize the SINR at the output of the receiver. It turns out that the SINR maximizing receiver uses a MMSE equalizer. The adaptation of the SINR maximizing equalizer receiver can be done in a semi-blind fashion at symbol rate, while requiring the same information (channel estimate) as the RAKE receiver. We considered a wide variety of symbol rate and chip rate adaptation strategies and we compared them in simulations.

1.1.6 Transmit Diversity Schemes for RAKE and Max-SINR

For the downlink in FDD mode, the UMTS norm specifies that the use of Transmission Diversity (TD) techniques is mandatory for the mobile station. Multiple transmitting antennas at the base station improve receiver performance due to the introduction of artificial diversity in the system and some schemes have been proposed for open loop systems (the transmitter doesn't know the downlink channel). In publication [2], we analysed the use of three different Downlink Transmission Diversity (TD) techniques, namely Space-Time TD (STTD), Orthogonal TD (OTD) and Delay TD (DTD). All of them were compared for the two receiver structures: RAKE and max-SINR receivers. The Max-SINR receiver structures proposed for the three TD modes are new and are shown to usually significantly outperform the RAKE schemes.

1.1.7 Reduced Complexity Max-SINR Receivers

In the discrete-time RAKE, only resolvable paths has to be considered (the temporal resolution is inversely proportional to the bandwidth, hence to the sampling rate). Note that for any RAKE to give a good sparse model, the positioning of fingers should be approached as an approximation problem (much like multipulse excitation modelling in speech coding) instead of putting fingers at all positions where the output of the pulse shaping MF plus correlator give non-zero contributions. So "sparse" matched filters have been studied.

In publications [3] and [4], we studied different structured implementations and adaptations of the max-SINR receiver, analysing their performances with respect to its theoretical expression and to the RAKE receiver.

The max-SINR equalizer, indeed, replaces at the same time the pulse shape and the channel matched filters, leaving complete freedom to the optimization process. Other possibilities rise when we want to impose a particular structure to the equalizer, such as the one of a RAKE receiver, that is a short FIR (pulse-shape) filter followed by a sparse (propagation channel) filter.

1.1.8 Intercell Interference Cancellation Receivers

An alternative solution to the ones presented in the previous section, which rather increases the overall complexity of the structured receiver, is the one in which we alternatively optimize for max SINR the coefficients of the sparse filter and those ones of the short FIR filter ([5]). This alternating algorithm is one of the algorithms we studied in the context of Equalizer Receivers and Intercell Interference Cancellation (presence of more base station transmitting to the mobile receiver) Receivers. In the case of a mobile terminal equipped with multiple sensors/antennas, the short FIR filter simply becomes a spatio-temporal MMSE equaliser.

The multi-sensor aspect improves the equalization performance and allows to suppress similarly structured intercell interference. In publications [6] and [7], we studied other downlink receiver structures for Intercell Interference Cancellation by exploiting excess codes (not-used user codes) in the WCDMA system. The existence of excess codes implies the existence of a noise subspace, which can be used to cancel the interference coming from a neighboring base station. In the case of aperiodic codes (such as in the FDD mode of UMTS), the noise subspace is time-varying due to the scrambling. This motivated us to introduce structured receivers that combine scrambling and descrambling operations with projections on code subspaces and linear time-invariant filters for equalization, interference cancellation and multipath combining. So the time-varying part of these receivers is limited to (de-)scrambling operations.

We basically used the hybrid structure introduced above, but, in the case of 2 transmitting BSs, we have 2 IC branches, one dedicated to intracell IC and the other to intercell IC. Branch Equalizers, Projectors and re-Channelling filters are designed in order to improve the performance of the linear receivers, such as the RAKE or the Max-SINR, by exploiting the structure of the received signal itself (the IC branch is indeed equivalent to a time-variant filter). In publication [7] we introduced also a new intra and intercell interference cancelling structures based on Polynomial Expansion approach, at symbol and at chip rates. These new structures are suitable also in case of Soft Handover with 2 BSs for the mobile receiver.

1.1.9 Downlink Channel Estimation

The RAKE receiver assumes a sparse/pathwise channel model so that the channel matched filtering gets done pathwise, with delay adjustment and decorrelation per path and maximum-ratio combining of path contributions at the symbol rate. Original RAKE receivers work with continuous delays, which are tracked by an Early-Late scheme. This requires signal interpolation and leads to suboptimal treatment of dif-

fuse portions in the channel impulse response. These disadvantages can be avoided by a discrete-time RAKE, operating at a certain oversampled rate.

Proper sparse modelling of the channel is an approximation problem that requires exploitation of the limited bandwidth of the pulse shape. In publication [8], we propose and simulate a number of sparse channel approximation algorithms along the lines of Matching Pursuit, of which the Recursive Early-Late (REL) approach appears most promising. We also analyse and simulate the effect of channel estimation on the RAKE output SINR.

In the classical channel estimation approach, a pilot sequence gets correlated with the received (pilot) signal. To estimate the path delays of the sparse channel, this approach looks for the positions of the maxima in this correlation (Early-Late technique). But due to oversampling and pulse-shape filtering, spurious maxima appear in the correlation, corresponding to the sidelobes of the pulse shape. REL technique derives from the basic Early-Late approach, and corresponds to applying the Matching Pursuit technique to the convolution between the FIR estimate of the overall channel and the pulse-shape matched filter. At each iteration, the pulse-shape contribution to a path gets subtracted from the convolution itself, ensuring better estimation for next path delays and amplitudes (the latter by Least-Square, LS).

In publications [9] and [10], we consider the estimation of mobile channels that are modelled as autoregressive processes with a bandwidth commensurate with the Doppler spread. Pilot based estimation leads to brute FIR channel estimates on a slot by slot basis. These estimates are then refined by Wiener filtering across slots that performs the optimal compromise between temporal decorrelation due to Doppler spread and slot-wise estimation error. We furthermore propose adaptive filtering techniques to implement the optimal filtering. To exploit the structure of the overall channel (convolution between pulse-shape transmitter filter, radio propagation channel and antialiasing receiver filter) the ”sparsification” of these refinements is then done again by the REL technique and shows better channel approximation w.r.t. to REL applied directly to the brute FIR channel estimates.

1.2 Issues not Covered in this Thesis

There are several important issues that we do not explore or deepen in this Thesis. Full synchronization is assumed between users on the downlink, and the receiver doesn’t need to estimate initially the transmission timing (slot timing). For a review of some methods for FDD downlink, take a look in [11] and [12] (and references therein).

Multi User Detection techniques applied on mobile stations (MS) for better Inter/Intracell Interference Cancellation, (semi)blind approaches for channel estimation and/or approximation and multi MS antennas implementation aspects are also issues not included in this work. All the three topics are considered hot in the research community, but they are also considered too complex to be implemented on a device like a cellular phone, which has complexity and power constraints. Different is the case when we deal with laptops or personal digital assistants (PDA), which can be used for applications that need more powerful digital signal processing and have the possibility to incorporate faster processors, bigger memories and efficient antenna arrays. (Downlink) System capacity is also an issue that is not covered.

1.3 Thesis Organization and Contributions

The remaining of the Thesis is organized in one background/notation chapter, four research chapters and a final concluding chapter.

In the second chapter 3^{rd} generation UMTS-FDD WCDMA system is introduced in a more technical matter, with emphasis on notation used later in the Thesis.

Third chapter is dedicated to the RAKE receiver, to discrete-time channel approximation and to zero-forcing and hybrid linear receivers. This chapter serves as reference chapter for the rest of the Thesis, in the sense that other structures performance are compared to those of the RAKE and the ZF receivers.

The fourth chapter will introduce and further explore the class of linear unstructured/structured max-SINR receivers, as well as their possible lower complexity implementations/adaptations and their application to multisensor mobile terminals. Results of this chapter are publications [1], [3], [4], [5].

Chapter five presents our work on Base Station Transmission Diversity and on Intercell Interference Cancellation based on the exploitation of the unused spreading codes in the system. The UMTS norm specifies that the use of a Transmission Diversity technique is mandatory at the mobile terminals, while it is optional at the base stations. We study 3 different schemes and present performance comparisons for all linear receivers introduced in previous chapters. A loading fraction smaller than one is foreseen for 3^{rd} generation systems, that means that a subset of the possible spreading codes, the excess codes, are not used. By exploiting the excess codes, the system can cancel interference coming from neighboring base stations. Also Polynomial Expansion (PE) is introduced for two new intra- and intercell interference cancellation structures, one at symbol rate and one at chip rate. Publications related to these issues

are [2], [6], [7].

In the last research chapter, the sixth, we propose different channel estimation and/or approximation techniques and a SINR analysis on its degradation due to channel estimation errors. First we study and simulate a number of sparse channel approximation algorithms along the lines of Matching Pursuit and secondly we model channel variations over slot periods with an autoregressive first-order process with bandwidth commensurate to the Doppler spread, so that adaptive optimal causal Wiener filtering is used to refine brute pilot based FIR channel estimates which are used afterwards for path extraction. Results of this chapter are publications [8], [10], [9].

Last chapter will eventually tell to the reader our conclusions, Thesis contributions and some ideas for further developments.

Chapter 2

3^{rd} Generation Wireless Systems : UMTS

This chapter briefly describes the european third generation standardization, illustrates the main features of the UMTS-FDD WCDMA downlink system and introduces the notation used along the Thesis.

2.1 Standardization of the Universal Mobile Telecommunication System

A long period of research preceded the selection of the 3G technology. The first project on the subject has been RACE I (Research of Advanced Communication technologies in Europe), which started in 1988 and was followed by RACE II and its CDMA-based CODIT (Code Division Testbed) and TDMA-based ATDMA (Advanced TDMA Mobile Access) air interfaces. Other propositions were coming from industries, see for example [14].

Mobile communications european research and development has been supported by the program ACTS (Advanced Communication Technologies and Services) started at the end of 1995. One of the projects included in ACTS was FRAMES (Future

Radio Wideband Multiple Access System), which was dedicated to define a proposal for a UMTS radio access system ([15]). Partners in this project were Nokia, Siemens, Ericsson, France Télécom, CSEM/Pro Telecom and some european universities. They proposed two modes in a harmonized radio access platform: wideband TDMA and wideband CDMA. ETSI received other proposals as candidates for UMTS Terrestrial Radio Access (UTRA) air interface and decided in June 1997 to form 5 concept groups.

- **OFDMA** Proposed by Telia, Lucent and Sony, this technology was mainly discussed in the japanese standardization forum.
- **ODMA** Basically not suitable for FDD mode because a terminal would need to be able to act as relay for other terminals out of the range of base stations, this Vodafone multiple access was afterwards integrated in the WTDMA/CDMA or WCDMA proposals.
- **Wideband TDMA/CDMA** This hybrid concept, based on the spreading option of the TDMA FRAMES mode, put CDMA on top of TDMA structure, led to lively discussions during the selection process because of the receiver complexity.
- **Wideband TDMA** Based on the non-spread option of the TDMA FRAMES mode, this proposal was basically a TDMA system with 1.6 MHz carrier spacing for wideband service implementation. "Higher capacity by interference averaging over the operator bandwidth and frequency hopping" was the claim of the supporters. But this system had the main limitation in the low bit rate services, due to the short minimum duration of a slot w.r.t. the frame timing. This implies the need of narrowband companion for a WTDMA system for voice services and makes uncompetitive this concept.
- **Wideband CDMA** This concept was formed from the CDMA FRAMES mode and was supported by Fujitsu, Panasonic, NEC and other worldwide companies too. The physical layer downlink solution was changed following other proposals that arrived to the concept group. The basic system features were:
  - wideband CDMA operation with 5 MHz
  - physical layer flexibility for integration of all data rates on a single carrier
  - reuse factor equal to one
  - transmission diversity
  - adaptive antennas
  - advanced receiver structures

The advanced state of the selection in Japan, where ARIB was going to adopt wideband CDMA, helped ETSI in the decision. All the proposals were evaluated until January 1998 when Wideband CDMA was selected as the standard for the UTRA air interface in the case of paired frequency bands, i.e. for the FDD operational mode, and when Wideband TDMA/CDMA was selected for operations with unpaired spectrum allocation, i.e. for TDD mode.

Similar technologies were developed around the world at the same time. ARIB in Japan chose as well WCDMA for both operational modes, FDD and TDD. TTA in Korea got initially to a mixed approach, choosing two air interfaces that were based on synchronous and asynchronous CDMA respectively. Towards the end of their standardization process, the koreans submitted some detailed proposal to ETSI and ARIB, so the final WCDMA respective proposal were quite harmonized. In the United States all the three existing second generation systems, GSM-1900, US-TDMA and IS-95, were evolving towards the 3^{rd} system.

This global development led to the creation of the 3^{rd} Generation Partnership Project (3GPP) to avoid to waste resources and to ensure compatibility for the equipments. Organizations involved in 3GPP (ETSI, ARIB, TTA and the american T1P1) agreed to join their efforts towards a common UTRA (now meaning Universal Terrestrial Radio Access) standardization. Also some worldwide manufactures and companies joined 3GPP through the organizations they were belonging to., as well as some marketing representatives like GSM Association, UMTS Forum and IPv6 Forum.

3GPP organized four Technical Specification Groups (TSG), the Radio Access Network TSG (RAN TSG), the Core Network TSG, the Service and System Aspects TSG and the Terminals TSG, to define by the end of 1999 the first release of the specifications. The most important TSG from a WCDMA technology point of view was the RAN TSG which was divided into four working groups and produced the Release-99 of UTRA air interface. The last specifications can always be obtained from 3GPP web site ([16]).

Collaboration of the partners within 3GPP during 1999 led to convergence and harmonisation between different CDMA based third generation solutions, cdma2000 still remaining on its own. The new standard consists of three operational modes: Multi Carrier (MC, based on multi-carrier of cdma2000), Direct Spread (DS, based on UTRA FDD) and Time Division Duplex (TDD, based on UTRA TDD). The main technical impacts of this phase of harmonisation were the change of chip rate for FDD and TDD from 4.096 Mcps to 3.84 Mcps and the inclusion of a common pilot channel in the FDD mode.

After Release-99, work has been carried on to include new features or corrections

and specify necessary extensions for connecting UTRA FDD to IS-41 based core networks or, respectively, cdma2000 to GSM based core networks.

2.1.1 Main Differences between WCDMA and 2^{nd} Generation Wireless Systems

Third generation systems are designed for multimedia communications and person-to-person telecommunications can be enhanced by higher data rates (up to 2 Mb/s) and quality, access to information and services on public or private networks and flexibility. This, together with the continuous evolution of the second generation systems, will allow new business opportunities for operators, manufacturers and content providers.

Second generation digital systems were initially deployed to provide speech services in macro cells. GSM (Global System for Mobile communications) and IS-95 are the basic 2^{nd} generation air interfaces and are evolving to provide other services such (interactive/multimedia) text messaging (SMS, EMS, MMS) and access to data networks. EDGE (Enhanced Data rates for GSM Evolution) and GPRS (General Packet Radio System) are second generation systems capable of providing third generation services due to its higher transfer data rates (up to 384 kb/s for EDGE and up to 144 Kb/s for GPRS). Co-existence and co-operation of second and third generation systems is necessary, anyway, within an initial period of few years, before the natural death of the 2^{nd} generation systems.

The main requirements and target performance of 3G systems are:

- full coverage and mobility for 144 Kb/s (384 Kb/s later) and limited coverage and mobility for 2 Mb/s
- variable bit rates to offer bandwidth on demand
- higher spectrum efficiency
- higher flexibility and multiplexing of new services with different qualities on a single connection (e.g. speech, video and packet data)
- asymmetric uplink and downlink traffic
- quality requirements for 10% frame error rate and 10^{-6} bit error rate
- coexistence and compatibility with second generation systems (inter-system handover for coverage enhancement and load balancing).

Thus, a larger bandwidth of 5 MHz is needed by 3G systems to be able to provide higher data rates, transmission diversity is needed to improve downlink capacity, advanced radio resource management algorithms are needed to handle different bit rates, quality requirements and services and to maximize the system throughput. Base station synchronisation is not needed in third generation systems, while 2^{nd} generation systems need GPS (Global Positioning System) via satellite connections for base station synchronisation, which makes more problematic the deployment of indoor and micro cells due to the lack of line-of-sight connection. The higher chip rate of WCDMA w.r.t. IS-95 gives more multipath diversity, so higher coverage, and higher trunking gain for high data rates.

2.2 Wideband DS-CDMA FDD Transmitted Signal Model

This work focuses on the baseband signalling and processing of the Wideband Direct Sequence (DS) Code Division Multiple Access (CDMA) FDD mode downlink (from the base station to mobile receivers) of the 3GPP UMTS proposal. The rest of this chapter is dedicated to the introduction of definitions, notations and hypotheses for the baseband signal model used throughout the dissertation. To describe the baseband construction of the noiseless transmitted signal $\bar{y}(t)$ we shall refer to Fig. 2.1.

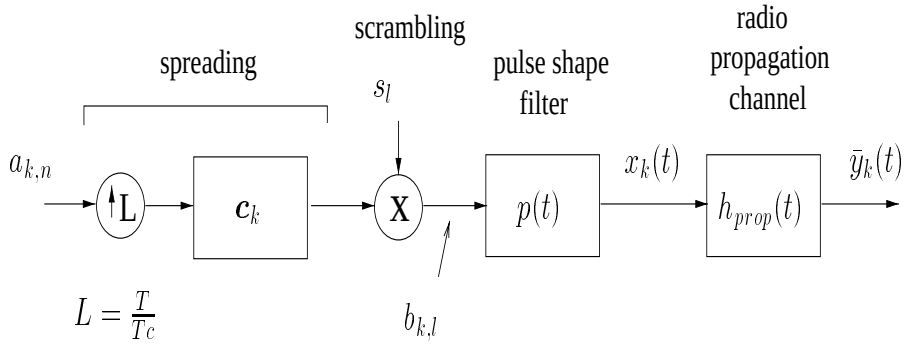

Figure 2.1: The transmission baseband chain

User's k-th symbol $a_{k,n}$ is first spread (spectrum expansion operation), i.e. repeated L times (chips), where $L = \frac{T}{T_c}$ is the processing gain or *spreading factor*, T is the symbol duration and T_c is the chip period, and then multiplied chip by chip with a user specific short (i.e. with period T) spreading sequence $\boldsymbol{c}_k = [c_{k,0}\ c_{k,1} \cdots c_{k,L-1}]^T$, and secondly scrambled, i.e. multiplied chip by chip with a pseudo-noise long (aperiodic w.r.t. T) base station specific chip sequence s_l. Indeed, in Fig. 2.1, the spreading operation is represented as a filtering of an upsampled symbol sequence with the

spreading sequence as impulse response. The chip sequence $b_{k,l}$ is then linearly modulated and the continuous-time baseband output signal is given by

$$x_k(t) = \sum_{l=-\infty}^{l=+\infty} p(t - lT_c) b_{k,l} \tag{2.1}$$

where the chip sequence $b_{k,l}$ can be written as

$$b_{k,l} = a_{k,\lfloor \frac{l}{L} \rfloor} c_{k,l \bmod L} \, s_l \, . \tag{2.2}$$

Along this work symbols $a_{k,n}$ are assumed to be i.i.d. and belonging to a normalized QPSK alphabet. The pulse-shape filter $p(t)$ proposed by the UMTS norm is the Root Raised Cosine (RRC) pulse with roll-off factor of $\alpha_{ps} = 0.22$ in frequency domain, that is in time domain

$$p(t) = \frac{\sin\left(\pi \frac{t}{T_c}(1-\alpha_{ps})\right) + 4\alpha_{ps}\frac{t}{T_c}\cos\left(\pi \frac{t}{T_c}(1+\alpha_{ps})\right)}{\pi \frac{t}{T_c}\left(1 - \left(4\alpha_{ps}\frac{t}{T_c}\right)^2\right)} \, .$$

So the effective bandwidth of the transmitted signal is $W_{eff} = \frac{1+\alpha}{T_c}$.

2.2.1 Frames and slots

In the UMTS FDD downlink there is one Dedicated Physical CHannel (DPCH), which forms a slot and is the result of a time-multiplexing of two dedicated subchannels, the data DPCH (DPDCH) and control DPCH (DPCCH), see Fig. 2.2. Most of the work of this Thesis assumes the use of the DPCH as transport channel. Each slot contains a fixed amount of chip periods, 2560, and since the official UMTS chip rate is 3.84 Mchips/sec, the chip period becomes 260.42 ns, every slot lasts for 0.6667 ms and the effective bandwidth is 4.68 MHz. There are 15 slot in each frame that lasts for 10 ms. Frames are finally organized in superframes of 720 ms. The DPCCH includes physical layer signalling, like training (pilot) bits, power control bits (TPC) or slot format indicator bits (TFCI, they indicate the use of multiple-rate simultaneous services in the system and they are not included in fixed rate services). Table 11 of 3GPP specification TS 25.211 ([17]) gives the exact number of bits/field for every slot format, while Table 12 in the same document specifies the pilot symbol patterns. The DPDCH contains user data bits. Note that here two consecutive bits represent real and imaginary parts of a QPSK symbol ($a_{k,n}$ in previous section).

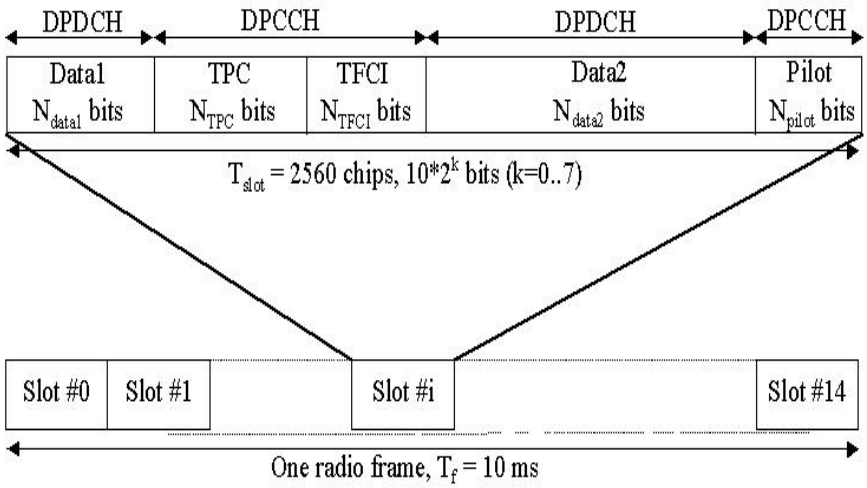

Figure 2.2: Frame/slot structure for downlink DPCH

2.2.2 Spreading and Scrambling

The mechanisms used to spread and scramble the symbol sequence are detailed in the 3GPP specification TS 25.213 ([18]). The spreading operation is necessary not only to widen the signal spectrum, but also to separate different users within a cell. The scrambling operation is needed to separate neighbours cells (base stations) and to render the transmitted/received signal cyclostationary at the chip level.

Because of the synchronicity of user signals and of the common downlink radio channel, the spreading codes (or channelisation codes) for the FDD downlink have been chosen to be orthonormal to each other, so that, in case of a channel equalizer receiver, codes are separable just by a simple correlation with the user-of-interest's channelisation code. Mathematically, if $\boldsymbol{c}_k$ is the k-th user spreading code, orthonormality is expressed by

$$\boldsymbol{c}_k^H \boldsymbol{c}_{k'} = \delta_{k,k'}$$

Within the Thesis, we will consider the spreading factor L constant for all active users in the system, even if the UMTS norm specifies that the system should support different data rates via Orthogonal Variable Spreading Factors (OVSF), Fig. 2.3.

Codes are generated with the help of the Walsh-Hadamard matrices, that is, codes are the (real-valued) columns (or rows) of the square (L by L) matrix $\boldsymbol{W}_L$ such that $\boldsymbol{W}_L^H \boldsymbol{W}_L = \boldsymbol{I}$, where $\boldsymbol{I}$ is the identity matrix of size L, the spreading factor. For

example, if $L = 4$:

$$\boldsymbol{W}_4 = \frac{1}{\sqrt{4}} \begin{bmatrix} 1 & 1 & 1 & 1 \\ 1 & -1 & 1 & -1 \\ 1 & 1 & -1 & -1 \\ 1 & -1 & -1 & 1 \end{bmatrix}$$

The first column (or row) is not usually used as a user code, being used instead as the code for the pilot channel. The spreading factor L can only be a power of 2, but the norm sets the possible values for L in the range $[4, \ldots, 512]$. In case of different user data rates, codes are assigned from the OVSF tree in Fig. 2.3; two codes can not be on same path towards the root of the tree.

The scrambling codes are frame periodic (38400 chips) and are segments of a Gold code of length $2^{18} - 1$. The polynomials that generate the real and imaginary parts of the code are $X^{18} + X^7 + X^1$ and $X^{18} + X^{10} + X^7 + X^5 + X^1$. Along the Thesis we consider the scrambling sequence as a unit magnitude complex (QPSK) i.i.d. sequence, independent from the symbol sequence as well; in this case the chip sequence $b_{k,l}$ can be considered white noise (chip rate i.i.d. sequence, hence stationary).

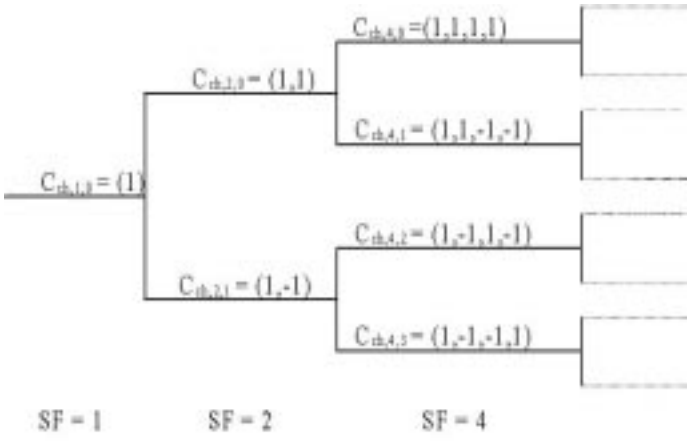

Figure 2.3: The OVSF code generation tree

It should be noted that UMTS TDD mode uses periodic (w.r.t. the symbol period T) scrambling codes of length $L = 16$, so that cyclostationarity of the transmitted/received signal is at symbol level.

2.3 Radio Propagation Channels

Reflection, diffraction and *scattering* (Fig. 2.4) are the phenomena affecting the radio

propagation in wireless communications ([19], [20], [21]). Depending on the envi-

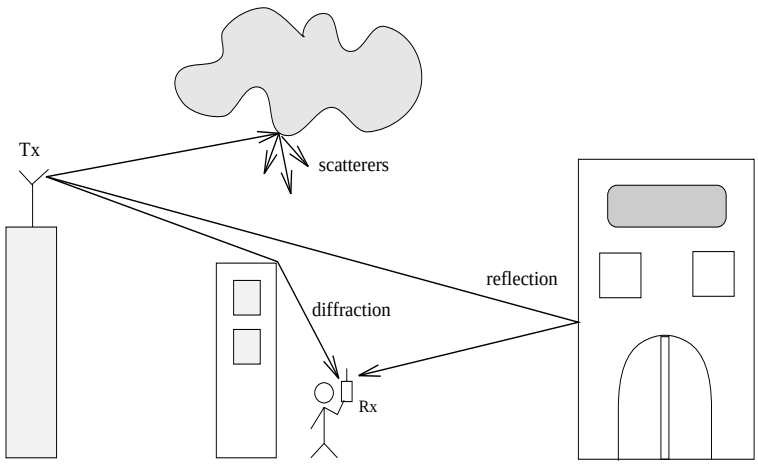

Figure 2.4: Propagation Mechanisms

ronment (indoor, urban, pedestrian, vehicular, rural, etc.) they distort, together or separately, the transmitted signal, which can be considered to pass through a filter $h_{prop}(t)$.

In terms of the power arriving at the receiver, the time-variations of the channel impulse response are mainly due to two types of attenuation, referred generally as fading. The *large-scale fading* is defined as the average signal power attenuation caused by mobility over large areas, where hills, building, trees, etc, are "shadowing" the transceivers; usually this type of fading is statistically modelled as a zero-mean log-normally distributed random variable. The *small-scale fading* is due to the superposition of a large number of multipath components impinging the transceiver antennas. It manifests itself as rapid variations of the amplitude and phase of the received signal, variations that depend on the carrier frequency, on the transmission rate and on the relative speeds of the transmitter and receiver. This kind of fading is modelled as a Rayleigh distributed random variable in the absence of a line of sight (LOS), while a Ricean distribution (non-zero mean) is used when a LOS component is present.

Generally, the total fading is considered as the superposition of small-scale fading to the large-scale fading and the received signal envelope undergoes variations like in Fig. 2.5.

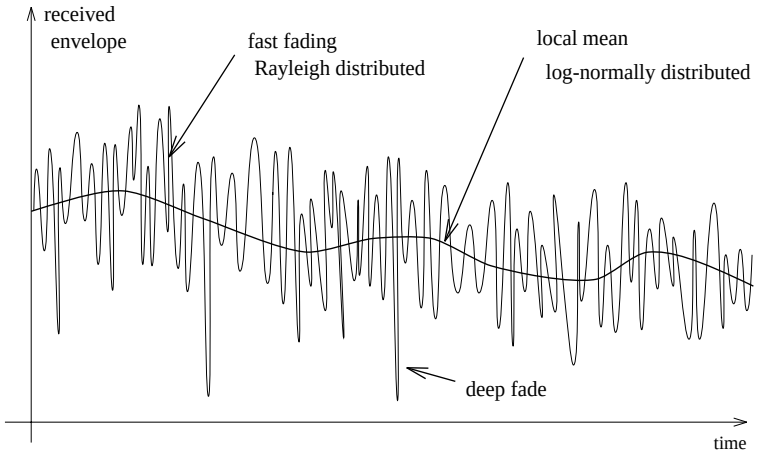

Figure 2.5: Propagation Mechanisms

2.3.1 Wide-Sense Stationary Uncorrelated Scattering (WSS-US) Model

The basic assumption behind this model is that multipath components arriving with different delays are uncorrelated ([23]). It has been shown that this channel is wide-sense stationary both in time and frequency. The model is described by 4 functions that represent the channel: the Multipath Intensity Profile (MIP) is a function of the delay, the the Doppler Power Spectrum (DPS) is a function of the Doppler-frequency shift, while the other two functions are, respectively, the Fourier transforms of the two above.

The MIP describes the power distribution in time of the multiple echoes of a single impulse sent through the channel; it also defines the maximum excess delay (or *delay spread*) of the channel as the time difference between the first and last (significant) received copy of the pulse. In an ideal environment, the MIP has just an ideal impulse with amplitude corresponding to the received power. By defining the delay spread as T_{ds}, we can distinguish between channels that show *frequency selective fading*, introducing some intersymbol-interference (ISI), when $T_{ds} > T$, and channel where this doesn't happen, or *flat fading* channels ($T_{ds} < T$). In this last case, all the multipath components arrive within a symbol period, so they are unresolvable in time if the sampling rate $\approx \frac{1}{T}$, the symbol level resolution.

2.3.2 Time Varying Multipath Channels

The Doppler Power Spectrum models the time variation of the channel, which is due to the mobility of the receivers (mobile stations) and/or of the environment objects.

If all is stationary, including the receiver, a continuous-time signal sent through the channel gets attenuated, but remains constant, i.e. the channel is time-invariant. The WSS-US model describes the time-variations of the channel in the Doppler frequency (shift) domain with the function $1/(\pi f_d \sqrt{1-(\nu/f_d)^2})$, where ν is the Doppler shift and f_d is the Doppler spread (spectral broadening); when the mobile moves along the line between itself and the base station (most critical case), $f_d = v/\lambda$, where v is the (positive or negative) mobile speed and $\lambda = c/f_c$ is the wavelength (c is light speed and f_c is the carrier frequency). $\frac{1}{f_d} = T_{ct}$ is the coherence time of the channel, that is the time a channel can be considered invariant over.

Along this work we shall consider a slow fading, frequency selective multipath channel. In this case the channel has a very long (compared to the symbol period) coherence time, and we can consider it invariant during a slot. We focus on channels that are represented by a set of delayed echoes ([24]) and that can be described by a Q tapped delay-line and considered to have a finite impulse response (FIR), that is

$$h_{prop}(t,\tau) = \sum_{p=1}^{Q} g_p(t)\delta(\tau - \tau_p(t))$$

2.3.2.1 Sparse Channel Approximation

When there are very few significant taps $M_p << Q$ in the Delay Power Profile (DPP), we say the radio channel is sparse and we can model its complex baseband representation as the sum of M_p delayed impulses with complex amplitudes, i.e.

$$h_{sp}(t,\tau) = \sum_{p=1}^{M_p} g_p(t)\delta(\tau - \tau_p(t)) \tag{2.3}$$

where $g_p(t)$ are WSS uncorrelated complex Gaussian processes. As we said in the previous section, we consider the channel to be constant over a slot period, so that amplitudes are independent of time t in the model. Delays change in a much slower fashion than the fading so we can set them as constant as well. The resulting model we will consider is then

$$h_{sp}(t) = \sum_{p=1}^{M_p} g_p\delta(t - \tau_p) \tag{2.4}$$

In Annex B of the specification TS 25.101 ([25]), UMTS norm specifies the propagation conditions in terms of relative delay and average power for each significant tap. Two examples are given here in Fig. 2.6. It is the case of a vehicular (suburban) environment with four equally spaced (by 1 chip period) taps with exponentially decaying

average power; the delay spread is considered short. Other channel models have non-multiple of chip period tap delays and more severe propagation conditions like the second example where the delay spread is very large (20 microseconds), the three taps have equal average power, but we are in a pedestrian (rural) environment; in this case the channel should not be considered constant over an entire slot.

Vehicular (suburban) Speed 120 Km/h		Pedestrian (rural) Speed 3 Km/h	
Relative Delays [ns}	Average Power [dB]	Relative Delays [ns}	Average Power [dB]
0	0	0	0
260 (1 chip)	-3	976 (3.75 chips)	0
521 (2 chips)	-6	20000 (76.9 chips)	0
781 (3 chips)	-9		

Figure 2.6: Two examples of UMTS radio channel propagation conditions

Reconsidering now the transmitted signal model, and including the radio propagation channel in the transmission chain, we can restate the signal transmitted by a user from the base station and passed through the channel (convolution) as

$$\begin{aligned} \bar{y}_k(t) &= \sum_{l=-\infty}^{l=+\infty} b_{k,l} \int_0^{N'T_c} p(t-\tau-lT_c) h_{sp}(\tau) d\tau \\ &= \sum_{l=-\infty}^{l=+\infty} b_{k,l} \sum_{p=1}^{M_p} g_p p(t-\tau_p-lT_c) \end{aligned} \tag{2.5}$$

where N' is the delay spread, in chips, of the sparse radio propagation channel $h_{sp}(t)$. Note that in the forward link the channel between the base station and a terminal is the same for all active users in the system.

2.4 Multiuser Downlink Received Discrete-Time Cyclostationary Signal

The baseband noiseless received signal $\bar{y}_k(t)$ can be reformulated by aggregating the radio propagation channel, the transmitter pulse shape filter and an antialiasing filter, like in the multiuser downlink signal model of Fig. 2.7.

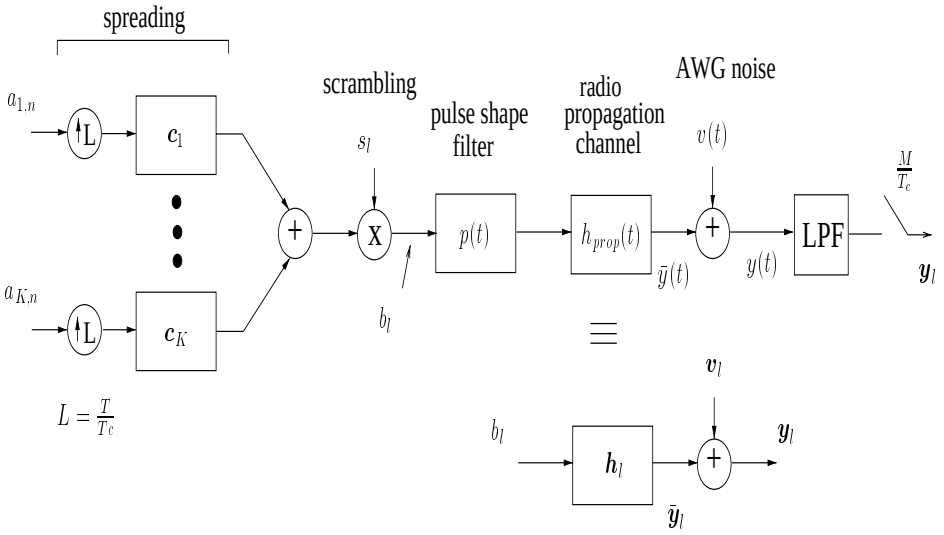

Figure 2.7: Multiuser Downlink Signal Model

Indeed, we can write the continuous-time overall channel as

$$h(t) = h_{sp}(t) * p(t) = \sum_{p=1}^{M_p} g_p p(t - \overline{\tau}_p) \, . \tag{2.6}$$

Note that the receiver antialiasing filter is an ideal low-pass filter with cut-off frequency corresponding to the sampling frequency W, which must be larger than the effective signal bandwidth $W_{eff} = \frac{1+\alpha}{T_c}$ to satisfy the well known Nyquist sampling theorem. It would suffice to oversample $M = 2$ times w.r.t. to chip rate $1/T_c$ to satisfy the theorem because $0 < \alpha \leq 1$. The continuous-time path delays τ_p are discretized to the resolution given by sampling at rate $W = \frac{M}{T_c}$.

Since the receiver samples M times per chip period, or eventually there are M sensors/antennas at the mobile receiver or we have a mix of M "phases", the overall channel (2.6) becomes in the discrete-time domain at chip instant l and oversampling phase m ($m \in [1, \ldots, M]$)

$$h_{m,l} = \sum_{p=1}^{M_p} g_p p(lT_c + (m-1)\frac{T_c}{M} - \overline{\tau}_p) \, , \tag{2.7}$$

so that $\boldsymbol{h}_l = \left[h_{1,l} \cdots h_{M,l}\right]^T$, represents the vectorized samples of the overall channel at chip period l and $\boldsymbol{h} = \left[\boldsymbol{h}_0^T \cdots \boldsymbol{h}_{N-1}^T\right]^T$ represents the entire overall channel that spans N chip periods, where $N = N' + \Delta$ and Δ is the effective duration, in chip periods, of the pulse shape filter $p(t)$.

Note that the overall channel $\boldsymbol{h}$ can be rewritten in matrix notation as

$$\boldsymbol{h} = \boldsymbol{P}\boldsymbol{g} = \begin{bmatrix} \vdots & & \vdots \\ p_{k-\overline{\tau}_1} & \cdots & p_{k-\overline{\tau}_{Mp}} \\ \vdots & & \vdots \end{bmatrix} \begin{bmatrix} g_1 \\ \vdots \\ g_{M_p} \end{bmatrix} \tag{2.8}$$

where p_k is the oversampled root raised cosine.

The total continuous-time noiseless received signal $\bar{y}(t)$ is the superposition of all the active user chip sequences, i.e.

$$\bar{y}(t) = \sum_{k=1}^{K} \sum_{l=-\infty}^{l=+\infty} b_{k,l}\ h(t - lT_c)$$

so, within the chip period l, the total discrete-time noiseless received signal is $\bar{\boldsymbol{y}}_l = [\bar{y}_{1,l} \cdots \bar{y}_{M,l}]^T$ with

$$\bar{y}_{m,l} = \sum_{k=1}^{K} \sum_{l'=0}^{N-1} h_{m,l'} b_{k,l-l'} \quad , \tag{2.9}$$

2.4.1 Additive White Gaussian Noise

Some noise gets added to the received signal $\bar{\boldsymbol{y}}_l$ at the front-end of the receiver. Unless differently stated we consider it as the sum of the thermal noise and of the intercell interference (coming from different base stations).

The thermal noise is modelled as a white Gaussian circular random variable with zero mean and a variance of N_0 (white stationary noise). It is also considered spatially white if the multiple sensors are sufficiently spaced apart (more than half of the wavelength). The noise spectrum is considered flat over any finite signal bandwidth. The use of a receiver antialiasing filter doesn't alter the whiteness of the thermal noise, while oversampling just amplifies its variance by the oversampling factor.

The intercell interference is a sum of contributions that are of the same form of the intracell contributions which are stationary vector processes. Hence the intercell interference plus thermal noise, $\boldsymbol{v}_l$, is stationary, with variance $\boldsymbol{R}_{vv} = \sigma_v^2 \boldsymbol{I}$.

The total sampled received signal, at chip rate, is therefore

$$\boldsymbol{y}_l = \sum_{k=1}^{K} \sum_{i=0}^{N-1} \boldsymbol{h}_i b_{k,l-i} + \boldsymbol{v}_l \ . \tag{2.10}$$

2.4.2 General Linear Receiver Structure

Fig. 2.8 shows a linear receiver in which a descrambler and a correlator for the user of interest's spreading code (user 1 in the Thesis) follow a general FIR filter $\boldsymbol{f}_l = [f_{1,l} \cdots f_{M,l}]$ whose input is at sampling rate and its output is at chip rate (MISO). We shall assume the filter $\boldsymbol{f}_l$ to be causal so that the receiver outputs symbol es-

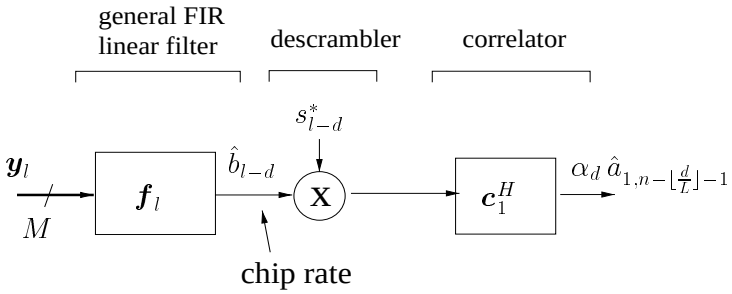

Figure 2.8: General Linear Receiver

timates for the user of interest with a certain delay. Let $\boldsymbol{h}(z) = \sum_{l=0}^{N-1} \boldsymbol{h}_l z^{-l}$ be the $M \times 1$ FIR channel transfer function and $\boldsymbol{f}(z) = \sum_{l=0}^{P-1} \boldsymbol{f}_l z^{-l}$ the $1 \times M$ FIR filter transfer function of length P chips. The cascade of channel and filter gives $\boldsymbol{f}(z)\boldsymbol{h}(z) = \sum_{l=0}^{P+N-2} \alpha_l z^{-l} = \boldsymbol{\alpha}(z)$.

The symbol estimate gets produced with a certain delay of $l_1{+}1$ symbol periods where $d = l_1 L + l_2$ $(l_1 = \lfloor \frac{d}{L} \rfloor, l_2 = d \bmod L)$. More precisely, the receiver outputs

$$\alpha_d\, \widehat{a}_{1,n-l_1-1} \;=\; \boldsymbol{c}_1^H\, X_n \tag{2.11}$$

where X_n is a vector of descrambled filter outputs,

$$X_n \;=\; \boldsymbol{S}^H_{n-l_1-1} Z_n \;,\;\; Z_n = \mathcal{T}(\boldsymbol{f})\boldsymbol{Y}_n \;, \tag{2.12}$$

Z_n is a vector of filter outputs, $\boldsymbol{S}_n =$ diag $\{s_{n,L-1}, \ldots, s_{n,1}, s_{n,0}\}$ is a diagonal matrix of scrambling code coefficients $s_{n,l} = s_{nL+l}$, $\mathcal{T}(\boldsymbol{f})$ is the block Toeplitz filtering matrix with $\boldsymbol{f} = \begin{bmatrix}\boldsymbol{f}_0 \cdots \boldsymbol{f}_{P-1}\end{bmatrix}$ (padded with zeros) as first row, and
$\boldsymbol{Y}_n = \left[\underline{Y}^T_{n,l_2}\, Y^T_{n-1} \cdots Y^T_{n-l_3}\, \overline{Y}^T_{n-l_3-1,l_4}\right]^T$ where $P{+}L{-}1{-}l_2 = l_3 L{+}l_4$,
$Y_n = \left[\boldsymbol{y}^T_{n,L-1} \cdots \boldsymbol{y}^T_{n,0}\right]^T$, $\underline{Y}_{n,l} = \left[\boldsymbol{y}^T_{n,l-1} \cdots \boldsymbol{y}^T_{n,0}\right]^T$, $\overline{Y}_{n,l} = \left[\boldsymbol{y}^T_{n,L-1} \cdots \boldsymbol{y}^T_{n,L-l}\right]^T$, and $\boldsymbol{y}_{n,l} = \boldsymbol{y}_{nL+l}$.

The structure of the vector $\boldsymbol{Y}_n$ of received data that contribute to the estimate $\widehat{a}_{1,n-l_1-1}$ is

$$\boldsymbol{Y}_n = \mathcal{T}(\boldsymbol{h}')\boldsymbol{S}_n \sum_{k=1}^{K} \boldsymbol{C}_k \boldsymbol{A}_{k,n} \;+ \boldsymbol{V}_n \tag{2.13}$$

where $\mathcal{T}(\boldsymbol{h}')$ is again a block Toeplitz filtering matrix with the zero padded $\boldsymbol{h}' = [\boldsymbol{h}_0 \cdots \boldsymbol{h}_{N-1}]$ as first block row, $\boldsymbol{S}_n$= blockdiag $\left\{\underline{\boldsymbol{S}}_{n,l_2}, \boldsymbol{S}_{n-1}, \ldots, \boldsymbol{S}_{n-l_5}, \overline{\boldsymbol{S}}_{n-l_5-1,l_6}\right\}$, $\boldsymbol{C}_k =$ blockdiag $\{\underline{\boldsymbol{c}}_{k,l_2}, \boldsymbol{c}_k, \ldots, \boldsymbol{c}_k, \overline{\boldsymbol{c}}_{k,l_6}\}$ (l_5 $\boldsymbol{c}_k$'s), $\boldsymbol{A}_{k,n} = [a_{k,n} \cdots a_{k,n-l_5-1}]^T$, $\boldsymbol{V}_n$ is defined like $\boldsymbol{Y}_n$, and $\underline{\boldsymbol{S}}_{n,l}$, $\overline{\boldsymbol{S}}_{n,l}$, $\underline{\boldsymbol{c}}_{k,l}$ and $\overline{\boldsymbol{c}}_{k,l}$ are defined similarly to $\underline{Y}_{n,l}$ and $\overline{Y}_{n,l}$ except that $\underline{\boldsymbol{S}}_{n,l}$ and $\overline{\boldsymbol{S}}_{n,l}$ are diagonal matrices, and $P+L+N-2-l_2 = l_5 L+l_6$.

We have for the filter-channel cascade

$$\mathcal{T}(\boldsymbol{f})\mathcal{T}(\boldsymbol{h}') = \mathcal{T}(\boldsymbol{\alpha}) = \mathcal{T}(\boldsymbol{\alpha}_d) + \mathcal{T}(\overline{\boldsymbol{\alpha}}_d) \tag{2.14}$$

where

$$\begin{aligned} &\boldsymbol{\alpha} = [\alpha_0 \cdots \alpha_{P+N-2}]\,,\ \boldsymbol{\alpha}_d = [0 \cdots 0\ \alpha_d\ 0 \cdots 0] \\ &\overline{\boldsymbol{\alpha}}_d = [\alpha_0 \cdots \alpha_{d-1}\ 0\ \alpha_{d+1} \cdots \alpha_{P+N-2}]\,. \end{aligned} \tag{2.15}$$

Equation 2.13 can be rewritten as a function of the overall channel using the commutative property of the convolution operation, that is

$$\boldsymbol{Y}_n = \sum_{k=1}^{K} \boldsymbol{B}_{k,n}\boldsymbol{h}\ + \boldsymbol{V}_n \tag{2.16}$$

where $\boldsymbol{B}_{k,n} = \mathsf{B}_{k,n} \otimes \boldsymbol{I}_M$ is a block Hankel matrix containing the user k-th chip sequence (after spreading and scrambling). This notation is useful for channel estimation by training sequences. For example, if $\boldsymbol{Y}_n$ is the received signal during training symbols and the user of interest is the number 1, the least-squares fitting problem to find the sparse channel parameters becomes

$$\arg\min_{\boldsymbol{\tau},\boldsymbol{g}} \|\boldsymbol{Y}_n - \boldsymbol{B}_{1,n}\overline{\boldsymbol{P}}\boldsymbol{g}\|^2 \tag{2.17}$$

where $\boldsymbol{\tau} = [\tau_1 \cdots \tau_{M_p}]$ and $\overline{\boldsymbol{P}}$ is similar to $\boldsymbol{P}$ of eq. 2.8, but with columns containing truncated (to 4 chip periods per side plus the central tap) versions of the RRC p_k since $\overline{\boldsymbol{P}}$ is stored at the mobile terminal. Note that, if the oversampling factor (multiplication of the sampling rate and the number of sensors) is high, the overall channel length is large and the matrix $\boldsymbol{P}$ can become rank deficient. A solution was proposed in [30] and consider the singular value decomposition (SVD) of $\boldsymbol{P}$ with the *effective* rank of this matrix. But a drawback of this approach is that if the radio propagation channel is truly sparse the orthonormal matrices coming from the SVD are not and their delays contribute at all positions in the overall channel. So if the channel is known to have sparse FIR impulse response, no gain comes from this approach.

2.5 Conclusions

We described in this chapter the general history of the standardization process for third generation wireless systems, in particular for the forward link of the UTMTS-FDD WCDMA norm, and their main differences with respect to the second generation systems like GSM. We revised the characteristics of the transmitted signal model, from the spreading and scrambling operations, through the radio propagation channel and the additive noise, till the received signal and sumbol estimates by a general linear receiver. Along the chapter we also introduced the notation used afterwards in the Thesis.

Chapter 3

RAKE Receiver and Channel Approximation

The conventional receiver for DS-CDMA communications is the RAKE receiver. The RAKE receiver is a matched filter, matched to the operations of spreading, pulse shape filtering and channel filtering. Such a matched filter maximizes the Signal-to-Interference-plus-Noise Ratio (SINR) at its output if the interference plus noise is white. This may be approximately the case if user-dependent scrambling (aperiodic spreading) is used. This is one option for the uplink in 3rd generation systems. However, this is not the case in the synchronous downlink with cell-dependent scrambling, orthogonal codes and a common channel. In this chapter we review the RAKE receiver, we set up its discrete-time representation, as well as the discrete-time approximation of the channel impulse response, and we introduce some alternatives to the RAKE receiver, like the linear equalizer and hybrid structures.

3.1 Pulse-shape and Channel Matched Filter Receiver

The classical continuous-time RAKE receiver (Fig. 3.1) is the reference receiver structure with which to compare other implementations. Assume the notation introduced in chapter 2. The RAKE receiver is a channel matched filter (MF), where the (over-

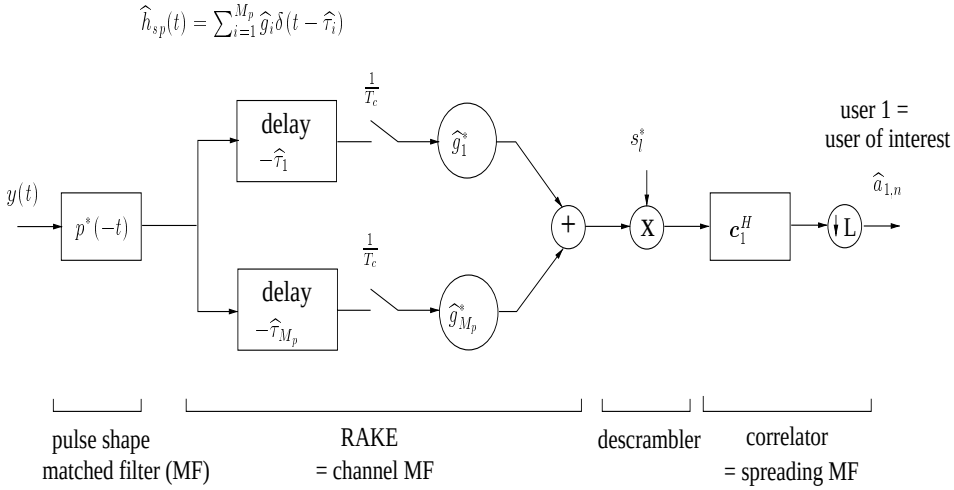

Figure 3.1: (reduced complexity) Continuous-time RAKE Receiver

all) channel is the convolution of the spreading sequence, the pulse shaping filter and the multipath propagation channel. The term RAKE refers to a sparse channel impulse response model in which the finite number of specular paths (M_p) leads to fingers (contributions at various delays) in the channel impulse response. The propagation channel MF is a MF to a sparsified estimation $\widehat{h}_{sp}(t)$ for the propagation channel $h_{prop}(t)$ (see section 2.3.2.1), in the sense that the convolution $p(t)$*$\widehat{h}_{sp}(t)$ should approximate the convolution $p(t)$*$h_{prop}(t)$.

In this classical implementation of the RAKE, there is one descrambler plus correlator per finger, unlike in Fig. 3.1 where, due to linearity, we moved forward in the circuit these two operations. The implementation in Fig. 3.1 is the least costly one if a general DSP implementation is considered (complexity issues are different with special purpose hardware for the correlator). The classical RAKE implementation allows estimating the channel taps (finger weights) at the outputs of the correlators and tracking of the delays (by dedoubling the fingers in an early-late fashion). However, this classical implementation, which uses continuous values for the delays, requires interpolators to generate samples of the received signal at these continuous-valued delays. The main complexity advantage of a discrete-time RAKE implementation is the avoidance of these interpolators.

3.2 From Continuous-time to Discrete-time

An alternative implementation is depicted in Fig. 3.2, in which a certain oversampling factor m is introduced with respect to the chip rate so that the sampling frequency satis-

fies the Nyquist criterion (corresponding to the bandwidth of the pulse-shaping filter). Since the Nyquist criterion is satisfied, the matched filtering for the propagation channel can be done in the discrete-time domain. This is indicated by the first equivalence in Fig. 3.2. Note that l is sampling time index while l' is the chip time index. The discrete-time propagation channel impulse response $\widehat{h}_{prop}[l]$ does not correspond to a simple sampled version of the continuous-time version $h_{prop}(t)$ however. Due to the fact that the sampling frequency is higher than the Nyquist rate and that the pulse shaping filter is nulling out a certain frequency band, $\widehat{h}_{prop}[l]$ should be, in general, such that the equivalence holds. If the sampling frequency exceeds the Nyquist rate, then the choice for $\widehat{h}_{prop}[l]$ is not unique. Since the sampling frequency satisfies the Nyquist criterion for the pulse shaping filter, the pulse shaping MF can be moved after the sampling operation if an anti-aliasing filter is introduced before the sampling operation, as shown by the second equivalence in Fig. 3.2. Now, the input to the discrete-time pulse shaping and propagation channel MFs is at the sampling rate whereas the corresponding output needs to be downsampled to the chip rate. A polyphase implementation of the discrete-time pulse shape MF and propagation channel MF can be realized for this multirate filtering operation.

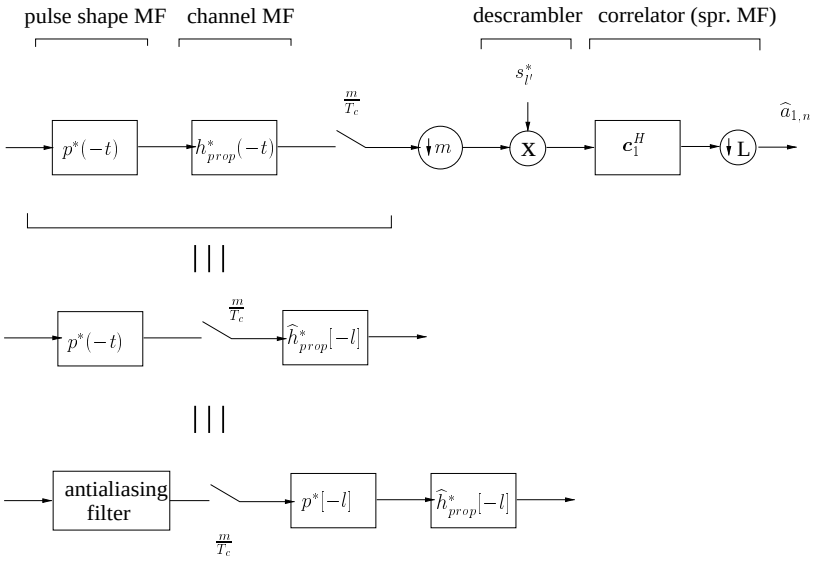

Figure 3.2: Discrete-time RAKE Receiver

Now, the approximation operation leading to the discrete-time propagation channel representation $\widehat{h}_{prop}[l]$ can be used to incorporate sparsification. Indeed, if the sampling frequency exceeds well the Nyquist rate (already with $m = 2$), then there is a large degree of nonuniqueness in the representation $\widehat{h}_{prop}[l]$. This is due to the fact that $p[l]$ has a nullspace that allows us to substitute $\widehat{h}_{prop}[l]$ by $\widehat{h}_{prop}[l] + n[l]$ to still have

a valid discrete-time propagation channel ($n[l] * p[l] = 0$). We can take advantage of these degrees of freedom to require $\widehat{h}_{prop}[l]$ to be sparse (have only a limited number of non-zero coefficients). If the true propagation channel $h_{prop}(t)$ is sparse, it would be good if its discrete-time representation $\widehat{h}_{prop}[l]$ could be equally sparse (see next section).

By using the matrix notation of chapter 2, the symbol estimate at the output of the discrete-time RAKE receiver, with a certain delay of $l_1 + 1$ symbol periods, is given by

$$\widehat{a}_{1,n-l_1-1} \;\propto\; \boldsymbol{c}_1^H \, S_{n-l_1-1}^H \mathcal{T}(\boldsymbol{h}^H) \boldsymbol{Y}_n \tag{3.1}$$

where $\boldsymbol{h}$ represents the overall discrete-time channel impulse response, including pulse-shape filter, propagation channel and receiver antialiasing filter, $\mathcal{T}(\boldsymbol{h}^H)$ is the block Toeplitz channel matched-filtering matrix, l_1 such that $d = l_1 L + l_2$ is the delay, in chip periods, given by the cascade channel/channel-matched-filter (l_2 is a chip period offset), and $\boldsymbol{Y}_n$ is the discrete-time received signal vector.

3.2.1 Channel Approximation

We have done some calculations to see what the SNR is (considering the approximation error as noise) by taking one (two) non-zero tap(s) in the discrete-time channel impulse response for each path in the continuous-time channel impulse response (see model block diagrams in Fig. 3.3 for 1 path and Fig. 3.4 for more paths).

In the case of 1 path approximation (Fig. 3.3) we have to find the amplitude A the minimizes the squared-error between a continuous-time pulse-shape (Root-Raised-Cosine with roll-off factor of 0.22) convolved with a pulse (delta-function) at an offset τ^o and an amplitude adjusted discrete-time truncated (4 chips per side) pulse-shape at zero delay. Mathematically the optimal amplitude for the discrete-time approximation becomes

$$A_{opt} = \arg\min_A \sum_k \epsilon_k^2 = \arg\min_A \sum_k \left(y_k - A p_k\right)^2$$

where p_k is the discrete-time truncated pulse-shape. We get $A_{opt} = \dfrac{\sum_k y_k p_k}{\sum_k p_k^2}$ and

$$SNR_{dB} = 10 \log 10 \left(\frac{\sum_k \epsilon_k^2 |_{A_{opt}}}{\sum_k y_k^2} \right)^{-1} = 10 \log 10 \left(1 - \frac{\left(\sum_k y_k p_k\right)^2}{\left(\sum_k y_k^2\right)\left(\sum_k p_k^2\right)} \right)^{-1}$$

We found that by oversampling with $m = 4$, the mean SNR (τ varying randomly and uniformly between 0 and $T_c/8$) is 17 dB when using just one tap. In Fig. 3.5 we

can see how the estimated amplitude A and the SNR vary with respect to the offset τ between the continuous-time delay and the discretized one. By taking two non-zero taps, the second being related to the pulse-shape derivative, but with $m = 2$, the mean SNR does not increase significantly with respect to the one-tap approximation. This last approach is not shown in the figures.

When approximating an entire continuous-time channel impulse response with one non-zero tap per path (see Fig. 3.4), our approach is to iteratively add one approximating tap (at the delay that minimize the approximation error) and there are basically 3 possibilities for the amplitude (re)estimation:

1 keeping the previous delays and amplitudes fixed for the new amplitude optimization

2 as in 1 but (re)optimizing all amplitudes together after having determined all discrete-time paths

3 (re)optimize all amplitudes at each possible new delay for the new approximating tap while keeping previously found delays fixed

The mean SNR for randomly chosen channel impulse responses (# of paths between 1 and 6, delay spread between 310e-9 and 20000e-9 s, random delays within the delay spread and negative-exponential distribution style for the amplitude variances) is 20.43 dB for approach 1, 20.92 dB for approach 2 and 22.06 dB for approach 3.

Since this SNR is much better than what the SINR of the received signal can be expected to be, this approximation error is negligible. So the discrete-time RAKE is a viable option. Of course, the approximation error can be reduced by assigning more than one discrete-time tap to a continuous-time path (assigning an extra tap to a strong path may be a better idea than to use that tap to model a weak path).

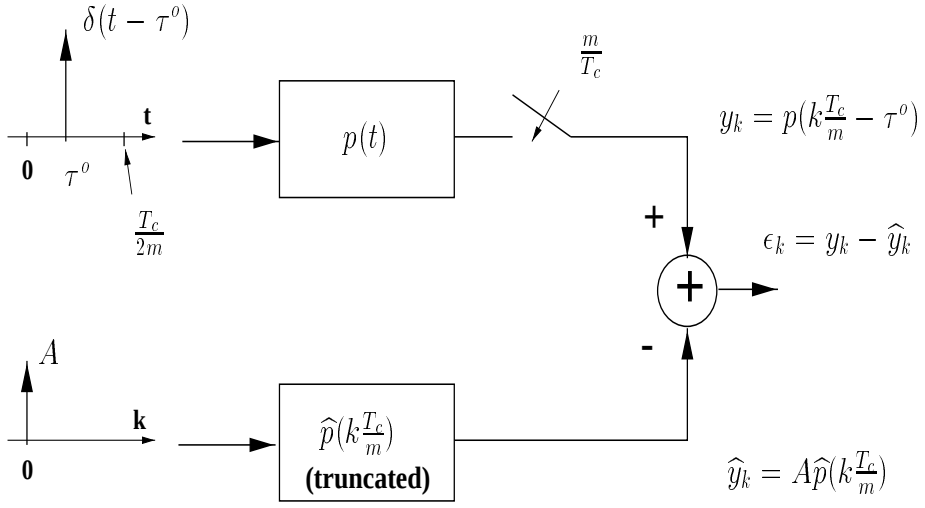

Figure 3.3: Delay Discretization Error Evaluation

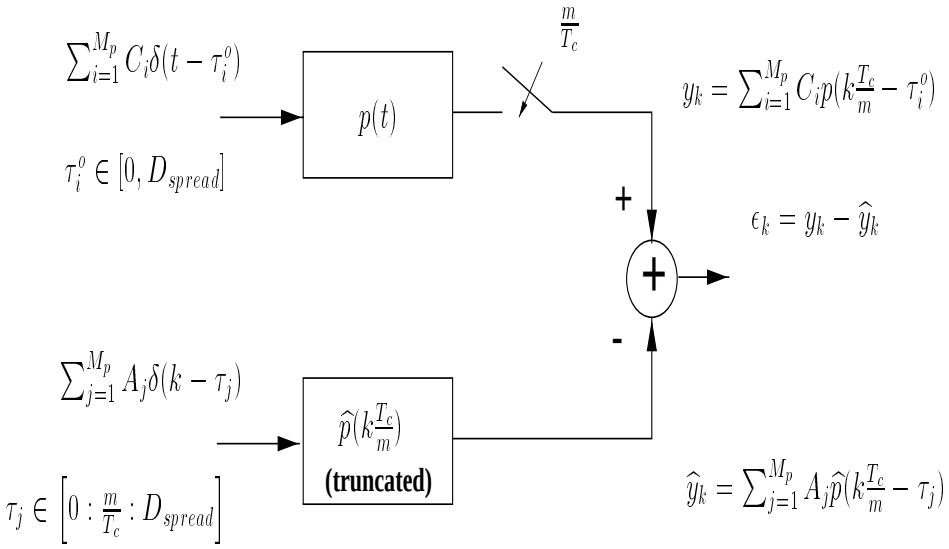

Figure 3.4: Channel Discretization Error Evaluation

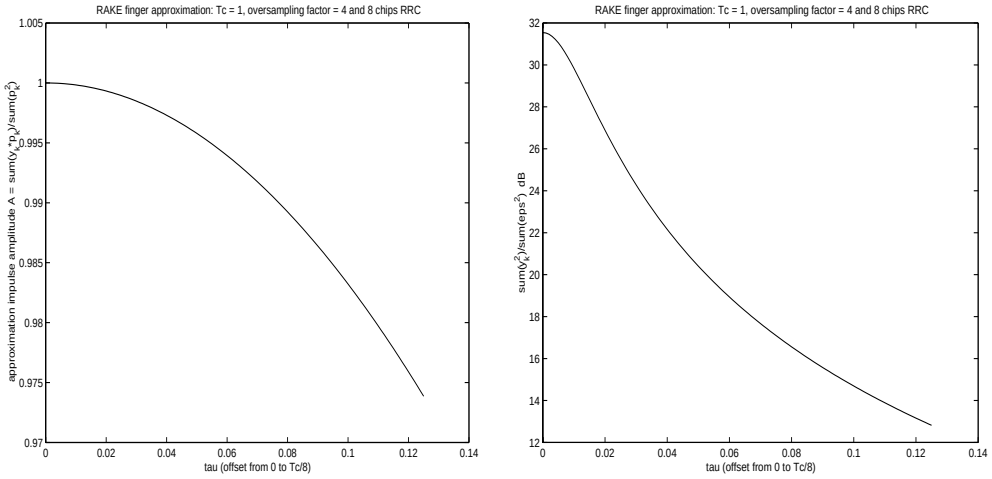

Figure 3.5: Amplitude and Error variation with offset τ

3.3 Equalizer Receivers and Hybrid Solutions

In [31], another receiver approach, based on channel equalization, is presented, the Zero Forcing (ZF) equalizer receiver. This approach was introduced independently also in [32] and [33]. Whereas the RAKE approach focuses on the noise (and inter-cell interference), the equalizer approach focuses on the intracell interference. If the base station does not use mobile-dependent beamforming, then the downlink channel towards a certain mobile is the same for the superposition of signals received by the mobile (even in the case of sectoring (non-ideal sectors), this reasoning could roughly be applied per sector). Indeed, if the channel gets zero-force equalized as first operation at the receiver, the codes become orthogonal again at the equalizer output. Hence the equalizer can be followed by a correlator to get rid of all intracell interference, see Fig. 3.6 where $\boldsymbol{w}$ replaces the channel matched filter $\boldsymbol{h}^H$ of the RAKE receiver.

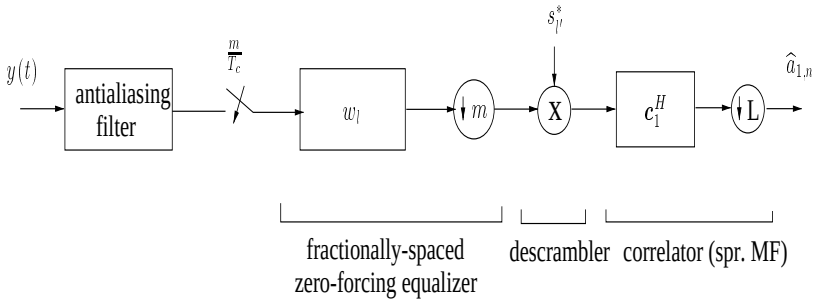

Figure 3.6: Equalizer receiver

The soft symbol estimate at the output of the Zero Forcing Equalizer receiver is given by

$$\widehat{a}_{1,n-l_1-1} \;=\; \boldsymbol{c}_1^H \, S_{n-l_1-1}^H \mathcal{T}(\boldsymbol{w}) \boldsymbol{Y}_n \tag{3.2}$$

where $\boldsymbol{w}\,\mathcal{T}(\boldsymbol{h}) \;=\; [0, \cdots, 0, 1, 0, \cdots, 0]$ with the 1 in the d-th position, being d the delay in chip periods given by the cascade channel/zero forcing equalizer.

By using a zero-forcing fractionally-spaced equalizer, the excess bandwidth can be used to cancel some of the intercell interference also (if multiple antennas are available, then this can be done even better). The problem with this approach is that a zero-forcing equalizer may produce quite a bit of noise enhancement. So between the RAKE receiver and the equalizer receiver, one or the other may be better, depending on whether the intracell interference dominates the intercell interference plus noise or vice versa, see Fig. 3.8. A natural solution to improve the equalizer approach would be to replace a zero-forcing design by a minimum mean square-error (MMSE) design which will be explored in the next chapter.

We investigated hybrid receiver structures combining the equalizer and RAKE components. The new structure consists of a RAKE preceded by an intracell interference canceller (IC), see Fig. 3.7. This IC has a desired signal suppression branch, which is build from a channel equalizer, followed by a projector that cancels the code of the signal of interest. This projector is then followed by re-filtering with the channel impulse response. At that point, the branch output contains the intracell interference in the same way as the received signal, and the signal of interest is removed. So by subtracting the branch output from the received signal, all intracell interference gets cancelled.

The new receiver structure acts similarly to the equalizer plus decorrelator receiver. However, noise plus intracell interference get treated differently and simulations show that the new receiver achieves improved performance, see Fig. 3.8. Further improvements can be obtained by replacing the refiltering coefficients by those resulting from a MMSE design.

3.4 Conclusions

This chapter was dedicated to the review of the traditional RAKE receiver, in its continuous- and discrete-time versions, to channel dicretization due to the introduction of oversampling w.r.t. the chip rate and some implications concerning the approximation of the continuous-time channel delays. We also introduced some linear receivers, like the Zero-Forcing receiver or hybrid solutions, that are capable of ameliorating the

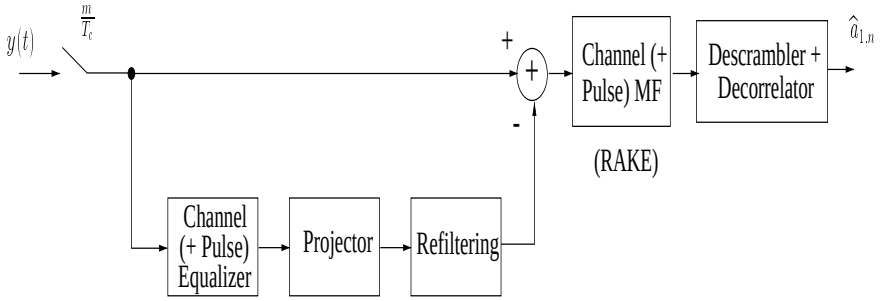

Figure 3.7: Hybrid RAKE-Equalizer structure

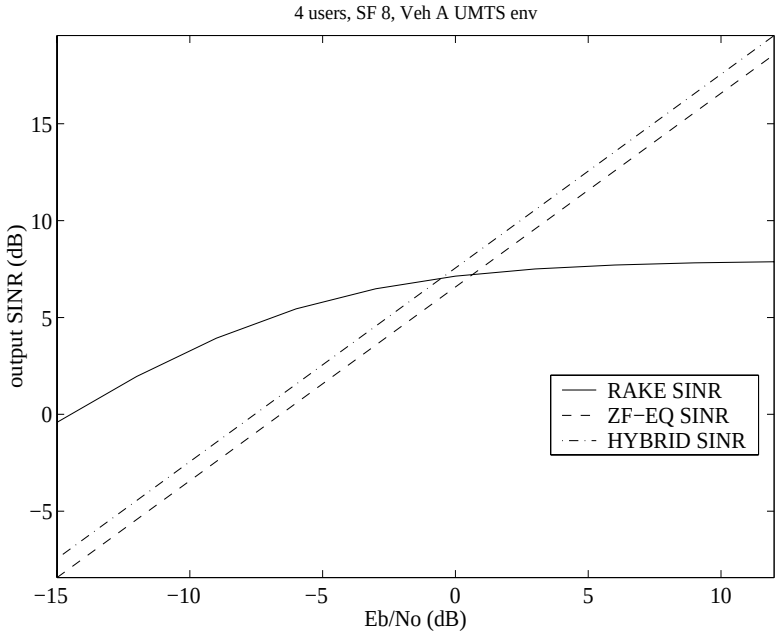

Figure 3.8: RAKE, ZF Equalizer, Hybrid structure SINR comparison

RAKE SINR performance in the high input SNR region. All these receivers are taken as references for SINR improvement using other linear structures.

Chapter 4

Max-SINR Receivers

We propose a restricted class of linear receivers for the downlink, exhibiting a limited or no complexity increase with respect to the RAKE receiver. The linear receivers in this class have the same structure as a RAKE receiver, but the channel matched filter gets replaced by an equalizer filter that is designed to maximize the SINR at the output of the receiver. The complexity of the equalizer filter is variable and can possibly be taken to be as low as in the RAKE receiver (same structure as the channel matched filter), while its adaptation guarantees improved performance with respect to (w.r.t.) the RAKE receiver. Various adaptation strategies and lower complexity structures are considered and compared.

4.1 Performance Criterion Selection

In section 3.3 we mentioned the fact that a natural solution to improve the Zero-Forcing equalizer performance, especially at low input SNR, would be to replace it by a MMSE design. Indeed, when cell-dependent scrambling is added to the orthogonal periodic spreading, then the received signal becomes cyclostationary with chip period (and hence stationary if sampled at chip rate) so that a time-invariant MMSE design becomes well-defined. Now, it may not be obvious a priori that such a MMSE equalizer leads to an optimal overall receiver. Due to the unique scrambler for the intracell users, the intracell interference after descrambling exhibits cyclostationarity with symbol pe-

riod and hence is far from white noise. As a result, the Signal to Interference plus Noise Ratio (SINR) at the output of a RAKE receiver can be far from optimal in the sense that other linear receivers may perform much better. That is the reason of our motivation to chose the SINR as the performance criterion for comparisons between the reference receiver, the RAKE, and other structures.

In this chapter we analyze the SINR at the output of a general linear equalizer and it turns out that the SINR maximizing receiver uses a MMSE equalizer. We call it the max-SINR receiver. The adaptation of the SINR maximizing equalizer receiver can be done in a semi-blind fashion at symbol rate, while requiring the same information (channel estimate) as the RAKE receiver. We consider a wide variety of symbol rate and chip rate adaptation strategies and compare them in simulations. Furthermore we analyse different implementations of the max-SINR receiver, due to the fact that we can impose to the receiver a structure more similar to the RAKE itself, that is a cascade of short FIR filter followed by sparse filter.

4.2 SINR for a General Linear Receiver

For the baseband downlink data model we shall refer to chapter 2, in particular to section 2.4. We recall here that an estimate of the user of interest symbol, with a certain delay of l_1+1 symbol periods, for a general linear receiver $\boldsymbol{f}$ followed by the descrambler and a decorrelator (see the figure in section 2.4.2) is given by

$$\alpha_d \widehat{a}_{1,n-l_1-1} \;=\; \boldsymbol{c}_1^H \, S_{n-l_1-1}^H \mathcal{T}(\boldsymbol{f}) \boldsymbol{Y}_n \;, \tag{4.1}$$

where the received signal $\boldsymbol{Y}_n$ has the structure

$$\boldsymbol{Y}_n = \mathcal{T}(\boldsymbol{h}') \boldsymbol{S}_n \sum_{k=1}^{K} \boldsymbol{C}_k \boldsymbol{A}_{k,n} \; + \boldsymbol{V}_n \;. \tag{4.2}$$

The scrambling diagonal matrix $\boldsymbol{S}_n$, the spreading matrices $\boldsymbol{C}_k$, the symbols matrices $\boldsymbol{A}_{k,n}$, the AWGN vector $\boldsymbol{V}_n$ and the Toeplitz filtering matrices $\mathcal{T}(\bullet)$ are defined in sections 2.2 to 2.4. $\boldsymbol{h}' = [\boldsymbol{h}_0 \cdots \boldsymbol{h}_{N-1}]$ is the first block row (padded with zeros) of the filtering matrix $\mathcal{T}(\boldsymbol{h}')$, $\boldsymbol{h}_l = [h_{1,l} \cdots h_{M,l}]^T$ and M is the oversampling factor at the receiver front-end.

For ease of notation (any other case can easily be handled as well), let's assume here that the filter length (in chips periods) is the same as of the channel, i.e. N chips. The filter-channel cascade results in

$$\mathcal{T}(\boldsymbol{f}) \mathcal{T}(\boldsymbol{h}') = \mathcal{T}(\boldsymbol{\alpha}) = \mathcal{T}(\boldsymbol{\alpha}_d) + \mathcal{T}(\overline{\boldsymbol{\alpha}}_d) \tag{4.3}$$

where in general $d = l_1 L + l_2$ chip periods ($l_1 = \lfloor \frac{d}{L} \rfloor$, $l_2 = d \mod L$); here, because of the same length for the filter with respect to the channel, $d = N$ chip periods and $\alpha_d = \boldsymbol{f}\boldsymbol{h}$ with $\boldsymbol{h} = \left[\boldsymbol{h}_0^T \cdots \boldsymbol{h}_{N-1}^T\right]^T$.

Let $n' = n - l_1 - 1$, $\boldsymbol{\alpha} = \boldsymbol{\alpha}_d + \overline{\boldsymbol{\alpha}}_d$ and $\sigma_k^2 = \mathrm{E}\,|a_{k,n}|^2$, where the user power is incorporated in the symbol constellation scaling. Due to the orthogonality of the codes, we have

$$\boldsymbol{c}_1^H \boldsymbol{S}_{n'}^H \mathcal{T}(\boldsymbol{\alpha}_d) \boldsymbol{S}_n \boldsymbol{C}_k \boldsymbol{A}_{k,n} = \alpha_d \, \delta_{1k} \, a_{k,n'} \tag{4.4}$$

where δ_{ik} is the Kronecker delta. As a result, we can decompose the receiver output $\alpha_d \, \widehat{a}_{1,n'}$ as

$$\alpha_d \, a_{1,n'} + \sum_{k=1}^{K} \boldsymbol{c}_1^H \boldsymbol{S}_{n'}^H \mathcal{T}(\overline{\boldsymbol{\alpha}}_d) \boldsymbol{S}_n \boldsymbol{C}_k \boldsymbol{A}_{k,n} + \boldsymbol{c}_1^H \boldsymbol{S}_{n'}^H \mathcal{T}(\boldsymbol{f}) \boldsymbol{V}_n \ . \tag{4.5}$$

We get for the mean square error of the symbol estimate, $\mathrm{MSE} = \mathrm{E}\,|\alpha_d a_{1,n'} - \alpha_d \widehat{a}_{1,n'}|^2 = |\alpha_d|^2 \, \mathrm{E}\,|a_{1,n'} - \widehat{a}_{1,n'}|^2$,

$$\begin{aligned} \mathrm{MSE} \ &= \boldsymbol{c}_1^H \mathrm{E}\left\{ \boldsymbol{S}_{n'}^H \mathcal{T}(\boldsymbol{f}) \boldsymbol{R}_{VV} \mathcal{T}^H(\boldsymbol{f}) \boldsymbol{S}_{n'} \right\} \boldsymbol{c}_1 + \\ &+ \sum_{k=1}^{K} \sigma_k^2 \, \mathrm{E}\left\{ \boldsymbol{c}_1^H \boldsymbol{S}_{n'}^H \mathcal{T}(\overline{\boldsymbol{\alpha}}_d) \boldsymbol{S}_n \boldsymbol{C}_k \boldsymbol{C}_k^H \boldsymbol{S}_n^H \mathcal{T}^H(\overline{\boldsymbol{\alpha}}_d) \boldsymbol{S}_{n'} \boldsymbol{c}_1 \right\} \end{aligned} \tag{4.6}$$

where $\boldsymbol{R}_{VV} = \mathrm{E}\,\boldsymbol{V}_n \boldsymbol{V}_n^H$ is the noise covariance matrix and the remaining expectation is over the random scrambling sequence.

Due to its i.i.d. character, we get for the noise contribution

$$\boldsymbol{c}_1^H \, \overline{\mathrm{diag}} \left\{ \mathcal{T}(\boldsymbol{f}) \boldsymbol{R}_{VV} \mathcal{T}^H(\boldsymbol{f}) \right\} \boldsymbol{c}_1 = \boldsymbol{f} \, \boldsymbol{R}_{VV} \, \boldsymbol{f}^H$$

where $\overline{\mathrm{diag}}\,\{A\}$ is a diagonal matrix containing the diagonal part of matrix A, and the block Toeplitz $\boldsymbol{R}_{VV}$ (chip rate cyclostationarity) changes dimensions as appropriate.

The interference contribution can be shown (appendix 4.A) to reduce to $\sigma_{tot}^2 \|\overline{\boldsymbol{\alpha}}_d\|^2$ where $\sigma_{tot}^2 = \frac{1}{L} \sum_{k=1}^{K} \sigma_k^2$. Hence, we get for the SINR at the linear receiver output, $\Gamma = \sigma_1^2 |\alpha_d|^2 / \mathrm{MSE}$,

$$\Gamma = \frac{\sigma_1^2 |\alpha_d|^2}{\boldsymbol{f} \boldsymbol{R}_{VV} \boldsymbol{f}^H + \sigma_{tot}^2 \|\overline{\boldsymbol{\alpha}}_d\|^2} = \frac{\sigma_1^2 |\alpha_d|^2}{\boldsymbol{f} \boldsymbol{A} \boldsymbol{f}^H - \sigma_{tot}^2 |\alpha_d|^2} \tag{4.7}$$

where matrix $\boldsymbol{A}$ is defined as

$$\boldsymbol{A} = \boldsymbol{R}_{VV} + \sigma_{tot}^2 \mathcal{T}(\boldsymbol{h}') \mathcal{T}^H(\boldsymbol{h}') \ . \tag{4.8}$$

In the case of the RAKE receiver, $\boldsymbol{f} = \boldsymbol{h}^H$ and the SINR becomes

$$\Gamma_{RAKE} = \frac{\sigma_1^2 \, \|\boldsymbol{h}\|^4}{\boldsymbol{h}^H \boldsymbol{R}_{VV} \boldsymbol{h} + \sigma_{tot}^2 \|\overline{\boldsymbol{\alpha}}_d^{RAKE}\|^2} \tag{4.9}$$

where $\boldsymbol{\alpha}^{RAKE} = \boldsymbol{h}^H \mathcal{T}(\boldsymbol{h}')$, so that $\alpha_d = \boldsymbol{h}^H \boldsymbol{h} = \|\boldsymbol{h}\|^2$. In the ZF equalizer case $\alpha_d^{ZF} = 1$ and $\overline{\boldsymbol{\alpha}}_d^{ZF} = 0$, so that

$$\Gamma_{ZF} = \frac{\sigma_1^2}{\boldsymbol{f}_{ZF} \boldsymbol{R}_{VV} \boldsymbol{f}_{ZF}^H} \tag{4.10}$$

where $\boldsymbol{f}_{ZF} = \boldsymbol{\alpha}_d \left(\mathcal{T}^H(\boldsymbol{h}')\mathcal{T}(\boldsymbol{h}')\right)^{-1} \mathcal{T}^H(\boldsymbol{h}')$ in the oversampling case.

4.3 An unbiased MMSE solution: the max-SINR receiver

The choice for the filter $\boldsymbol{f}$ that leads to maximum receiver output SINR is unique up to a scale factor and can be found as the solution to the following problem

$$\boldsymbol{f}_{MAX} = \arg \max_{\boldsymbol{f}:\boldsymbol{f}\boldsymbol{h}=1} \Gamma = \arg \min_{\boldsymbol{f}:\boldsymbol{f}\boldsymbol{h}=1} \boldsymbol{f}\boldsymbol{A}\boldsymbol{f}^H \,. \tag{4.11}$$

The solution (by Lagrange multiplier) is

$$\boldsymbol{f}_{MAX} = \left(\boldsymbol{h}^H \boldsymbol{A}^{-1} \boldsymbol{h}\right)^{-1} \boldsymbol{h}^H \boldsymbol{A}^{-1} \tag{4.12}$$

and the maximum SINR becomes ($\alpha_d^{MAX} = 1$)

$$\Gamma_{MAX} = \frac{\sigma_1^2}{\left(\boldsymbol{h}^H \boldsymbol{A}^{-1} \boldsymbol{h}\right)^{-1} - \sigma_{tot}^2} \,. \tag{4.13}$$

Due to the stochastic model for the scrambling sequence, the users' chip sequences are independent i.i.d. sequences. As a result, $\boldsymbol{y}_l$ is stationary. Using (4.2) we get for $\boldsymbol{R}_{YY}$

$$\begin{aligned}
\boldsymbol{R}_{YY} &= \boldsymbol{R}_{VV} + \sum_{k=1}^{K} \sigma_k^2 \mathcal{T}(\boldsymbol{h}')\, \mathrm{E}\left\{\boldsymbol{S}_n \boldsymbol{C}_k \boldsymbol{C}_k^H \boldsymbol{S}_n^H\right\} \mathcal{T}^H(\boldsymbol{h}') \\
&= \boldsymbol{R}_{VV} + \sum_{k=1}^{K} \sigma_k^2 \mathcal{T}(\boldsymbol{h}')\, \overline{\mathrm{diag}}\, \left\{\boldsymbol{C}_k \boldsymbol{C}_k^H\right\} \mathcal{T}^H(\boldsymbol{h}') \\
&= \boldsymbol{R}_{VV} + \sum_{k=1}^{K} \sigma_k^2 \mathcal{T}(\boldsymbol{h}')\, \frac{1}{L}\boldsymbol{I}\, \mathcal{T}^H(\boldsymbol{h}') \\
&= \boldsymbol{R}_{VV} + \sigma_{tot}^2 \mathcal{T}(\boldsymbol{h}') \mathcal{T}^H(\boldsymbol{h}') = \boldsymbol{A} \quad !
\end{aligned} \tag{4.14}$$

Consider now the MMSE receiver to estimate linearly the desired user chip sequence $b_{1,l-d}$ from the data Y_l. That MMSE receiver is

$$\widehat{b}_{1,l-d} = \boldsymbol{R}_{b_{1,l-d}Y_l} \boldsymbol{R}_{YY}^{-1} Y_l = \frac{\sigma_1^2}{L} \boldsymbol{h}^H \boldsymbol{R}_{YY}^{-1} Y_l \tag{4.15}$$

which is hence proportional to the filter for the max SINR receiver (see (4.12)). In fact, $\boldsymbol{f}_{MAX}$ is the unbiased MMSE receiver (coefficient of $b_{1,l-d}$ in $\widehat{b}_{1,l-d}$ is 1). Furthermore, the filter $\boldsymbol{f}_{MAX}$ also leads to the unbiased MMSE estimate $\widehat{a}_{1,n-l_1-1}$ at the output of the receiver we are considering. So, this receiver corresponds to the cascade of an (unbiased if $\alpha_d = 1$) MMSE receiver for the desired user's chip sequence, followed by a descrambler and a correlator. In the noiseless case, the MMSE receiver $\boldsymbol{f}_{MAX}$ becomes a ZF equalizer. In fact, the max-SINR receiver is related to the linear MMSE receiver which is

$$\widehat{a}_1 = \boldsymbol{R}_{a_1 Y} \boldsymbol{R}_{YY}^{-1} Y = \sigma_a^2 \boldsymbol{c}_1^H \boldsymbol{S}^H \mathcal{T}^H(\boldsymbol{h}) \boldsymbol{R}_{YY}^{-1} Y \tag{4.16}$$

where we omitted time indices and we assume that the FIR LMMSE is based on a stretch of signal Y. $\boldsymbol{S}$ is a diagonal matrix containing the scrambling sequence over a certain symbol period, $\boldsymbol{R}_{a_1 Y} = \mathrm{E}_{a,v} a_1 Y^H$, $\boldsymbol{R}_{YY} = \mathrm{E}_{a,v} Y Y^H$ where $\mathrm{E}_{a,v}$ denotes expectation over symbols and noise. Due to the scrambling sequence, $\boldsymbol{R}_{YY}$ is time-varying and the whole LMMSE is time-varying. The max-SINR is obtained when $\boldsymbol{R}_{YY}$ is computed using $\mathrm{E}_{a,v,s}$, so by averaging over the scrambler also, considered as an i.i.d. sequence. In that case $\sigma_a^2 \mathcal{T}^H(\boldsymbol{h}) \boldsymbol{R}_{YY}^{-1}$ is of the form $\mathcal{T}(\boldsymbol{f})$ where $\boldsymbol{f}$ is an MMSE (chip rate) equalizer. So the LMMSE receiver becomes a MMSE equalizer-descrambler-correlator cascade.

4.3.1 Max-SINR Parameter Estimation Strategies

Construction from Theoretical Expression and h

Assume that a training signal is available to estimate the channel, so that we consider $\boldsymbol{h}$ to be known. Assume that the noise plus intercell interference is white so that $\boldsymbol{R}_{VV}$ is of the form $\boldsymbol{R}_{VV} = \sigma_v^2 \boldsymbol{I}$. Then the only two parameters we need to estimate (further) in order to be able to construct $\boldsymbol{f}_{MAX}$ are σ_v^2 and σ_{tot}^2. In the case of oversampling we can obtain σ_v^2 and σ_{tot}^2 from

$$\begin{aligned} \sigma_v^2 &= \lambda_{min}(\boldsymbol{R}_{YY}) \\ M\sigma_v^2 + \sigma_{tot}^2 \|\boldsymbol{h}\|^2 &= \mathrm{E}\,\|\boldsymbol{y}_l\|^2 \end{aligned} \tag{4.17}$$

where $\lambda_{min}(.)$ denotes the minimal eigenvalue and note that the signal part of $\boldsymbol{R}_{YY}$ is singular. In practice we estimate the quantities on the right of the equations in (4.17) from data. Although we believe that $\boldsymbol{R}_{VV} = \sigma_v^2 \boldsymbol{I}$ is a good approximation, work on more general noise covariance models is ongoing.

Construction from $\widehat{\boldsymbol{R}}_{YY}$ and $\boldsymbol{h}$

If we again assume that $\boldsymbol{h}$ is available via training data, and we estimate $\boldsymbol{R}_{YY}$, then we can simply construct $\widehat{\boldsymbol{f}}_{MAX} \sim \boldsymbol{h}^H \widehat{\boldsymbol{R}}_{YY}^{-1}$ or this quantity can also be estimated directly (without forming $\widehat{\boldsymbol{R}}_{YY}^{-1}$) via an LMS-like algorithm. Note that Y_l at all chip periods is available for estimating $\boldsymbol{R}_{YY}$ (chip rate cyclostationarity).

Linearly Constrained MOE Approach

Again we assume that $\boldsymbol{h}$ is available via training data. From (4.5) and (4.14), we get for the variance of the receiver output (often mistakenly called output energy)

$$E|\boldsymbol{c}_1^H X_n|^2 = |\alpha_d|^2(\sigma_1^2 - \sigma_{tot}^2) + \boldsymbol{f}\boldsymbol{R}_{YY}\boldsymbol{f}^H \ . \tag{4.18}$$

Hence we can obtain the max SINR receiver filter from the following linearly constrained Minimum Output Energy (MOE) criterion

$$\boldsymbol{f}_{MAX} = \arg \min_{\boldsymbol{f}:\boldsymbol{f}\boldsymbol{h}=1} E|\boldsymbol{c}_1^H X_n|^2 \tag{4.19}$$

in which we replace the statistical average by a temporal average. To obtain a better estimation quality, it would be desirable to be able to perform the temporal averaging at the chip rate. To that end, consider the receiver output at an intermediate chip period

$$\boldsymbol{c}_1^H X_{n,m} = \boldsymbol{c}_1^H \, \boldsymbol{S}_{n',m}^H \mathcal{T}(\boldsymbol{f}) \boldsymbol{Y}_{n,m} \ . \tag{4.20}$$

$\boldsymbol{S}_{n',m} = \text{diag}\{s_{n'+1,m-1}, \ldots, s_{n'+1,0}, s_{n',L-1}, \ldots, s_{n',m}\}$ and $X_{n,m}$ are like $\boldsymbol{S}_{n'}$ and X_n but shifted m chips into the future so that $X_n = X_{n,0}$ and $\boldsymbol{S}_{n'} = \boldsymbol{S}_{n',0}$, and $\boldsymbol{Y}_{n,m} = [\boldsymbol{y}_{nL+l_2-1+m}^T \, \boldsymbol{y}_{nL+l_2-2+m}^T \cdots \boldsymbol{y}_{nL+l_2-P-L+1+m}^T]^T$. With $\mathcal{T}(\boldsymbol{f})\boldsymbol{Y}_{n,m} = \mathcal{Y}_{n,m}\boldsymbol{f}^T$ for a certain structured matrix $\mathcal{Y}_{n,m}$, we can write

$$\begin{aligned} E|\boldsymbol{c}_1^H X_{n,m}|^2 &= \boldsymbol{f}\,\boldsymbol{R}^*\,\boldsymbol{f}^H \\ \text{where} \quad \boldsymbol{R} &= E\{\mathcal{Y}_{n,m}^H \boldsymbol{S}_{n,m}\boldsymbol{c}_1\boldsymbol{c}_1^H\boldsymbol{S}_{n,m}^H\mathcal{Y}_{n,m}\} \end{aligned}$$

so that $\boldsymbol{f} = \left(\boldsymbol{h}^H\boldsymbol{R}^{-*}\boldsymbol{h}\right)^{-1}\boldsymbol{h}^H\boldsymbol{R}^{-*}$. It can be shown that $|\boldsymbol{c}_1^H X_{n,m}|^2 = \boldsymbol{f}\boldsymbol{R}_{VV}\boldsymbol{f}^H + \sigma_{tot}^2\|\overline{\boldsymbol{\alpha}}_d\|^2 + |\alpha_d|^2 f_m$ where $f_m = \sum_{k=1}^K \sigma_k^2 \|\boldsymbol{c}_1^H\mathcal{T}(\boldsymbol{\alpha}_d)\boldsymbol{C}_{k,m}\|^2/|\alpha_d|^2$ and $\boldsymbol{C}_{k,m}$ is like $\boldsymbol{C}_k$ but considered m chips later. So the part of $|\boldsymbol{c}_1^H X_{n,m}|^2$ that varies with m only depends on $\boldsymbol{f}$ through α_d, which is fixed by the linear constraint. So when temporal averaging is performed over all chip periods, the filter estimate $\boldsymbol{f}$ will still converge to $\boldsymbol{f}_{MAX}$. As far as the estimation quality is concerned however, the MSE on the filter estimate is proportional to the excess OE, which in turn is proportional to the MOE. To

lower the MOE at intermediate chip instants, it may be advantageous to consider instead the receiver output $\boldsymbol{c}_{1,m}^H X_{n,m}$ where $\boldsymbol{c}_{1,m} = [c_{1,m-1} \cdots c_{1,0}\, c_{1,L-1} \cdots c_{1,m}]^T$ is $\boldsymbol{c}_1$ shifted cyclically over m chips. In this case $|\alpha_d|^2 f_m = \sum_{k=1}^K \sigma_k^2 \|\boldsymbol{c}_{1,m}^H \mathcal{T}(\boldsymbol{\alpha}_d)\boldsymbol{C}_{k,m}\|^2$ whereas the rest of the OE is unchanged. The receiver output in this case is produced by implementing the despreading like the descrambling (multiplication) followed by a sliding summation over L chips.

Blind Approach Exploiting Unused Codes [34]

Assume that the receiver knows that the codes $[\boldsymbol{c}_{K+1} \cdots \boldsymbol{c}_L] = \boldsymbol{C}^\perp$ are not used. Then we can introduce the following blind (channel knowledge not required) criterion

$$\boldsymbol{f}_B = \arg \min_{\boldsymbol{f}:\|\boldsymbol{f}\|=1} \frac{\mathrm{E}\,\|\boldsymbol{C}^{\perp H} X_n\|^2}{\mathrm{E}\,\|X_n\|^2} \,. \tag{4.21}$$

In [34] it is shown that $\boldsymbol{f}_B = \boldsymbol{f}_{MAX}$. In the numerical examples below, we actually consider the following variation $\boldsymbol{f}_B = \arg\min \frac{\mathrm{E}\,\|\boldsymbol{C}^{\perp H} X_n\|^2}{\mathrm{E}\,\|\boldsymbol{c}_1^H X_n\|^2}$.

4.3.2 Numerical examples

Various simulations with different sets of parameters have been performed. All the K users are considered synchronous and use the same spreading factor. The FIR channel is the convolution of a sparse Vehicular A UMTS channel and a pulse shape (root-raised cosine with roll-off factor of 0.22). The UMTS chip rate (3.84 Mchips/sec) is assumed, leading to the channel length of $N = 19$ chips. An oversampling factor of $M = 2$ is used in these simulations. Two cases of user power distribution are considered: all interferers have the same power and the user of interest has either the same power also or 15dB less power (near-far situation).

The spreading factor (SF) is indicated at the top of the figures, which show the performance of various receiver instances in terms of the output signal-to-interference-and-noise (SINR) ratios versus the SNR at the receiver when the length of all the FIR filters, in chips, is the same ($P = N$). In Figures 4.1-4.3, we compare the theoretical RAKE (dashed), ZF equalizer (dash-dot) and max-SINR (solid) with the estimated max SINR (dotted) obtained via the first of the four methods of section 4.3.1 (using only 5 symbol periods of data!).

Fig. 4.1 refers to a highly loaded system with equal distribution of average power between users, while Fig. 4.2 refers to the same system but with a near-far problem for the user of interest. We can note how the max SINR receiver suffers much less from the near-far effect than the RAKE. In the SNR range of interest, the max SINR receiver

performs between 2dB and 10dB better then the RAKE, while the ZF equalizer suffers a lot from the noise enhancement in that SNR range. It can be noted that the adapted max-SINR receiver has close to optimal performance. Fig. 4.3 presents the same near-far situation but with $L = 128$ and $K = 100$ users; performances are similar.

In the next set of three figures we compare the performances of the three theoretical receivers (RAKE, ZF Equalizer and max-SINR receiver) with three estimated versions of the max-SINR structure: sparse-dots curves refer to the second method of section 4.3.1, dense-dots curves refer to the third method and x's curves refer to the blind method.

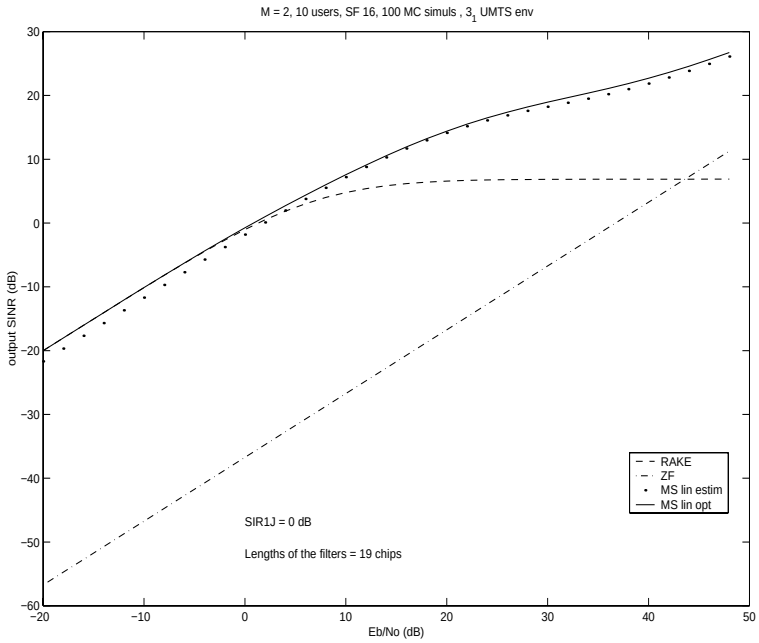

Figure 4.1: Output SINR versus E_b/N_0, high loaded system, Veh environment, spreading factor 16 and equal power distribution

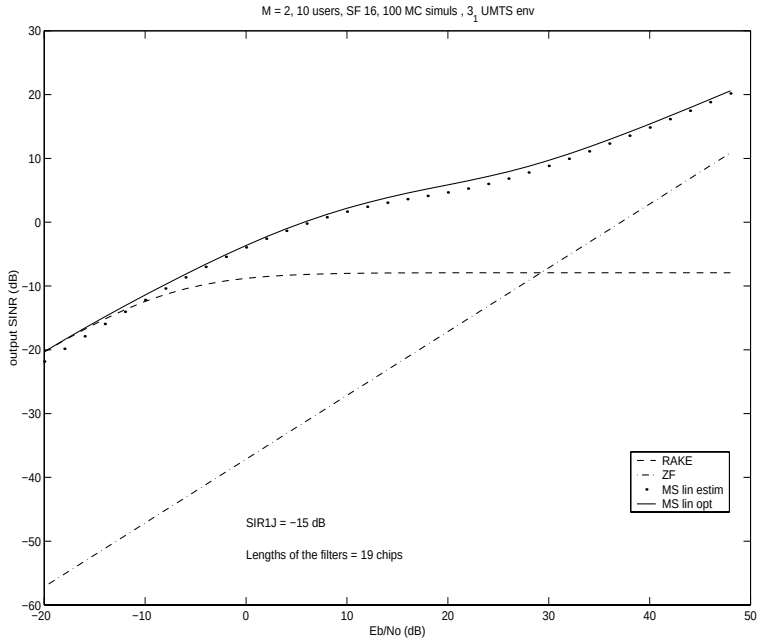

Figure 4.2: Output SINR versus E_b/N_0, high loaded system, Veh environment, spreading factor 16 and near-far situation

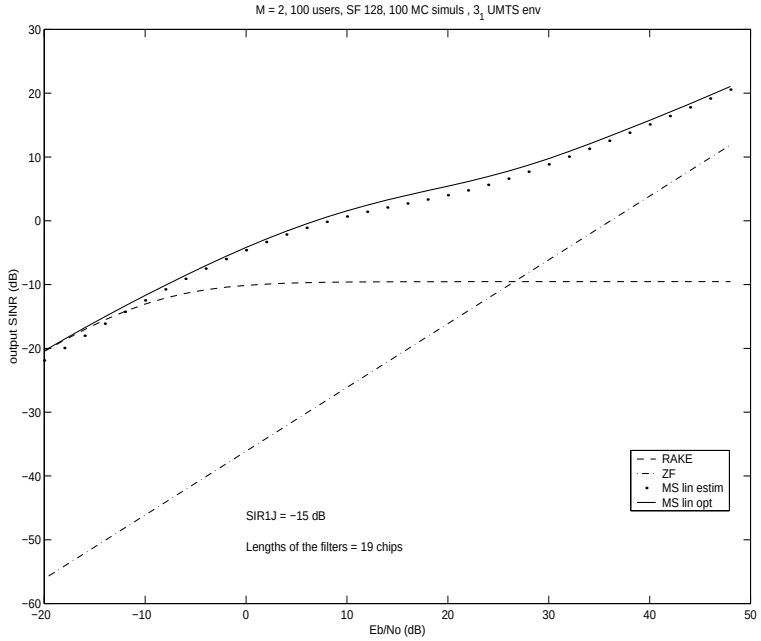

Figure 4.3: Output SINR versus E_b/N_0, high loaded system, Veh environment, spreading factor 128 and near-far situation

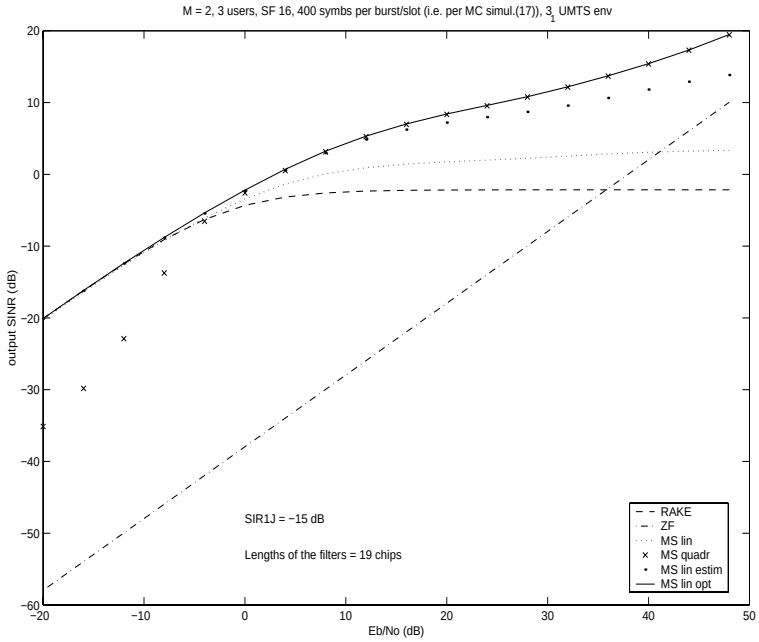

Figure 4.4: Output SINR versus E_b/N_0, high loaded system, Veh environment, spreading factor 16 and equal power distribution

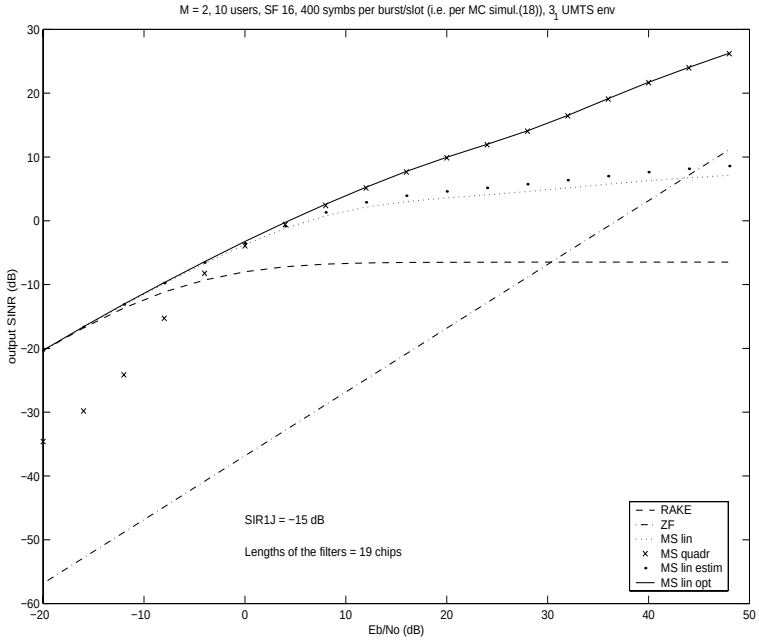

Figure 4.5: Output SINR versus E_b/N_0, high loaded system, Veh environment, spreading factor 16 and near-far situation

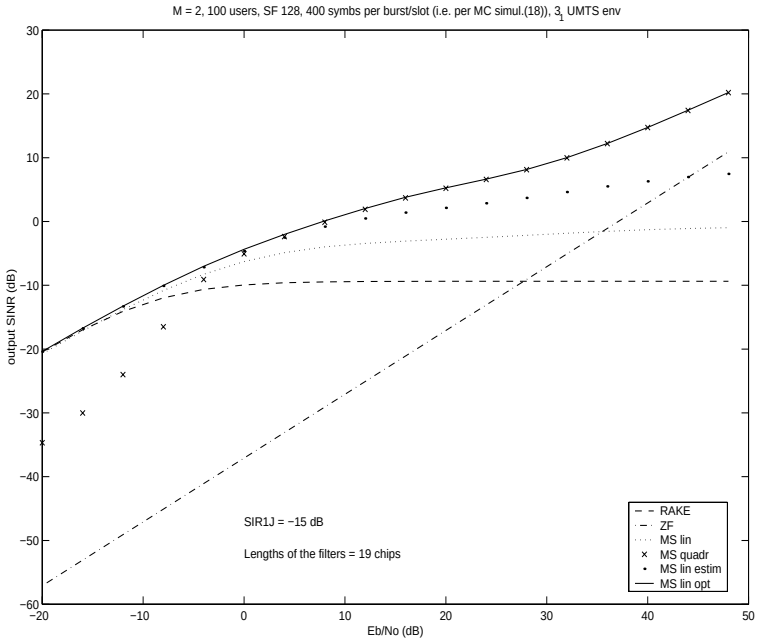

Figure 4.6: Output SINR versus E_b/N_0, high loaded system, Veh environment, spreading factor 128 and near-far situation

4.4 Reduced complexity Max-SINR Receivers

We study different implementation of the max-SINR receiver, analysing their performances with respect to its theoretical expression and to the RAKE receiver. Assume that $\boldsymbol{h}$ is known (via training signal), noise plus intercell interference is white ($\boldsymbol{R}_{VV} = \sigma_v^2 \boldsymbol{I}$) with a known variance σ_v^2 and σ_{tot}^2 is known by construction. The equalizer filter $\boldsymbol{f}_{MAX}$ presented in section 4.3,

$$\boldsymbol{f}_{MAX} = \left(\boldsymbol{h}^H \boldsymbol{R}_{YY}^{-1} \boldsymbol{h}\right)^{-1} \boldsymbol{h}^H \boldsymbol{R}_{YY}^{-1} \ , \tag{4.22}$$

with $\boldsymbol{R}_{YY} = \boldsymbol{R}_{VV} + \sigma_{tot}^2 \mathcal{T}(\boldsymbol{h}')\mathcal{T}^H(\boldsymbol{h}')$, replaces at the same time the pulse shape and the channel matched filters, leaving complete freedom to the optimization process. Other possibilities rise when we want to impose a particular structure to the receiver. For example we force the equalizer to be a cascade of a short FIR (spatio)temporal filter (like a pulse-shape matched filter) and of a sparse (spatio)temporal filter (like the propagation channel matched filter).

4.4.1 Structured Max-SINR Receivers

Root Raised Cosine MF

The pulse shape adopted by the 3G UMTS norm is the root raised cosine (RRC) with roll-off 0.22. If we want to impose match filtering with this pulse shape, what is left to be optimized to maximize the output SINR are the coefficients of the matched filter for the propagation channel. In fact, we can write the overall channel $\boldsymbol{h}$ as

$$\boldsymbol{h} = \boldsymbol{P}\boldsymbol{h}_{prop} = \boldsymbol{P}_{sp}\boldsymbol{g} \tag{4.23}$$

where $\boldsymbol{P}$ is the convolution matrix of the root raised cosine $p(t)$ and $\boldsymbol{h}_{prop}$ is the vector of samples of the multipath propagation channel (MPC). Due to the sparseness of the MPC (train of pulses), $\boldsymbol{P}$ can be reduced to $\boldsymbol{P}_{sp}$ (selected columns) and $\boldsymbol{h}_{prop}$ to $\boldsymbol{g}$ (non-zero coefficients). The receiver filter is then factored into a RRC matched filter (represented by a convolution matrix as $\boldsymbol{P}$ or $\boldsymbol{P}_{sp}$) and an optimized (sparse) filter:

$$\boldsymbol{f} = \boldsymbol{f}_{prop}\boldsymbol{P}^H = \boldsymbol{f}_{sp}\boldsymbol{P}_{sp}^H \tag{4.24}$$

The max-SINR optimization problem in (4.11) gives in this case the following solution:

$$\boldsymbol{f}_{RRC} = \left(\boldsymbol{h}^H \boldsymbol{B} \left(\boldsymbol{B}^H \boldsymbol{R}_{YY} \boldsymbol{B}\right)^{-1} \boldsymbol{B}^H \boldsymbol{h}\right)^{-1} \boldsymbol{h}^H \boldsymbol{B} \left(\boldsymbol{B}^H \boldsymbol{R}_{YY} \boldsymbol{B}\right)^{-1} \boldsymbol{B}^H \tag{4.25}$$

where $\boldsymbol{B}$ can be $\boldsymbol{P}$ or $\boldsymbol{P}_{sp}$. In the latter case, just a number of coefficients corresponding to the number of paths in the MPC get optimized. As we will note in section 4.4.2, optimizing only the non-zero coefficients in the sparse MPC gives only modest gains w.r.t. the RAKE receiver. A better strategy could be the one in which we optimize those coefficients that corresponds to the biggest taps in the MPC, instead of taking as fixed the delays as in 4.25. The number of coefficients can also be augmented w.r.t. the number of paths in the MPC itself. The equation 4.25 is still applicable, but $\boldsymbol{B}$ is replaced by a different optimized convolution matrix P.

Propagation channel MF

Another choice of optimization is the one in which we impose to match filter with the propagation (sparse) channel, but we optimize the pulse shape MF coefficients in order to maximize the output SINR. In this case, the receiver filter is factored into an optimized pulse shape matched filter and a propagation channel matched filter:

$$\boldsymbol{f} = \boldsymbol{h}_{prop}^{H} \boldsymbol{P}_{opt} = \boldsymbol{p}_{opt}^{H} \boldsymbol{T}^{H}(\boldsymbol{h}_{prop}) \tag{4.26}$$

being $\boldsymbol{p}_{opt}$ the optimized finite-length pulse shape (from (4.12)) and $\boldsymbol{T}(\boldsymbol{h}_{prop})$ the convolution matrix of the (sparse) MPC. The max-SINR filter is:

$$\boldsymbol{f}_{h_{prop}} = \left(\boldsymbol{h}^{H} \boldsymbol{T}(\boldsymbol{h}_{prop}) \boldsymbol{B} \boldsymbol{T}^{H}(\boldsymbol{h}_{prop}) \boldsymbol{h}\right)^{-1} \boldsymbol{h}^{H} \boldsymbol{T}(\boldsymbol{h}_{prop}) \boldsymbol{B} \boldsymbol{T}^{H}(\boldsymbol{h}_{prop}) \tag{4.27}$$

where $\boldsymbol{B} = \left(\boldsymbol{T}^{H}(\boldsymbol{h}_{prop}) \boldsymbol{R}_{YY} \boldsymbol{T}(\boldsymbol{h}_{prop})\right)^{-1}$.

4.4.2 Numerical Examples

We evaluate the loss of the structured max-SINR receivers with respect to its theoretical optimal version. A near-far situation for the user of interest (10 dB less power than all other users) is taken into account. In the figures below, “RAKE” refers to the RAKE receiver, “ZF” refers to the ZF equalizer (for the overall channel), and for the max-SINR curves, “theor” refers to the fully optimized max-SINR, “RRC-taps” refers to the RAKE but with the sparse channel coefficients optimized (eq. 4.25), “G-sp” refers to the RAKE but with the pulse shape MF replaced by an optimized filter (eq. 4.27), and “RRC-nx” refer to a receiver filter consisting of the pulse shape MF and a sparse filter with n times more coefficients than the number of paths, in positions corresponding to the positions of the largest coefficients in the overall channel MF. When optimizing filters w.r.t. the RAKE, the lengths of the filters are kept. In Fig. 4.7, the environment is UMTS Indoor B, spreading factor is 16, with 10 users. In Fig. 4.8, the

environment is UMTS Vehicular A, spreading factor is 64, with 10 users. We see that the constrained optimized receivers show saturation, due to the fact that their number of degrees of freedom is not large enough to perform zero-forcing equalization. Nevertheless, in the SNR region of interest (0-20dB), the reduced complexity techniques show useful gains w.r.t. the RAKE receivers.

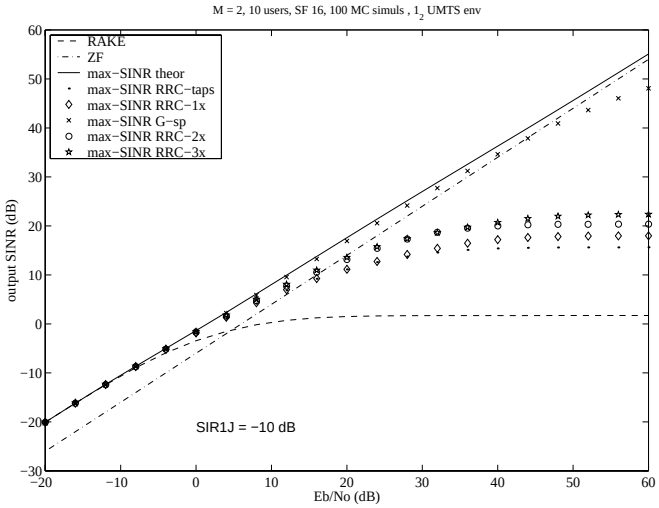

Figure 4.7: Output SINR versus E_b/N_0: Ind B environment, high loaded system, spreading factor 16 and near-far situation

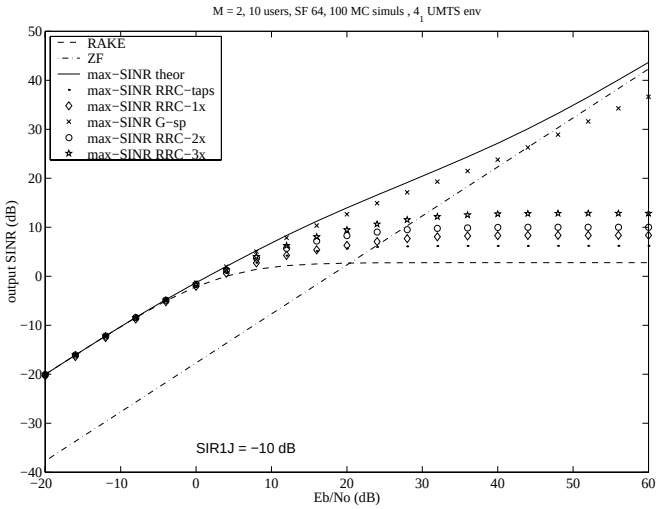

Figure 4.8: Output SINR versus E_b/N_0: Veh environment, medium loaded system, spreading factor 64 and near-far situation

4.5 Multi-sensor Receivers

In the case of a mobile terminal equipped with multiple sensors, the receivers become spatio-temporal receivers (2D). For example, the max-SINR equalizer simply becomes a spatio-temporal MMSE equaliser. The multi-sensor aspect improves the equalization performance and allows to suppress similarly structured intercell interference. In its reduced complexity version, the 2D max-SINR equaliser gets factored (as in the RAKE) into a short FIR filter and a sparse filter that spans the delay spread of the channel. The FIR filter can be spatiotemporal or just temporal. In the latter case, it can be identical or different for the different antennas. The sparse filter is spatiotemporal.

Filtering by the short filter needs to be carried out at chip rate, while filtering with the sparse filter is implemented by combining after the correlator (at symbol rate) as in the RAKE. Various choices are possible for the FIR filter and the sparse filter. These choices lead to a certain SINR at the output of the overall receiver. The maximization of the SINR can be transformed into a quadratic optimization problem subject to a linear constraint. For the FIR filter, the linear constraint is that the inner product with the pulse shape matched filter should be fixed. For the sparse filter, the inner product with the propagation channel matched filter should be fixed. Subject to these constraints, still various choices are possible for the filters.

The adaptation of the SINR maximizing version of the receiver can be done in a semi-blind fashion at symbol rate, while requiring the same information (channel estimate) as the RAKE receiver. The complexity of the receiver gets essentially determined by the choice of either a spatiotemporal or a temporal solution for the FIR filter, by the number of coefficients in the various filters, and by the complexity of the adaptation mechanisms if any parts of the receiver get adapted.

The multiuser baseband downlink data model has been introduced chapter 2, in particular to section 2.4. Being the MS equipped with multiple sensors, we add a superscript j ($j = 1 \cdots J$) to denote the j-th antenna. So, by stacking the M samples per chip period in vectors, we get for the sampled received signal at MS antenna j during chip period l

$$\boldsymbol{y}_l^j = \sum_{k=1}^{K} \sum_{i=0}^{N-1} \boldsymbol{h}_i^j b_{k,l-i} + \boldsymbol{v}_l^j \,, \tag{4.28}$$

where

$$\boldsymbol{y}_l^j = \begin{bmatrix} y_{1,l}^j \\ \vdots \\ y_{M,l}^j \end{bmatrix}, \boldsymbol{h}_l^j = \begin{bmatrix} h_{1,l}^j \\ \vdots \\ h_{M,l}^j \end{bmatrix}, \boldsymbol{v}_l^j = \begin{bmatrix} v_{1,l}^j \\ \vdots \\ v_{M,l}^j \end{bmatrix} \tag{4.29}$$

The overall channel $\boldsymbol{h}^j$ is assumed to have a delay spread of N chips due to contributions from M_p paths. The multipath description of the channel for oversampling phase m at antenna j and during chip period l is

$$h^j_{m,l} = \sum_{p=1}^{M_p} g^j_p \; p(lT_c + \frac{(m-1)T_c}{M} - \tau_p) \tag{4.30}$$

For antenna j, $\{g^j_p\}$ is the complex amplitude of path p with corresponding delay $\{\tau_p\}$ (the delays for a given path are equal for all J MS antennas). In the case of J multiple MS antennas, the total received signal from a BS and the overall channel impulse response during chip period l are

$$\begin{array}{rcl} \boldsymbol{y}_l & = & \left[(\boldsymbol{y}^1_l)^T \cdots (\boldsymbol{y}^J_l)^T\right]^T \\ \boldsymbol{h}_l & = & \left[(\boldsymbol{h}^1_l)^T \cdots (\boldsymbol{h}^J_l)^T\right]^T \; . \end{array} \tag{4.31}$$

The unconstrained max-SINR filter $\boldsymbol{f}_{MAX}$ of equation 4.22 is still valid. Here it becomes simply spatiotemporal and replaces at the same time the temporal pulse-shape matched filter on each antenna and the 2D sparse propagation channel matched filter.

4.5.1 Path-Wise (PW) Receivers

Other possibilities arise when we impose a particular structure on the receiver. We shall here focus on structured equalizers that are the cascade of a short spatiotemporal FIR filter followed by a sparse spatiotemporal filter. The RAKE is a particular instance of this structure, with the FIR filter being the pulse shape matched filter per antenna, and the sparse filter being the 2D matched filter to the 2D sparse propagation channel. We shall here consider several choices for the short FIR filter, with the sparse filter portion being optimized for max SINR. The constrained equalizer structure considered here is depicted in Fig. 4.9: filter $\boldsymbol{f}_l$ gets replaced by a cascade. The resulting receiver structure is depicted in 4.10.

4.5.1.1 Pulse-Shape MF Equalizer

The pulse shape adopted by the 3G UMTS norm is a root raised cosine (RRC) with roll-off 0.22. In a first instance, we shall take the short FIR filter to simply be the pulse shape matched filter, as in the RAKE receiver. However, the sparse filter coefficients are optimized for maximum SINR. This receiver structure was introduced in [35] as the GRAKE and independently in [3]. To analyse this receiver structure, we can write

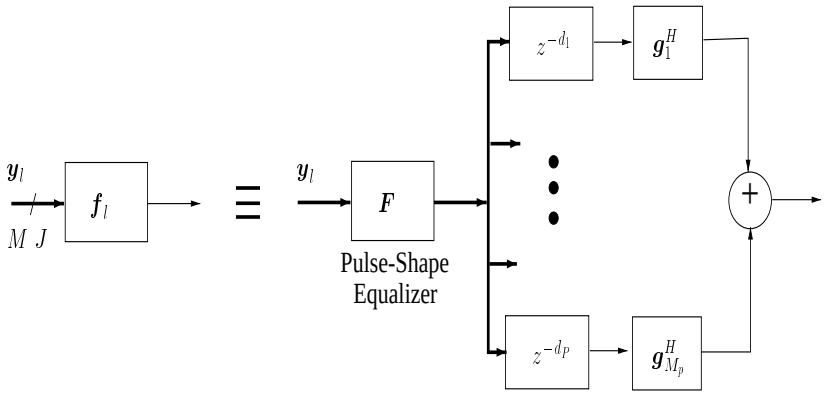

Figure 4.9: The structured equalizer

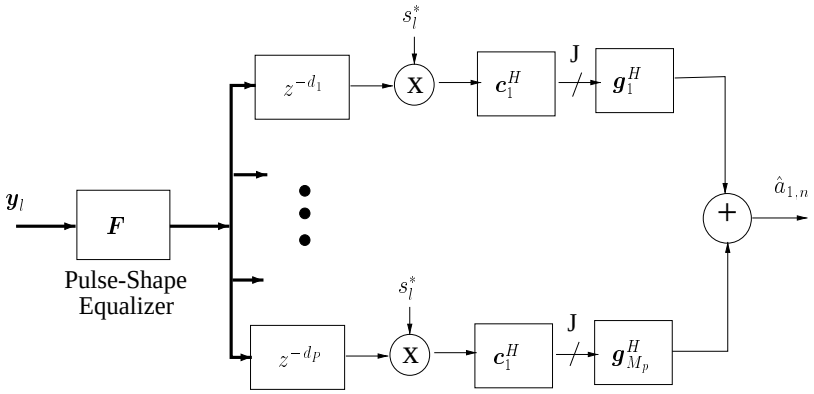

Figure 4.10: The path-wise equalizer RAKE structure

the overall channel $\boldsymbol{h}$ in (4.30) as

$$\boldsymbol{h} = \mathcal{T}(\boldsymbol{p} \otimes \boldsymbol{I}_J)\, \boldsymbol{h}_{prop} = \mathcal{P}_{sp}\boldsymbol{g} \tag{4.32}$$

where $\mathcal{T}(\boldsymbol{p} \otimes \boldsymbol{I}_J)$ is the convolution matrix of the discrete-time root raised cosine $\boldsymbol{p}$ and $\boldsymbol{h}_{prop}$ is the vector of samples of the multipath propagation channel (MPC). Due to the sparseness of the MPC (train of pulses), $\mathcal{T}(\boldsymbol{p} \otimes \boldsymbol{I}_J)$ can be reduced to $\mathcal{P}_{sp}$ (selected columns) and $\boldsymbol{h}_{prop}$ to $\boldsymbol{g}$ (the non-zero coefficients of $\boldsymbol{h}_{prop}$). The receiver filter is then factored into a truncated RRC matched filter (represented by a convolution matrix as $\mathcal{T}(\boldsymbol{p} \otimes \boldsymbol{I}_J)$ or $\mathcal{P}_{sp}$) and an optimized (sparse) filter:

$$\boldsymbol{f} = \boldsymbol{f}_{prop}\, \mathcal{T}^H(\boldsymbol{p} \otimes \boldsymbol{I}_J) = \boldsymbol{f}_{sp}\, \mathcal{P}_{sp}^H\ . \tag{4.33}$$

Optimizing the coefficients of the spatiotemporal (temporally) sparse filter $\boldsymbol{f}_{sp}$ for maximum SINR at the output of the overall receiver, we get for the SINR

$$\Gamma_{GRAKE} = \frac{\sigma_1^2}{\left(\boldsymbol{h}^H \mathcal{P}_{sp}^H \left(\mathcal{P}_{sp}\boldsymbol{R}_{YY}\mathcal{P}_{sp}^H\right)^{-1} \mathcal{P}_{sp}\boldsymbol{h}\right)^{-1} - \sigma_{tot}^2} \tag{4.34}$$

For improved performance, the tap positions in $\boldsymbol{f}_{prop}$ do not necessarily correspond to the taps in the propagation channel $\boldsymbol{h}_{prop}$. Also, increasing the number of taps beyond the number of paths (such that more than one tap per path is available) will obviously improve performance, but at the cost of an increase in complexity. In the GRAKE, the channel impulse response as seen at the input of the sparse filter is the channel impulse response filtered by the pulse shape matched filter, or hence the sparse propagation channel filtered by the pulse shape correlation sequence. The sampled pulse shape correlation sequence would be a delta function if no oversampling would be used. In the case of oversampling however, it contains a number of nonzero samples. Hence, putting more than one tap per finger in the sparse filter of the receiver will improve performance.

4.5.1.2 PW Equalizer

In the unconstrained equalizer-correlator receiver, the optimal equalizer $\boldsymbol{f}_{MAX}$ is essentially a MMSE equalizer $\boldsymbol{h}^H \boldsymbol{R}_{YY}^{-1} = \boldsymbol{h}_{prop}^H \mathcal{T}^H(\boldsymbol{p} \otimes \boldsymbol{I}_J)\, \boldsymbol{R}_{YY}^{-1}$. Hence, a logical choice for the short FIR filter in the path-wise structured equalizer would be a pathwise equalizer, or hence a MMSE pulse shape equalizer (corresponding to $(\boldsymbol{p} \otimes \boldsymbol{I}_J)\, \boldsymbol{R}_{YY}^{-1}$). The resulting receiver is still depicted in Fig. 4.10. One may remark that in that case, the channel as seen at the input of the sparse filter is the cascade of the channel impulse response and the pulse shape equalizer and hence also the cascade of the sparse propagation channel and the equalized pulse shape (cascade of the pulse shape and its MMSE equalizer). This equalized pulse shape should have approximately one significant nonzero coefficient. Hence, the sparse filter with one tap per path appears to be well adapted in this case.

The spatiotemporal FIR MMSE equalizer for the pulse shape is of the form

$$\boldsymbol{F} = (\boldsymbol{p} \otimes \boldsymbol{I}_J)\, \boldsymbol{R}_{YY}^{-1} \tag{4.35}$$

where $\boldsymbol{R}_{YY}$ now is the covariance matrix spanning $2Q+1$ chip periods, and $\boldsymbol{p}$ contains $2Q+1$ blocks of size $M \times M$, that are filled with the M (oversampling) phases of the pulse shape (matched filter) in the time span $(-Q, Q)$ chip periods. The resulting $\boldsymbol{F}$ contains MJ rows, each row corresponding to the pulse shape equalizer for a particular sampling phase and a particular antenna. The receiver filter (overall equalizer) is now again factored into a short FIR filter, being the pulse shape equalizer, and an optimized (sparse) filter:

$$\boldsymbol{f} = \boldsymbol{f}_{prop}\, \mathcal{T}(\boldsymbol{F}) = \boldsymbol{f}_{sp}\, \mathcal{F}_{sp}\ . \tag{4.36}$$

Optimizing the coefficients of the spatiotemporal (temporally) sparse filter $\boldsymbol{f}_{sp}$ for maximum SINR at the output of the overall receiver, we get for the SINR

$$\Gamma_{PWeqRAKE} = \frac{\sigma_1^2}{\left(\boldsymbol{h}^H \mathcal{F}_{sp}^H \left(\mathcal{F}_{sp} \boldsymbol{R}_{YY} \mathcal{F}_{sp}^H\right)^{-1} \mathcal{F}_{sp} \boldsymbol{h}\right)^{-1} - \sigma_{tot}^2} \tag{4.37}$$

4.5.1.3 Averaged PW Equalizer and per-antenna Equalizer

The spatiotemporal MMSE equalization of the pulse shape leads to nonnegligible complexity unless Q is kept very small. To simplify the equalization operation, we can average the RX signal covariance matrix over the antennas to obtain $\overline{\boldsymbol{R}}_{YY}$ with which we construct a temporal pulse shape equalizer

$$\overline{\boldsymbol{F}} = \boldsymbol{p}\, \overline{\boldsymbol{R}}_{YY}^{-1} \ , \tag{4.38}$$

We then apply this temporal equalizer to each antenna signal, hence

$$\boldsymbol{F} \ = \ \overline{\boldsymbol{F}} \otimes \boldsymbol{I}_J \ . \tag{4.39}$$

The SINR for the averaged PW equalizer (APWeqRAKE) can be obtained by substituting in (4.36) and (4.37) the temporal pulse shape equalizer $\boldsymbol{F}$ in (4.39).

An alternative strategy would be to have an optimized temporal equalizer per antenna instead of an averaged one, that is we take

$$\overline{\boldsymbol{F}}_j = \boldsymbol{p}\, \overline{\boldsymbol{R}}_{Y_j Y_j}^{-1} = [\overline{F}_{j,Q} \cdots \overline{F}_{j,-Q}] \tag{4.40}$$

and $\boldsymbol{F} = [\boldsymbol{F}^{(Q)} \cdots \boldsymbol{F}^{(-Q)}]$ where $\boldsymbol{F}^{(q)}$ is constructed from $\{\overline{F}_{j,q}\}_{j=1}^{p}$. The SINR for the per-antenna equalizer (PAEeqRAKE) can be, again, obtained by substituting $\boldsymbol{F}$ in (4.36) and (4.37).

4.5.1.4 Joint Alternating Equalizer

The best structurally constrained receiver can be obtained by optimizing both the FIR and the sparse filters for maximum SINR. This can be done by alternating optimizations. Initializing $\boldsymbol{F}$ as the 2D pulse-shape matched filter, we can indeed optimize the coefficients of the sparse spatiotemporal filter, as in the GRAKE receiver, subject to the linear constraint $\boldsymbol{f}_{sp}\boldsymbol{g} = 1$. Then we can maximize the SINR w.r.t. the FIR filter $\boldsymbol{F}$. We shall take for $\boldsymbol{F}$ a different temporal filter for each antenna (so not a spatiotemporal filter). The constraint on each of these temporal FIR filters (for the different antennas) is that the inner product with the pulse shape matched filter should be one. Then we can reoptimize $\boldsymbol{f}_{sp}$ and so on until convergence. Equations. (4.22) and (4.36)

tell us how to implement each one of these iterations, where firstly $\boldsymbol{f}_{sp}$ and secondly $\boldsymbol{F}$ are optimized. The SINR for the joint-iterative equalizer (JiveRAKE) can be, again, obtained by substituting expressions of $\boldsymbol{f}_{sp}$ and $\boldsymbol{F}$ in (4.36) and using Eq. (4.13) (with $\boldsymbol{A} = \boldsymbol{R}_{YY}$ and $\alpha_d = 1$).

4.5.1.5 Polynomial Expansion Extensions

The work done in [7] (see also [36] for background) allows us to apply the chip-rate Polynomial Expansion (PE) theory to the path-wise receiver structures of previous section. We can write the received chip-rate signal $\boldsymbol{y}_l = \boldsymbol{H}(z)b_l + \boldsymbol{v}_l$, where $\boldsymbol{H}(z)$ is the channel transfer function at chip rate. The equalizer output $\boldsymbol{x}_l = \boldsymbol{F}(z)\boldsymbol{x}_l$ can be rewritten as $\boldsymbol{x}_l = \boldsymbol{D}(z)b_l + \boldsymbol{F}(z)\boldsymbol{v}_l$, where $\boldsymbol{D}(z) = \boldsymbol{F}(z)\boldsymbol{H}(z)$, and an estimate of the user of interest (user 1) symbol can be obtained by $\hat{a}_1(n) = \boldsymbol{c}_1^H \boldsymbol{S}_n^H \boldsymbol{D}^{-1}(z)\boldsymbol{X}_n$, being $\boldsymbol{X}_n$ a concatenation of $\boldsymbol{x}_l$ over a symbol period. Computation of the exact inverse of $\boldsymbol{D}(z)$ would lead to high complexity, so we can approximate it by polynomial expansion, assuming that the main tap ($\alpha_d = \alpha_0 = 1$) of $\boldsymbol{D}(z)$ is dominant in magnitude over all the other taps (close to zero forcing), $\boldsymbol{D}^{-1}(z) = \sum_{i=0}^{\infty} (\boldsymbol{I} - \boldsymbol{D}(z))^i$. As a result, an estimate of the user of interest symbols, at first order polynomial expansion, can be rewritten as $\hat{a}_1(n) = \boldsymbol{c}_1^H \boldsymbol{S}_n^H \bar{\boldsymbol{F}}(z)\boldsymbol{Y}_n$ with $\bar{\boldsymbol{F}}(z) = \boldsymbol{F}(z)\,(2\boldsymbol{I} - \boldsymbol{H}(z)\boldsymbol{F}(z))$. The corresponding implementation is depicted in Fig. 4.11. Both filters $\boldsymbol{f}$'s can be structured and optimized jointly for max SINR. Matrix $\Pi = \boldsymbol{I}$ for chip-rate PE, while for symbol-rate PE $\Pi = \boldsymbol{S}_l^H \boldsymbol{P} \boldsymbol{S}_l$, where S is the scrambler and $\boldsymbol{P}$ projects on the used codes subspace.

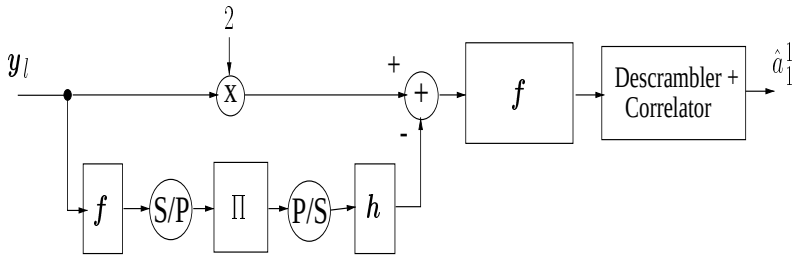

Figure 4.11: Polynomial Expansion structure

4.5.1.6 Numerical Examples

The FIR channel is the convolution of a sparse channel with 4 (environment 3) or 8 taps (environment 6, two separated clusters of 4 taps each) and a pulse shape (root-raised cosine with roll-off factor of 0.22). The UMTS chip rate (3.84 Mchips/sec) is assumed,

leading to a maximum overall channel length of $N = 12$ chips for environment 3 and of $N = 20$ chips for environment 6. An oversampling factor of $M = 2$ or $M = 4$ is used in the simulations and it is indicated in the title of each figure. The spreading factor (SF) is 32 and there are 9 intracell users per active BS. All intracell and intercell interferers have the same power as the user of interest.

The figures show the performance of various receiver instances in terms of the output signal-to-interference-and-noise (SINR) ratios versus the SNR at the receiver when the complexity for all the FIR filters is comparable. In the figure legends, "RAKE" refers to the performance of the RAKE receiver (continuous line), "Unc. max-SINR" to the unconstrained max-SINR receiver of Eq. 4.22 (dashed line), "G-RAKE" to the receiver of section 4.5.1.1 (dotted line), "PWeq-RAKE" to the path-wise equalizer of section 4.5.1.2 (star line), "Avg PWeq-RAKE" and "PAeq-RAKE" to the receivers of section 4.5.1.3 (dashed-dotted and dashed-dotted-diamond lines respectively) and "JIeq-RAKE" to the Joint Iterative receiver of section 4.5.1.4 (dashed-star line).

In the cases of 1 MS antenna and 1 or 2 BS transmitting (Fig. 4.12 and Fig. 4.13), all the path-wise receivers easily outperform the RAKE, with the GRAKE receiver performing generally worse then the other path-wise structures. We can notice that all the considered structures saturate for high input SNR, due to the fact that there are not enough degrees of freedom to obtain complete cancellation of the intracell and/or intercell interference (zero-forcing).

When 2 MS antennas are implemented (Fig. 4.14 and Fig. 4.15), zero-forcing is possible for the unconstrained max-SINR receiver as well as for the JIeqRAKE (the high-SNR zero-forcing asymptote is not visible on the SNR scale of Fig. 4.14). The other receiver structures perform similarly, with the GRAKE being the best. When 3 MS antennas are implemented and 2 BS are transmitting (Fig. 4.16 and Fig. 4.17), we have similar performance for all the receivers.

4.6 Conclusions

We proposed a class of downlink linear receivers that maximize the SINR at their output, possibly keeping the complexity as low as the complexity of the RAKE receiver, from which they take the structure, replacing the channel matched filter by an (cascade of) equalizer optimized for obtaining the maximum output SINR. It turns out that such a SINR maximizing is indeed an MMSE equalizer for the chip sequence of the user of interest. We analysed various implementations of this max-SINR receiver, trying to decrease the complexity given by its theoretical formulation. Therefore we introduced structured max-SINR receivers, by exploiting the nature of the channel seen by

the receiver itself, i.e. the convolution of the radio propagation channel and the pulse shaping filter. We studied as well the possibility for the mobile station to have multiple sensors, which is in its own a better solution to improve intercell interference cancellation, so we introduced various path-wise spatio-temporal equalizers, along which the most promising is the one that alternatingly maximizes the pulse shape equalizer and the radio propagation channel equalizer.

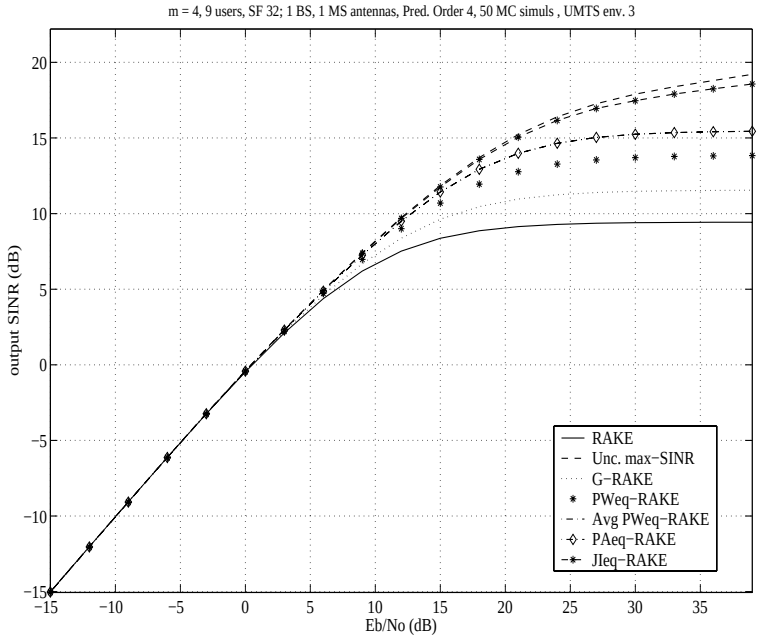

Figure 4.12: Output SINR versus E_b/N_0, 1 MS antenna and 1 transmitting BS

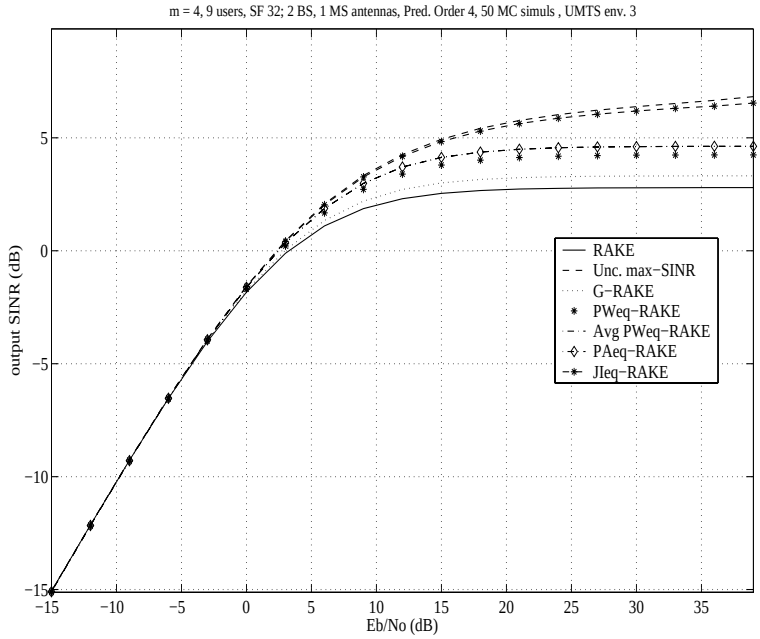

Figure 4.13: Output SINR versus E_b/N_0, 1 MS antenna and 2 transmitting BS

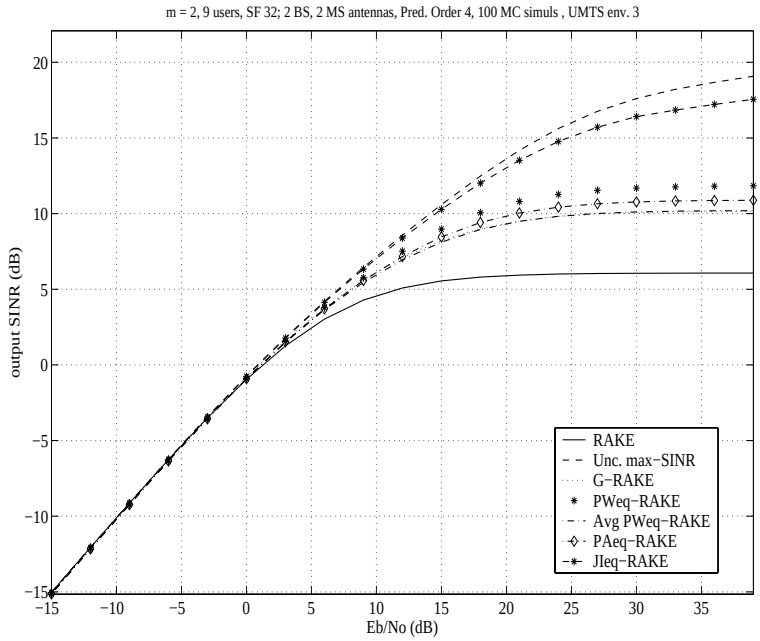

Figure 4.14: Output SINR versus E_b/N_0, 2 MS antenna and 2 transmitting BS

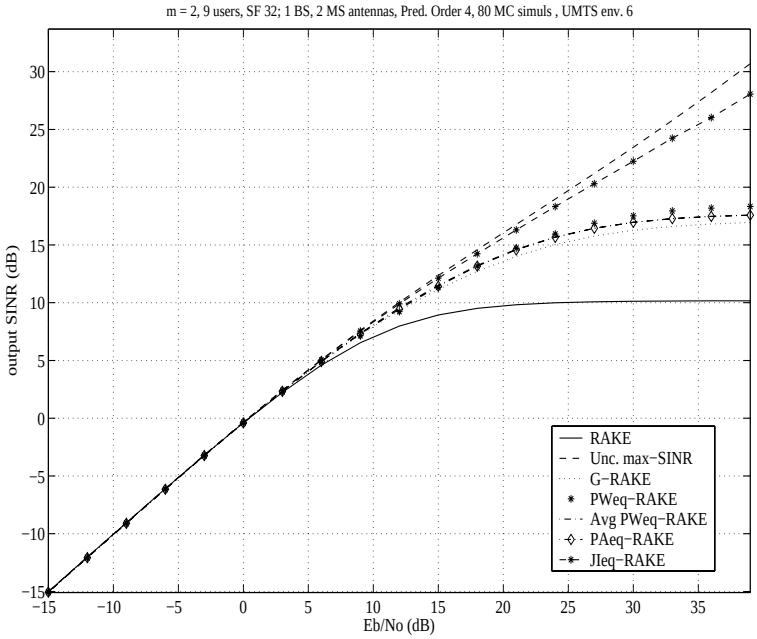

Figure 4.15: Output SINR versus E_b/N_0, 2 MS antenna and 1 transmitting BS

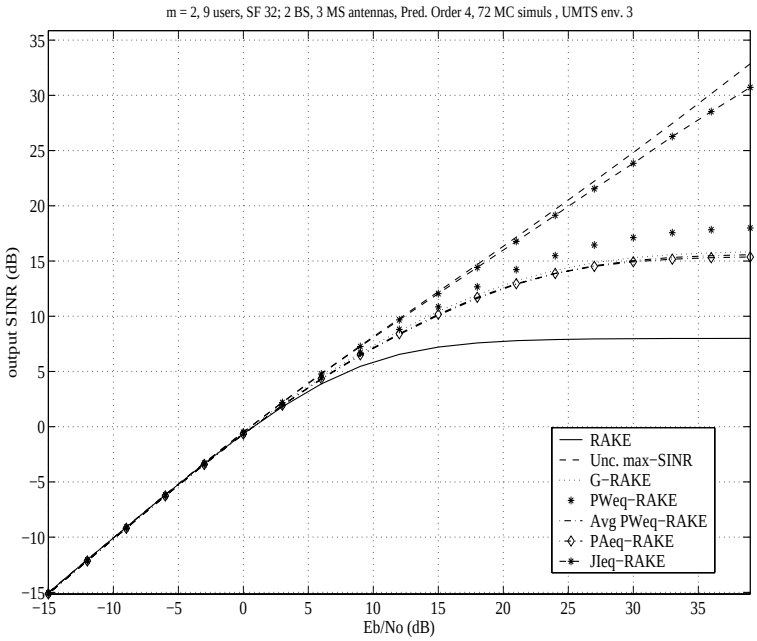

Figure 4.16: Output SINR versus E_b/N_0, 3 MS antenna and 2 transmitting BS

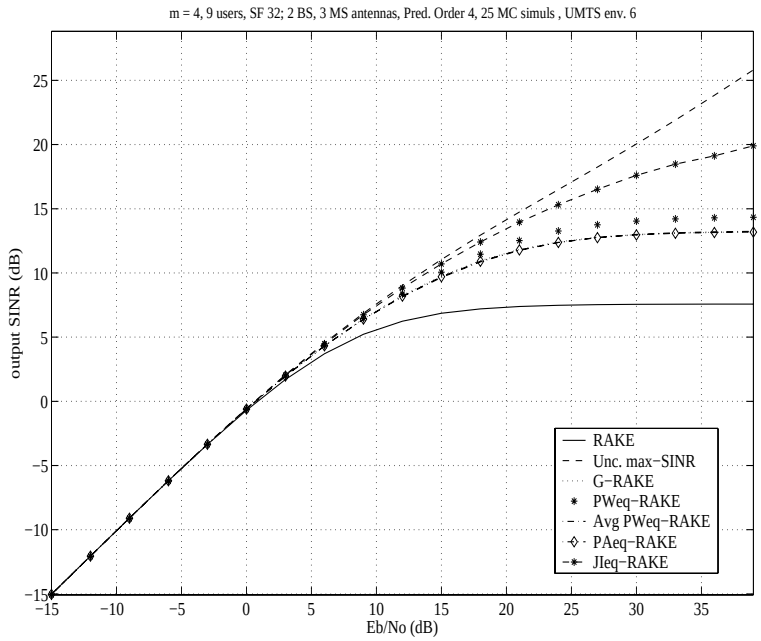

Figure 4.17: Output SINR versus E_b/N_0, 3 MS antenna and 2 transmitting BS

4.A Proof of equation 4.7

We shall analyse the following expression

$$E|\boldsymbol{x}^H \boldsymbol{S}_1^H \boldsymbol{A} \boldsymbol{S}_2 \boldsymbol{y}|^2$$

where, $\boldsymbol{x}$ and $\boldsymbol{y}$ are column vectors (spreading codes), $\boldsymbol{A}$ is a (block) Toeplitz convolution matrix and $\boldsymbol{S}_1$, $\boldsymbol{S}_2$ are diagonal scrambling matrices with $\boldsymbol{S}_1$ contained in $\boldsymbol{S}_2$, so that $s_{2,j} \in \{s_{1,i}\}, j \in I_1$, otherwise $s_{2,j}, j \in I_2 \setminus I_1$; assume furthermore that $|s_{1,i}| = |s_{2,j}| = 1$.

We can then rewrite the above expression as

$$E\left\{ \sum_{i,j} \sum_{k,l} x_i^* s_{1,i}^* A_{i,j} s_{2,j} y_i y_k^* s_{2,k}^* A_{l,k}^* s_{1,l} x_l \right\}$$

and consider the following (j,k) cases:

- $\mathbf{j} \in I_1, k \in I_2 \setminus I_1$: we get $E\{\bullet\} = 0$
- $\mathbf{j} \in I_2 \setminus I_1, k \in I_1$: we get $E\{\bullet\} = 0$
- $\mathbf{j} \in I_2 \setminus I_1, k \in I_2 \setminus I_1$: independency between s_1 and s_2

$$\begin{aligned} \Rightarrow \; E\{\bullet\} &= \sum_{i,j} \sum_{k,l} x_i^* A_{i,j} y_i y_k^* A_{l,k}^* \underbrace{E\{s_{1,i}^* s_{1,l}\}}_{=\delta_{i,l}} \underbrace{E\{s_{2,j} s_{2,k}^*\}}_{=\delta_{j,k}} \\ &= \sum_i \sum_{j \in I_2 \setminus I_1} |x_i^* A_{i,j} y_j|^2 \\ &= \left\| \left(\boldsymbol{A} \begin{bmatrix} \boldsymbol{I} & & \\ & \boldsymbol{0} & \\ & & \boldsymbol{I} \end{bmatrix} \right) \odot \left(\boldsymbol{x}\boldsymbol{y}^H \right)^* \right\|_F^2 \end{aligned}$$

where $\odot$ is the product element-by-element between two matrices.

- $\mathbf{j} \in I_1, k \in I_1$: we have $E\{\bullet\} \neq 0$ only when pair by pair equal indices or when all the 4 indices are equal. Because s is complex, we should associate s and s^*. One contribution ($l = i, k = j \neq i$) is

$$\begin{aligned} E\{\bullet\} &= \sum_i x_i^* A_{i,j} y_j |s_{1,i}|^2 \sum_{j \neq i} y_j^* A_{i,j}^* x_i |s_{2,j}|^2 \\ &= \sum_i \sum_{j \in I_1 \neq i} |x_i^* A_{i,j} y_j|^2 \\ &= \left\| \left(\boldsymbol{A} \begin{bmatrix} \boldsymbol{0} & & \\ & \boldsymbol{I} & \\ & & \boldsymbol{0} \end{bmatrix} - \overline{\text{diag}} \left(\boldsymbol{A} \begin{bmatrix} \boldsymbol{0} & & \\ & \boldsymbol{I} & \\ & & \boldsymbol{0} \end{bmatrix} \right) \right) \odot \left(\boldsymbol{x}\boldsymbol{y}^H \right)^* \right\|_F^2 \end{aligned}$$

where $\overline{\text{diag}}\,\{\boldsymbol{T}\}$ indicates a diagonal matrix containing the diagonal of $\boldsymbol{T}$.

When $l = i = k = j$ we have

$$\begin{aligned} E\{\bullet\} &= \sum_i |x_i^* A_{i,i} y_i|^2 \\ &= \left\| \overline{\text{diag}} \left(\boldsymbol{A} \begin{bmatrix} \boldsymbol{0} & & \\ & \boldsymbol{I} & \\ & & \boldsymbol{0} \end{bmatrix} \right) \odot \left(\boldsymbol{x}\boldsymbol{y}^H\right)^* \right\|_F^2 . \end{aligned}$$

Other contribution ($i = j, k = l \neq i$) is

$$\begin{aligned} E\{\bullet\} &= \sum_i x_i^* A_{i,i} y_i \sum_{l \neq i} x_l A_{l,l}^* y_l^* \\ &= \left| \boldsymbol{x}^H \overline{\text{diag}} \left(\boldsymbol{A} \begin{bmatrix} \boldsymbol{0} & & \\ & \boldsymbol{I} & \\ & & \boldsymbol{0} \end{bmatrix} \right) \boldsymbol{y} \right|^2 - \left\| \overline{\text{diag}} \left(\boldsymbol{A} \begin{bmatrix} \boldsymbol{0} & & \\ & \boldsymbol{I} & \\ & & \boldsymbol{0} \end{bmatrix} \right) \odot \left(\boldsymbol{x}\boldsymbol{y}^H\right)^* \right\|_F^2 \end{aligned}$$

Adding up all the non-zero contribution we can finally rewrite $E|\boldsymbol{x}^H \boldsymbol{S}_1^H \boldsymbol{A} \boldsymbol{S}_2 \boldsymbol{y}|^2$ as

$$\underbrace{\left\| \boldsymbol{A} \odot \left(\boldsymbol{x}\boldsymbol{y}^H\right)^* \right\|_F^2}_{Term\,1} + \underbrace{\left| \boldsymbol{x}^H \overline{\text{diag}} \left(\boldsymbol{A} \begin{bmatrix} \boldsymbol{0} & & \\ & \boldsymbol{I} & \\ & & \boldsymbol{0} \end{bmatrix} \right) \boldsymbol{y} \right|^2}_{Term\,2} - \underbrace{\left\| \overline{\text{diag}} \left(\boldsymbol{A} \begin{bmatrix} \boldsymbol{0} & & \\ & \boldsymbol{I} & \\ & & \boldsymbol{0} \end{bmatrix} \right) \odot \left(\boldsymbol{x}\boldsymbol{y}^H\right)^* \right\|_F^2}_{Term\,3} .$$

We can extend this analysis for the case $\boldsymbol{y} \to \mathcal{Y}$, i.e. $\mathcal{Y}\mathcal{Y}^H = \sum_i \boldsymbol{y}_i \boldsymbol{y}_i^H$. For example we have $Term\,1 = \sum_i \sum_j \sum_k |x_i^* A_{i,j} y_{j,k}|^2$, which becomes

$$\begin{aligned} & \sum_{i,j} x_i^* A_{i,j} \underbrace{\left(\sum_k y_{j,k} y_{j,k}^* \right)}_{\left(\mathcal{Y}\mathcal{Y}^H\right)_{j,j}} A_{i,j}^* x_i \\ = & \sum_{i,j} A_{i,j} \left(\mathcal{Y}\mathcal{Y}^H\right)_{j,j} A_{i,j}^* \left(\boldsymbol{x}\boldsymbol{x}^H\right)_{i,i} \\ = & \sum_{i,j} A_{i,j} \left(\mathcal{Y}\mathcal{Y}^H\right)_{j,j} \left(\boldsymbol{A}^H\right)_{j,i} \left(\boldsymbol{x}\boldsymbol{x}^H\right)_{i,i} \\ = & \sum_{i,j} \left[\boldsymbol{A}\, \overline{\text{diag}}\, \left(\mathcal{Y}\mathcal{Y}^H\right)\right]_{i,j} \left[\boldsymbol{A}^H \overline{\text{diag}}\, \left(\boldsymbol{x}\boldsymbol{x}^H\right)\right]_{j,i} \\ = & Tr\{\boldsymbol{A}\, \overline{\text{diag}}\, \left(\mathcal{Y}\mathcal{Y}^H\right) \boldsymbol{A}^H \overline{\text{diag}}\, \left(\boldsymbol{x}\boldsymbol{x}^H\right)\} \end{aligned}$$

where $Tr\{\bullet\}$ takes the trace of the argument matrix.

$Term\,2$, which can be restated as

$$\sum_k \boldsymbol{x}^H \overline{\text{diag}} \left(\boldsymbol{A} \begin{bmatrix} \boldsymbol{0} & & \\ & \boldsymbol{I} & \\ & & \boldsymbol{0} \end{bmatrix} \right) \boldsymbol{y}_k \boldsymbol{y}_k^H \overline{\text{diag}}^H \left(\boldsymbol{A} \begin{bmatrix} \boldsymbol{0} & & \\ & \boldsymbol{I} & \\ & & \boldsymbol{0} \end{bmatrix} \right) \boldsymbol{x} \ ,$$

becomes

$$\boldsymbol{x}^H \overline{\text{diag}} \left(\boldsymbol{A} \begin{bmatrix} \boldsymbol{0} & & \\ & \boldsymbol{I} & \\ & & \boldsymbol{0} \end{bmatrix} \right) \mathcal{Y}\mathcal{Y}^H \overline{\text{diag}}^H \left(\boldsymbol{A} \begin{bmatrix} \boldsymbol{0} & & \\ & \boldsymbol{I} & \\ & & \boldsymbol{0} \end{bmatrix} \right) \boldsymbol{x} \ .$$

We can rewrite $Term\,3$, that is

$$\sum_i \sum_{j \in I_1} \sum_k x_i^* A_{i,j} y_{j,k} y_{i,k}^* A_{j,i}^* x_j \ ,$$

like

$$\begin{aligned}
& \sum_i \sum_{j \in I_1} x_i^* A_{i,j} \left(\sum_k y_{j,k} y_{i,k}^* \right) A_{j,i}^* x_j \\
= & \sum_i \sum_{j \in I_1} x_i^* A_{i,j} \left(\mathcal{Y}\mathcal{Y}^H \right)_{i,j}^* \left(A_{i,j}^* \right) x_j \\
= & \ \boldsymbol{x}^H \left(\boldsymbol{A} \begin{bmatrix} \boldsymbol{0} & & \\ & \boldsymbol{I} & \\ & & \boldsymbol{0} \end{bmatrix} \odot \left(\mathcal{Y}\mathcal{Y}^H \right)^* \odot \begin{bmatrix} \boldsymbol{0} & & \\ & \boldsymbol{I} & \\ & & \boldsymbol{0} \end{bmatrix} \boldsymbol{A}^H \right) \boldsymbol{x} \\
= & \ Tr \left\{ \overline{\text{diag}} \left(\boldsymbol{A} \begin{bmatrix} \boldsymbol{0} & & \\ & \boldsymbol{I} & \\ & & \boldsymbol{0} \end{bmatrix} \right) \overline{\text{diag}} \left(\mathcal{Y}\mathcal{Y}^H \right) \overline{\text{diag}}^H \left(\boldsymbol{A} \begin{bmatrix} \boldsymbol{0} & & \\ & \boldsymbol{I} & \\ & & \boldsymbol{0} \end{bmatrix} \right) \overline{\text{diag}} \left(\boldsymbol{x}\boldsymbol{x}^H \right) \right\} \ .
\end{aligned}$$

Remembering that $\boldsymbol{\alpha} = \boldsymbol{\alpha}_d + \overline{\boldsymbol{\alpha}}_d$, we can apply the above analysis to our problem of equation 4.6, but considering $\mathcal{T}(\boldsymbol{\alpha})$ instead of $\mathcal{T}(\boldsymbol{\alpha}_d)$ (L is the spreading factor). By setting $\boldsymbol{x} = \boldsymbol{c}_1$, $\boldsymbol{S}_1 = \boldsymbol{S}_{n'}$, $\boldsymbol{A} = \mathcal{T}(\boldsymbol{\alpha})$, $\boldsymbol{S}_2 = \boldsymbol{S}_n$ and $\mathcal{Y} = \boldsymbol{C}_k$, we get

$$\begin{aligned}
& \sum_{k=1}^K \sigma_k^2 \, \text{E} \left\{ \boldsymbol{c}_1^H S_{n'}^H \mathcal{T}(\boldsymbol{\alpha}) \boldsymbol{S}_n \boldsymbol{C}_k \boldsymbol{C}_k^H \boldsymbol{S}_n^H \mathcal{T}^H(\boldsymbol{\alpha}) S_{n'} \boldsymbol{c}_1 \right\} \\
= & \sum_{k=1}^K \sigma_k^2 \left(Term\,1 + Term\,2 + Term\,3 \right) \\
= & \sum_{k=1}^K \sigma_k^2 \frac{L \|\boldsymbol{\alpha}\|^2}{L^2} + \sum_{k=1}^K \sigma_k^2 \underbrace{\|\boldsymbol{c}_1^H \mathcal{T}(\boldsymbol{\alpha}_d) \boldsymbol{C}_k\|^2}_{|\alpha_d|^2 \delta_{1,k}} - \sum_{k=1}^K \frac{\sigma_k^2}{L^2} \underbrace{Tr\{\mathcal{T}(\boldsymbol{\alpha}_d) \mathcal{T}^H(\boldsymbol{\alpha}_d)\}}_{|\alpha_d|^2 L} \\
= & \sum_{k=1}^K \frac{\sigma_k^2}{L} \|\overline{\boldsymbol{\alpha}}_d\|^2 + \sigma_1^2 |\alpha_d|^2
\end{aligned}$$

where the first term in the last equality is the multiple access interference (intracell) and second term is the signal of interest energy (numerator of the SINR).

Chapter 5

Intercell Interference Cancellation and Transmit Diversity

In this chapter we discuss the exploitation of the unused codes of a CDMA system at the mobile station for intercell interference cancellation. Furthermore, we analyse the use of three different Transmission Diversity (TD) schemes, namely Space-Time TD (STTD), Orthogonal TD (OTD) and Delay TD (DTD). All of them are compared for the two receiver structures: RAKE and max-SINR receivers.

5.1 Exploiting Excess Codes for IIC

The deployment of third generation CDMA-based wireless systems foresees a loading fraction that is smaller than one, i.e. the number of users per cell is scheduled to be significantly less than the spreading factor to attain an acceptable performance. This means that a base station can set apart a subset of the codes, the excess codes, that it will not use. In the case of periodic codes (such as in the TDD mode of UMTS), the existence of excess codes implies the existence of a noise subspace, which can be used to cancel the interference coming from a neighboring base station. We introduce a SINR maximizing linear receiver to perform this interference reduction. In the case of aperiodic codes (such as in the FDD mode of UMTS), the noise subspace is time-varying.

In this case, we introduce structured receivers that combine scrambling and descrambling operations with projections on code subspaces and linear time-invariant filters for equalization, interference cancellation and multipath combining. So the time-varying part of these receivers is limited to (de-)scrambling operations.

5.1.1 Linear Receivers and Hybrid Solutions

Fig. 5.1 shows the downlink signal model in baseband. For each base station j, $j = 1, 2$, the K^j users are assumed to transmit linearly modulated signals over the same linear multipath channel $h^j(t)$; the BS 2 is considered the interfering one. Additive noise $v(t)$ is then included in the received signal $y(t)$.

The symbol and chip periods T and T_c are related through the spreading factor L: $T = LT_c$, which is assumed here to be common for all the users and for the two base stations. The total chip sequences b_l^j are the sum of the chip sequences of all the users for each BS j. Every user chip sequence is given by the product between the n-th symbol of the k-th user and an aperiodic spreading sequence $w_{k,l}^j$ which is itself the product of a periodic Walsh-Hadamard (with unit energy) spreading sequence $\boldsymbol{c}_k^j = \left[\boldsymbol{c}_{k,0}^j\, \boldsymbol{c}_{k,1}^j\, \cdots\, \boldsymbol{c}_{k,L-1}^j\right]^T$, and a base-station specific unit magnitude complex scrambling sequence s_l^j with zero mean and variance 1, $w_{k,l}^j = c_{k,l \bmod L}^j s_l^j$:

$$b_l^j = \sum_{k=1}^{K^j} b_{k,l}^j = \sum_{k=1}^{K^j} a_{k,\lfloor \frac{l}{L} \rfloor}^j w_{k,l}^j \qquad j = 1, 2\ . \tag{5.1}$$

The scrambling operation is a multiplication of chip rate sequences. The spreading operation is represented by a filtering of an upsampled symbol sequence with the spreading sequence as impulse response. The chip sequences $b_l^{1,2}$ get transformed into a continuous-time signals by filtering them with the pulse shape $p(t)$ and then pass through the multipath propagation channels $h^1(t)$ and $h^2(t)$ (from BS 1 and from BS 2 to the mobile station respectively) to yield the total received signal $y(t)$. The receiver samples M times per chip the lowpass filtered received signal. Stacking the M samples per chip period in vectors, we get for the sampled received signal

$$\boldsymbol{y}_l = \boldsymbol{y}_l^1 + \boldsymbol{y}_l^2 + \boldsymbol{v}_l, \quad \boldsymbol{y}_l^j = \sum_{k=1}^{K^j} \sum_{i=0}^{N-1} \boldsymbol{h}_i^j b_{k,l-i}^j \quad j = 1, 2 \tag{5.2}$$

where

$$\boldsymbol{y}_l^j = \begin{bmatrix} y_{1,l}^j \\ \vdots \\ y_{M,l}^j \end{bmatrix}, \boldsymbol{h}_l^j = \begin{bmatrix} h_{1,l}^j \\ \vdots \\ h_{M,l}^j \end{bmatrix}, \boldsymbol{v}_l = \begin{bmatrix} v_{1,l} \\ \vdots \\ v_{M,l} \end{bmatrix}\ . \tag{5.3}$$

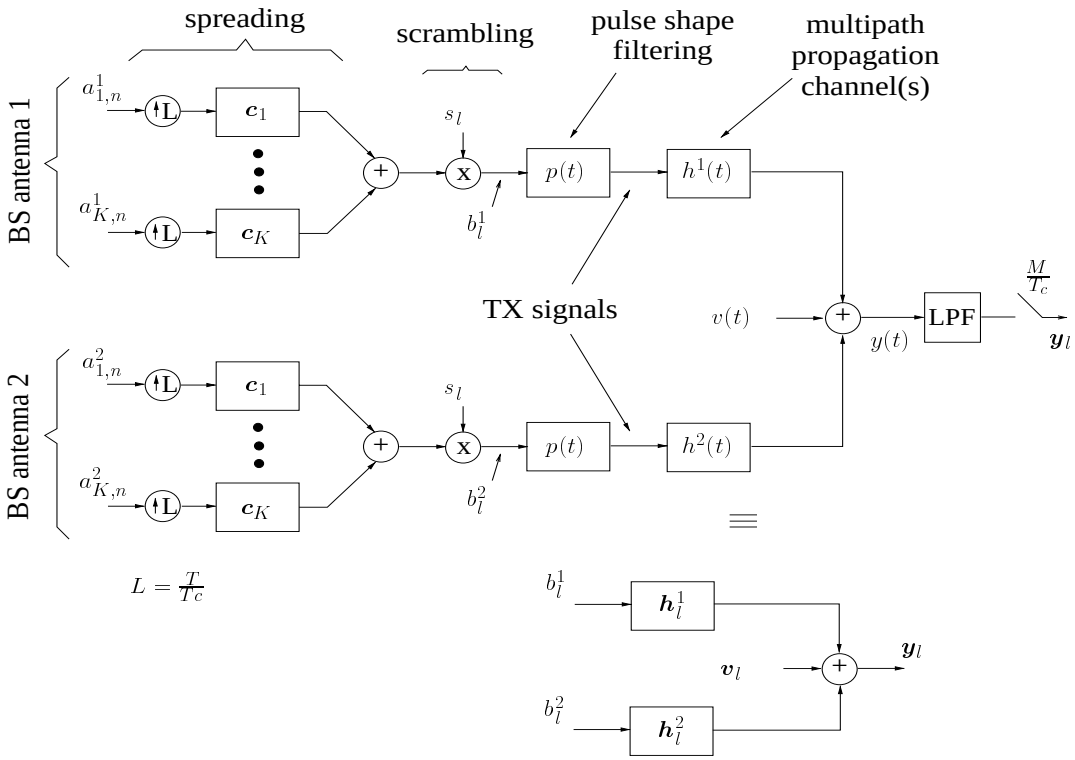

Figure 5.1: Downlink signal model for Intercell Interference Cancellation (IIC)

Here $\boldsymbol{h}_l^j$ represents the vectorized samples of the overall channel $h^j(t)$, including pulse shape, propagation channel and receiver filter. The overall channels $h^j(t)$ are assumed to have the same delay spread of N chips.

In the case where the scrambling sequence is aperiodic and where we model it and the symbol sequences as independent i.i.d. sequences, then the chip sequences $b_l^{1,2}$ are sums of independent white noises (chip rate i.i.d. sequences, hence stationary) and hence are white noises. The intracell contribution to $\boldsymbol{y}_l$ then is a stationary (vector) process (the continuous-time counterpart is cyclostationary with chip period). The intercell interference is a sum of contributions that are of the same form as the intracell contribution so its contribution to $\boldsymbol{y}_l$ is also a stationary vector process. The remaining noise is assumed to be white stationary noise. Hence the sum of intercell interference and noise, $\boldsymbol{v}_l$, is stationary.

When the scrambling sequence is periodic with (symbol) period T, the chip sequences $b_l^{1,2}$ are stationary (vector) processes with symbol period; the intracell contribution to $\boldsymbol{y}_l$ is then also stationary with symbol period. The intercell contribution is again of the same form of the intracell interference (while the noise stays white stationary), so that the received signal is cyclostationary with symbol period.

Linear Structures

Fig. 5.2 shows a linear receiver in which a descrambler and a correlator follow a general FIR filter $\boldsymbol{f}_l$ whose input is at sampling rate and its output is at chip rate. In the

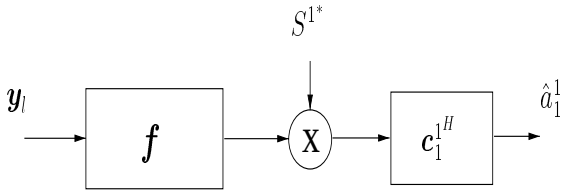

Figure 5.2: General Linear Receiver for IIC

case of a RAKE receiver implementation, $\boldsymbol{f}$ is a channel matched filter $\boldsymbol{h}^{1^H}$ which is equivalent to consider the BS 2 as an additive noise and to maximize the SNR at the filter output. To maximize the SINR at the receiver output while taking into account the intracell interference, the filter $\boldsymbol{f}$ can be adapted to be the Max-SINR filter (see [1]). These two approaches are well suitable for a system with one BS, but they are here used for comparison with other structures designed to take better into account the presence of an interfering base station (see next sections).

Hybrid Structures

Fig. 5.3 shows one instance of an hybrid structure where an Interference Cancellation (IC) Branch precedes a linear receiver as in Fig. 5.2. The IC branch is formed by an equalizer, a descrambler, a projector, a scrambler and a filter; different implementation are possible and are presented in the following subsections. This approach is conceived to perform intracell or intercell interference cancellation in order to improve the performances of the linear receivers presented above by exploiting the structure of the received signal itself (the IC branch is indeed equivalent to a time-variant filter).

Structure 1 Here the base station 1 is considered in the IC branch and intracell interference cancellation is performed by reconstructing the orthogonality between user codes of BS 1 after the equalizer and projecting this signal into the subspace of the used spreading codes, but the user of interest. Then, by "re-channelling" the scrambler output, the intracell interference can be subtracted from the received signal $\boldsymbol{y}_l$ and is possible to apply a RAKE receiver. This structure allows also to decrease the intercell interference plus noise because the projector output space include both of them. The equalizer could be either a Zero-Forcing (ZF) or a Minimum Mean Square Error (MMSE) equalizer: the former enhances the intercell interference plus noise but re-

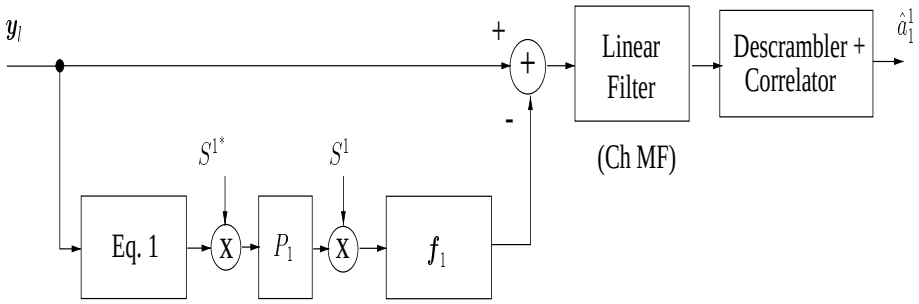

Figure 5.3: Hybrid Structure 1 for IIC

stores the orthogonality, while the latter perturbs the structure of the signal received from the BS 1 but does not increase so much the intercell interference plus noise. The "re-channelling" filter could either be the channel $\boldsymbol{h}^1$ or a filter adapted to minimize the intercell interference plus noise variance. We can guess that when a ZF equalizer is used, this adaptation works better than in using a MMSE equalizer because in the first case the intercell interference plus noise is more important.

Structure 2 In this structure, the BS 2 is considered in the IC branch; the equal-

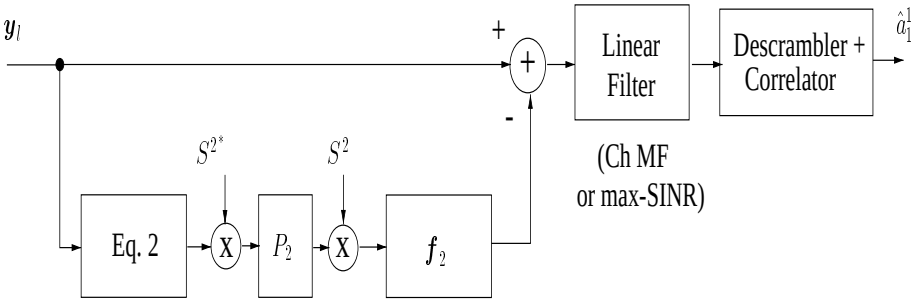

Figure 5.4: Hybrid Structure 2 for IIC

izer and the "re-channelling" filter can again be described as for Structure 1 above, but the projection is into the complete subspace of used spreading codes of BS 2. In this approach it is possible to implement either a RAKE receiver or a max-SINR receiver after the subtractor, being the latter conceivable due to the absence of the signal from BS 2 in the subtractor output signal.

Structure 3 This structure combines the single-branch approaches of previous subsections. The equalizers and the projections are defined as before, while the two filters $\boldsymbol{f}_1$ and $\boldsymbol{f}_2$ can be equal to the corresponding BS channels $\boldsymbol{h}^1$ and $\boldsymbol{h}^2$ or jointly adapted to have minimum interference plus noise variance at the subtractor output.

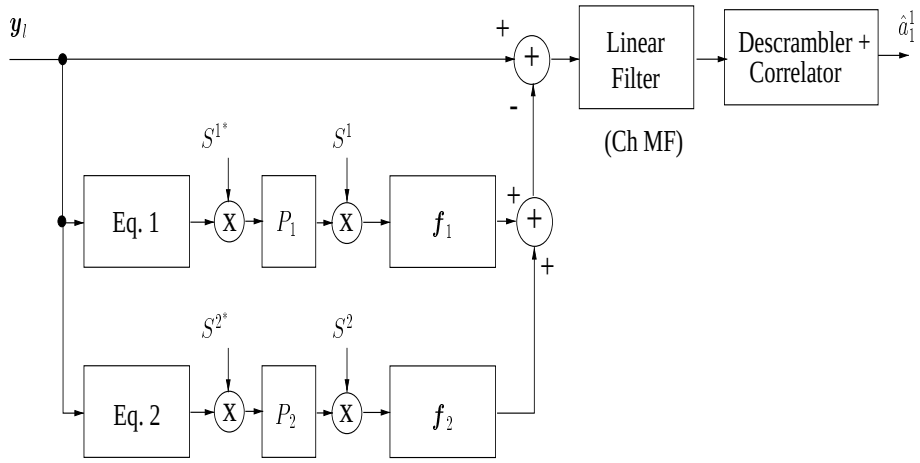

Figure 5.5: Hybrid Structure with two IC branches

The linear receiver after the subtractor can be in this case just a RAKE receiver, due to the simultaneous cancellation of intracell and intercell interference.

5.1.1.1 Numerical Examples

Fig. 5.6 to Fig. 5.14 present some of the simulations that we have performed to evaluate the various structures. In the legends of these figures, MS refer to max-SINR receiver. The K^j users of base station j are considered synchronous between them and with the users of the other BS, with the same spreading factor $L = 32$ and using the same downlink channel $\boldsymbol{h}^j$ which is a FIR filter, convolution of a sparse Vehicular A UMTS channel and a pulse shape (root-raised cosine with roll-off factor of 0.22). The channel length is $N = 19$ chips, due to the UMTS chip rate of 3.84 Mchips/sec. An oversampling factor of $M = 2$ is assumed. Two possible user power distributions are simulated: all interferers (intracell and intercell) have the same power and the user of interest has either the same power also or 10dB less power (near-far situation). Two possible base-station dependent scrambling sequences are simulated: aperiodic and periodic (with symbol period) scrambling. Every simulation gives 10 curves: the first two in the legend represent the linear structures, the simple RAKE and the max-SINR receivers; the third to the sixth in the legend are referring to the structures in which the "re-channelling" filters are the channels themselves, $\boldsymbol{f}_j = \boldsymbol{h}^j$ $j = 1, 2$, while the last four in the legend are the same structures but with $\boldsymbol{f}_j$ optimized to minimize the intercell interference plus noise variance at the subtractor output. The names in the legend "Si-x-RAKE" or "Si-x-MS" refer to the structure i with "re-channelling" filter x (channel or optimized filter) and output linear filter RAKE or max-SINR. In the case of structure 3 H refers to the use of the two channels $\boldsymbol{h}^1$ and $\boldsymbol{h}^2$ and F to the use of the

jointly optimized filters $\boldsymbol{f}_1$ and $\boldsymbol{f}_2$.

The first two figures, Fig. 5.6 and Fig. 5.7, show the performances in implementing respectively a ZF equalizer or a MMSE equalizer in the IC branches. We can well see how the MMSE versions work much better than the ZF ones. In Fig. 5.7, all the curves are above the simple RAKE curve. Another remark is that when a MMSE equalizer is implemented, the optimization of the filters $\boldsymbol{f}_j$ is practically not necessary, which is not the case of ZF equalizers (as we stated for structure 1). So the following figures for aperiodic scrambling are always supposing the use of MMSE equalizers and in this case the hybrid structure 3 works always much better than all the other structures. Fig. 5.8 confirms even more this result showing the case of near-far situation for the user of interest; the hybrid structure 3 is the best one on all the range of interest for E_b/N_0.

Fig. 5.9 and Fig. 5.10 show that all the structures are sensitive to the number of users in the system, but again the structure 3 is better because is less sensitive, especially in the case of optimization of the "re-channelling" filters.

Fig. 5.11 to Fig. 5.14 present the case when the scrambling for the two base stations is periodic with symbol period. In all simulations the simple max-SINR receiver ([1]) is performing the best for all E_b/N_0. All the hybrid solutions show a saturation for high E_b/N_0, but the optimized (in terms of $\boldsymbol{f}_j$) hybrid structures 3 and 2 seem to perform better than the other hybrid structures. In these simulations we used ZF equalizations in the IC branches because a MMSE equalization is here (periodic scrambling) not conceivable, due to the fact that the signals are not anymore cyclostationary with chip period but they are cyclostationary with symbol period.

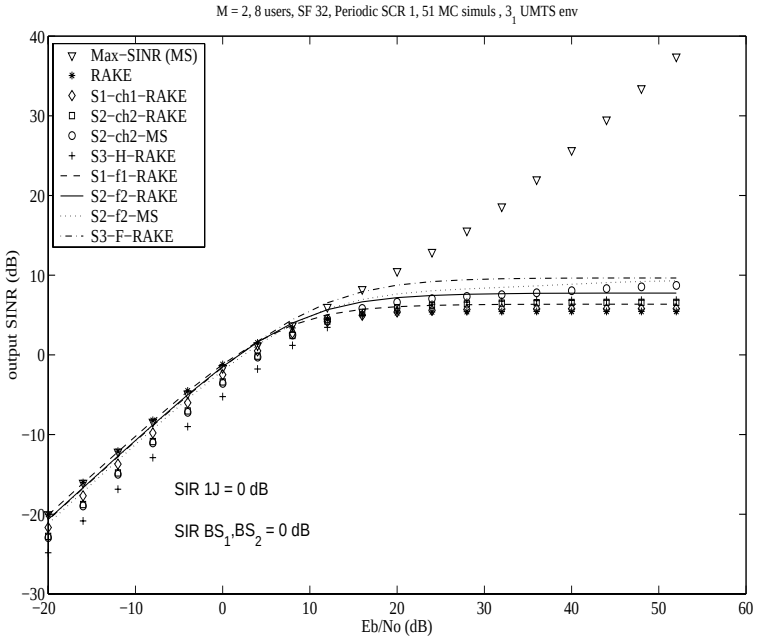

Figure 5.6: Output SINR versus E_b/N_0, 25% loaded BSs, spreading factor 32 and equal power distribution, aperiodic scrambling, ZF equalizers

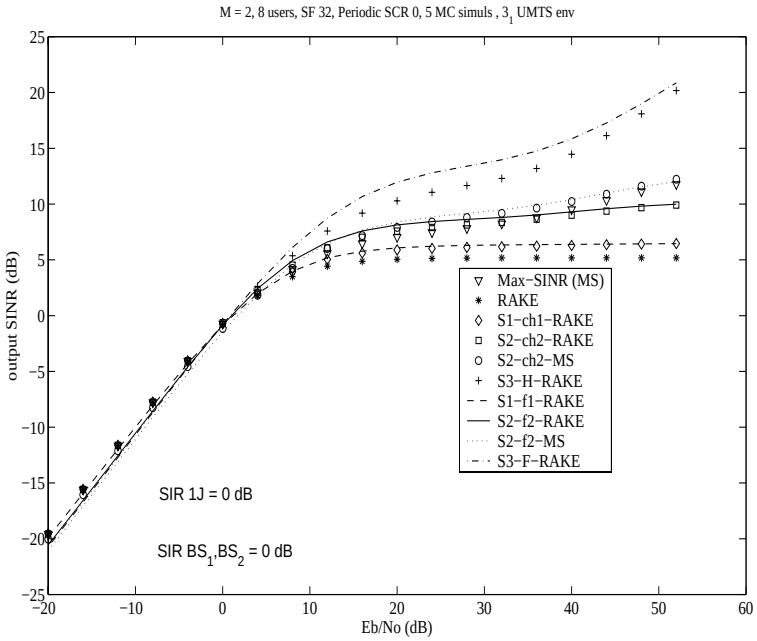

Figure 5.7: Output SINR versus E_b/N_0, 25% loaded BSs, spreading factor 32 and equal power distribution, aperiodic scrambling, MMSE equalizers

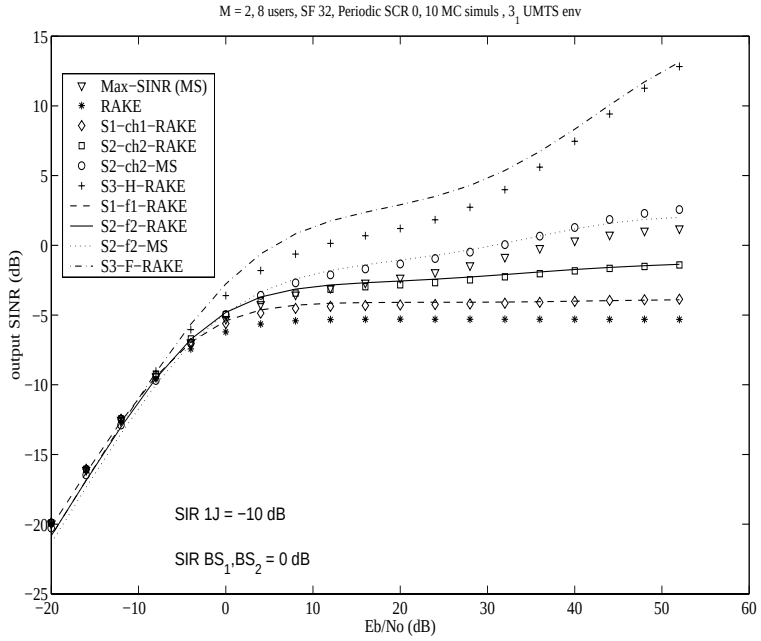

Figure 5.8: Output SINR versus E_b/N_0, 25% loaded BSs, spreading factor 32 and near-far situation, aperiodic scrambling, MMSE equalizers

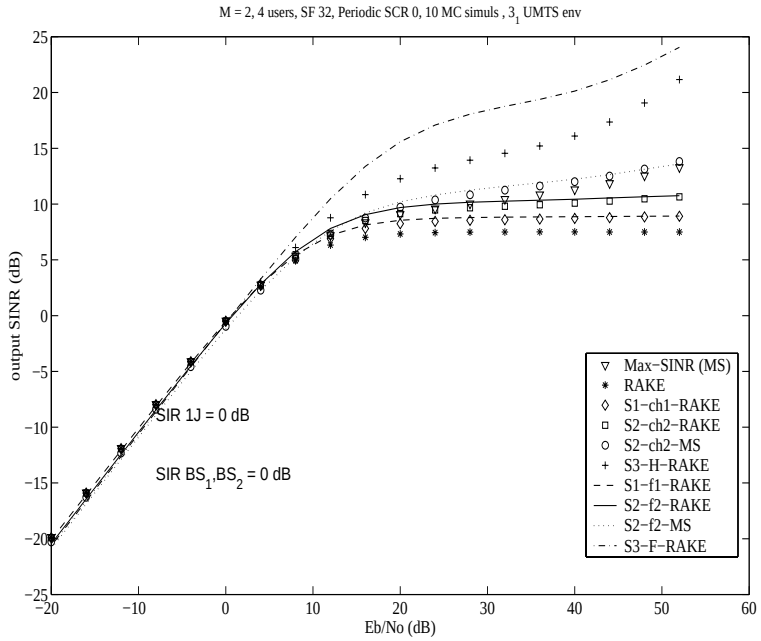

Figure 5.9: Output SINR versus E_b/N_0, 12.5% loaded BSs, spreading factor 32 and equal power distribution, aperiodic scrambling, MMSE equalizers

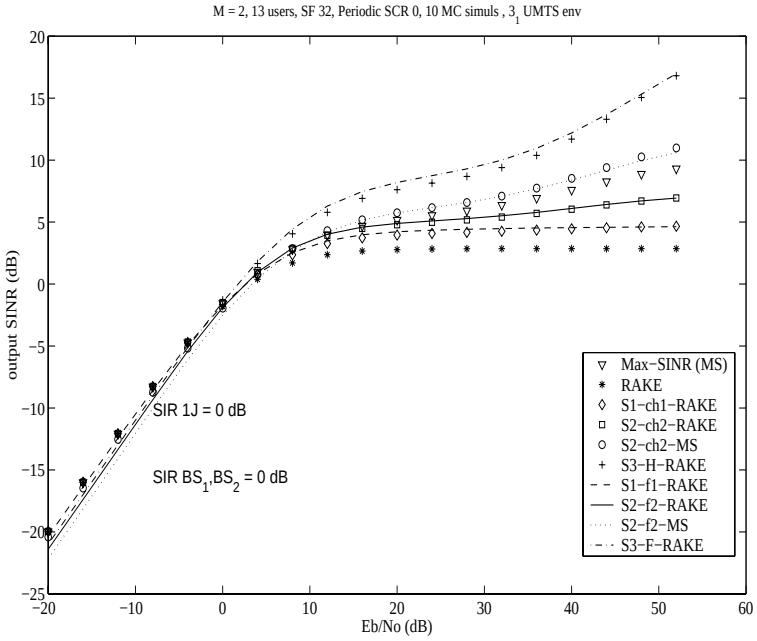

Figure 5.10: Output SINR versus E_b/N_0, 40.6% loaded BSs, spreading factor 32 and equal power distribution, aperiodic scrambling, MMSE equalizers

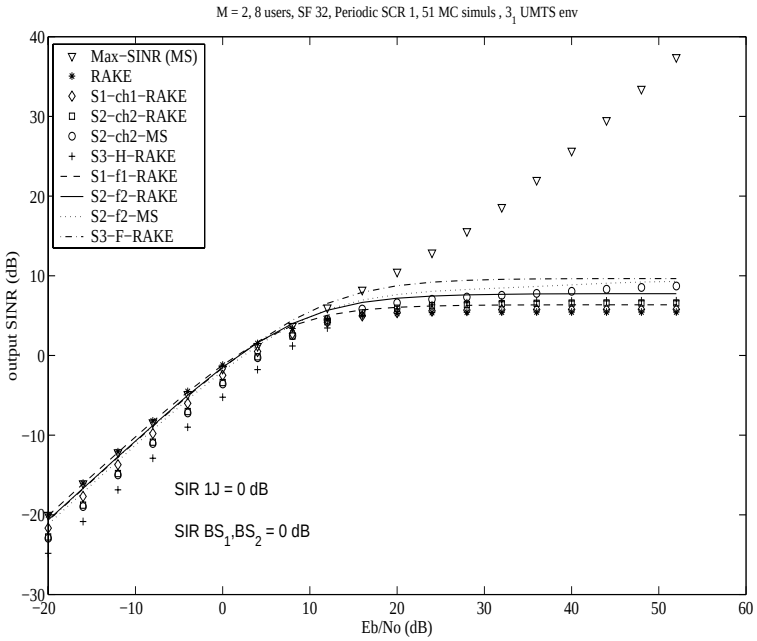

Figure 5.11: Output SINR versus E_b/N_0, 25% loaded BSs, spreading factor 32 and equal power distribution, periodic scrambling, ZF equalizers

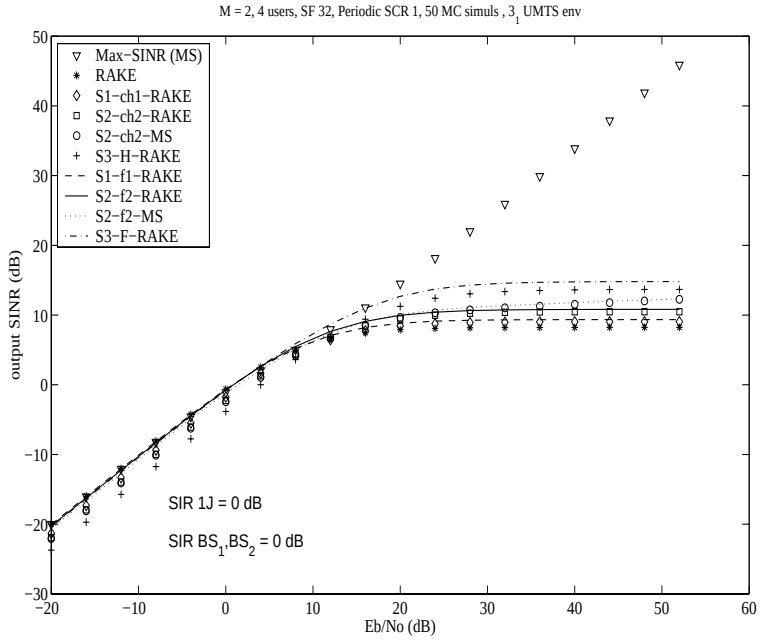

Figure 5.12: Output SINR versus E_b/N_0, 12.5% loaded BSs, spreading factor 32 and equal power distribution, periodic scrambling, ZF equalizers

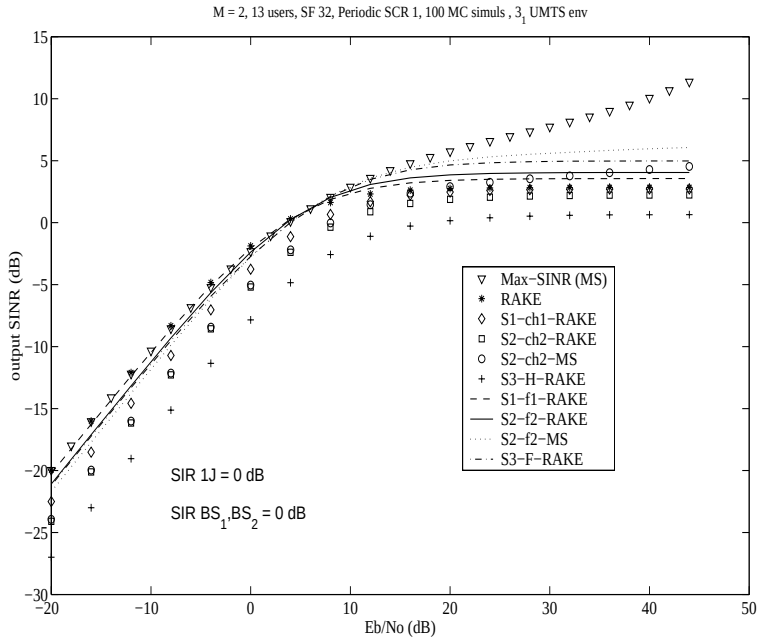

Figure 5.13: Output SINR versus E_b/N_0, 40.6% loaded BSs, spreading factor 32 and equal power distribution, periodic scrambling, ZF equalizers

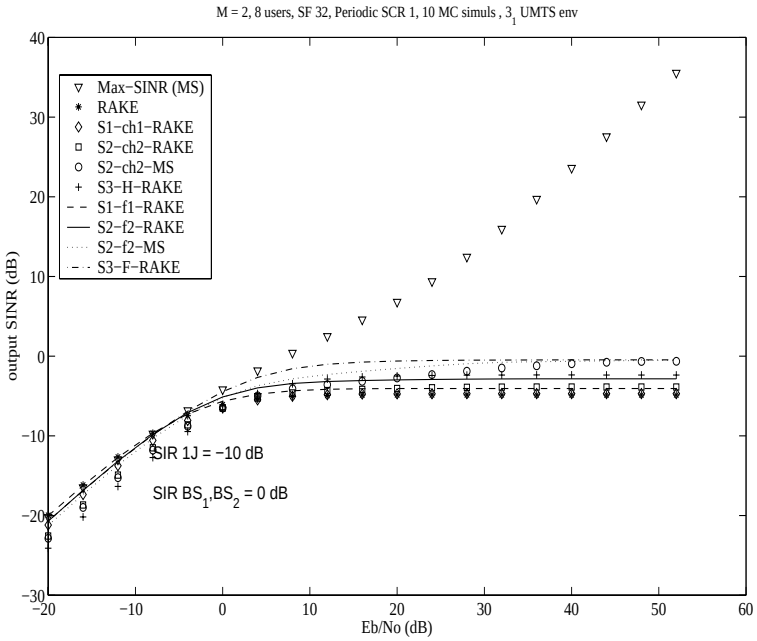

Figure 5.14: Output SINR versus E_b/N_0, 25% loaded BSs, spreading factor 32 and near-far situation, periodic scrambling, ZF equalizers

5.1.2 Polynomial Expansion IC Structures

5.1.2.1 Symbol Rate PE IC Structure

A vector of received signal over one symbol period n can be written as:

$$\boldsymbol{Y}[n] = \boldsymbol{H}_1(z)\,\boldsymbol{S}_1[n]\,\boldsymbol{C}_1\boldsymbol{A}_1[n] + \boldsymbol{H}_2(z)\,\boldsymbol{S}_2[n]\,\boldsymbol{C}_2\boldsymbol{A}_2[n] + \boldsymbol{V}[n] \qquad (5.4)$$

As shown in Fig. 5.15, $\boldsymbol{H}_j(z) = \sum_{i=0}^{M_j-1} \boldsymbol{H}_j[i]\,z^{-i}$ is the $Lmq \times L$ channel transfer function at symbol rate. The block coefficients $\boldsymbol{H}_j[i]$ correspond to the $M_j = \lceil \frac{L+N_j+d_j-1}{L} \rceil$ parts of the block Toeplitz matrix (with $mq \times 1$ sized blocks) with $\boldsymbol{h}^j$ as first column. d_j is the TX delay between BS j and the mobile, expressed in chip periods. $\boldsymbol{h}^j$ comprises the delay in the channel and hence its top entries may be zero. The $L \times L$ matrices $\boldsymbol{S}_j[n]$ are diagonal and contain the scrambler of BS j for symbol period n. The vectors $\boldsymbol{A}_j$ contain the K_j symbols of BS j for symbol period n, and $\boldsymbol{C}_j$

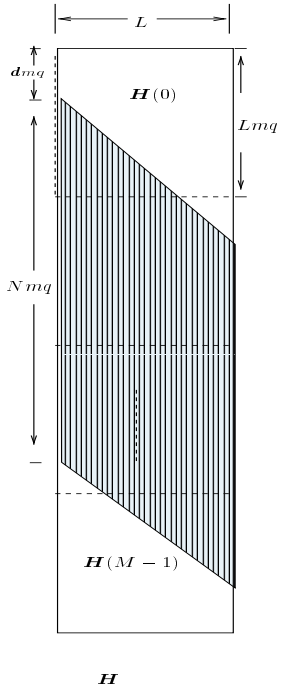

Figure 5.15: Channel impulse response $\boldsymbol{H}(z)$.

is the $L \times K_j$ matrix of the K_j active codes for BS j. Equation (5.4) can be rewritten as

$$\begin{aligned} \boldsymbol{Y}[n] &= [\boldsymbol{H}_1(z)\boldsymbol{S}_1[n]\boldsymbol{C}_1 \;\; \boldsymbol{H}_2(z)\boldsymbol{S}_2[n]\boldsymbol{C}_2]\boldsymbol{A}[n] + \boldsymbol{V}[n] \\ &= \widetilde{\boldsymbol{G}}(z)\boldsymbol{A}[n] + \boldsymbol{V}[n] \end{aligned} \qquad (5.5)$$

where $\boldsymbol{A}$ is the $(K = K_1 + K_2) \times 1$ vector containing all the transmitted symbols for the two BS. $\widetilde{\boldsymbol{G}}(z)$ is a $Lmq \times K$ channel-plus-spreading symbol rate filter, and

is time-varying due to the scrambling. The condition $K < Lq$ (or even $K < Lmq$) guarantees the existence of an FIR left inverse filter for $\widetilde{\boldsymbol{G}}(z)$, and allows zero-forcing interference cancellation. The calculation of an exact inverse of the channel would lead to high complexity due to the time-varying nature of the scrambler. Hence we will provide a good approximation to this inverse with acceptable complexity based on polynomial expansion [36].

Let $\boldsymbol{X}[n]$ be the $K \times 1$ correlator output, then:

$$\begin{aligned} \boldsymbol{X}[n] &= \widetilde{\boldsymbol{F}}(z)\boldsymbol{Y}[n] \\ &= \begin{bmatrix} \boldsymbol{C}_1^H \boldsymbol{S}_1^H[n]\boldsymbol{F}_1(z) \\ \boldsymbol{C}_2^H \boldsymbol{S}_2^H[n]\boldsymbol{F}_2(z) \end{bmatrix} (\widetilde{\boldsymbol{G}}(z)\boldsymbol{A}[n] + \boldsymbol{V}[n]) \\ &= \boldsymbol{M}(z)\boldsymbol{A}[n] + \widetilde{\boldsymbol{F}}(z)\boldsymbol{V}[n] \end{aligned} \tag{5.6}$$

where $\boldsymbol{F}_j(z) = \frac{\boldsymbol{H}_j^H(z^{-*})}{\|h_j\|^2}$ are the channel matched filters and $\boldsymbol{M}(z) = \widetilde{\boldsymbol{F}}(z)\widetilde{\boldsymbol{G}}(z)$. Let $\boldsymbol{F}_j(z)\boldsymbol{H}_j(z) = \boldsymbol{D}_{jj}(z) = \sum_i \boldsymbol{D}_{jj}[i]\, z^{-i}$. We assume that $diag\{\boldsymbol{D}_{jj}[0]\} = I$. As a result, if $\boldsymbol{M}(z) = \sum_i \boldsymbol{M}[i]\, z^{-i}$, $diag\{\boldsymbol{M}[0]\} = I$. In order to obtain the estimate of $\boldsymbol{A}[n]$, we initially consider the processing of $\boldsymbol{X}[n]$ by a decorrelator:

$$\begin{aligned} \widehat{\boldsymbol{A}}[n] &= \boldsymbol{M}(z)^{-1}\boldsymbol{X}[n] \\ &= (\boldsymbol{I} + \overline{\boldsymbol{M}}(z))^{-1}\boldsymbol{X}[n] \end{aligned} \tag{5.7}$$

The correlation matrix $\boldsymbol{M}(z)$ has a coefficient $\boldsymbol{M}[0]$ with a dominant unit diagonal in the sense that all other elements of the $\boldsymbol{M}[i]$ are much smaller than one in magnitude. Hence, the polynomial expansion approach suggests to develop $(\boldsymbol{I} + \overline{\boldsymbol{M}}(z))^{-1} = \sum_{i=0}^{\infty}(-\overline{\boldsymbol{M}}(z))^i$ up to some finite order, which leads to

$$\widehat{\boldsymbol{A}}^{(-1)}[n] = 0 \tag{5.8}$$

$$i \geq 0 \quad \widehat{\boldsymbol{A}}^{(i)}[n] = \boldsymbol{X}[n] - \overline{\boldsymbol{M}}(z)\, \widehat{\boldsymbol{A}}^{(i-1)}[n] \ . \tag{5.9}$$

In practice, we may want to stop at the first-order expansion, the quality of which depends on the degree of dominance of the diagonal of the static part of $\boldsymbol{M}(z)$ with respect to its off-diagonal elements and the dynamic part.

At first order, the expression for the user of interest (user one) becomes:

$$\begin{aligned} \widehat{\boldsymbol{a}}_1^1[n] &= \boldsymbol{e}_1^H \widehat{\boldsymbol{A}}^{(1)}[n] \\ &= \boldsymbol{e}_1^H(\boldsymbol{X}[n] - \overline{\boldsymbol{M}}(z)\, \widehat{\boldsymbol{A}}^{(0)}[n]) \\ &= \boldsymbol{e}_1^H(2\boldsymbol{X}[n] - \boldsymbol{M}(z)X[n]) \\ &= \boldsymbol{e}_1^H \widetilde{\boldsymbol{F}}(z)(2\boldsymbol{Y}[n] - \widetilde{\boldsymbol{G}}(z)X[n]) \\ &= \boldsymbol{c}_1^{1\,H}\boldsymbol{S}_1^H[n]\boldsymbol{F}_1(z)(2\boldsymbol{Y}[n] - \widetilde{\boldsymbol{G}}(z)\,\widetilde{\boldsymbol{F}}(z)\,\boldsymbol{Y}[n]) \end{aligned} \tag{5.10}$$

The corresponding structure is shown in Fig. 5.16, where $\boldsymbol{P}_j$ denotes the projection on all the active codes $\boldsymbol{C}_j$ of BS j, (in the Hybrid Structures considered earlier, $\boldsymbol{P}_1$ denoted the projection onto the interfering active codes of BS 1).

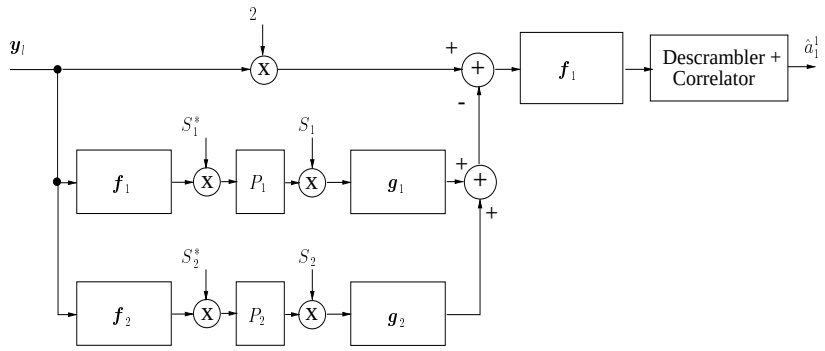

Figure 5.16: Symbol Rate Polynomial Expansion Structure.

In our development so far (decorrelator approach) the equalizer $\boldsymbol{f}_1$ (resp. $\boldsymbol{f}_2$) was the normalized matched filter to $\boldsymbol{h}_1$ (resp $\boldsymbol{h}_2$). An improved approach consists of using MMSE chip rate equalizers for the respective BS channels, normalized to have $\boldsymbol{f}_1\boldsymbol{h}_1 = 1$ (resp. $\boldsymbol{f}_2\boldsymbol{h}_2 = 1$). The idea behind this modification is to make the diagonal more dominant, leading to a more accurate first order expansion for the inverse. A second modification consists of replacing the re-channelling filters $\boldsymbol{g}_j$, which were so far the channel impulse responses $\boldsymbol{h}_j$, by Wiener filters so that the polynomial expansion moves from a decorrelator approach to a MMSE approach. It appears that taking $\boldsymbol{g}_j$ to be a scalar multiple of $\boldsymbol{h}_j$, in which the scalar is adjusted for MMSE after the subtraction process, may yield most of the attainable improvement.

5.1.2.2 Chip Rate PE IC Structure

In the symbol rate approach above, polynomial expansion was applied to the composite operation of spreading, scrambling, channelling, equalization, descrambling and despreading. This composite operation takes symbol rate inputs and outputs. Alternatively, we may want to apply the polynomial expansion to only the channelling and equalization operations, in which case we take chip rate inputs and outputs. To take advantage of the previously introduced notation, we shall nevertheless consider a rep-

resentation at the symbol rate

$$\begin{aligned} \boldsymbol{Z}[n] &= \boldsymbol{F}(z)\boldsymbol{Y}[n] = \begin{bmatrix} \boldsymbol{F}_1(z) \\ \boldsymbol{F}_2(z) \end{bmatrix} \boldsymbol{Y}[n] \\ &= \boldsymbol{F}(z)(\boldsymbol{G}(z)\widetilde{\boldsymbol{A}}[n] + \boldsymbol{V}[n]) \\ &= \boldsymbol{F}(z)([\boldsymbol{G}_1(z)\ \boldsymbol{G}_2(z)]\begin{bmatrix} \boldsymbol{S}_1[n]\boldsymbol{C}_1 & 0 \\ 0 & \boldsymbol{S}_2[n]\boldsymbol{C}_2 \end{bmatrix}\boldsymbol{A}[n] + \boldsymbol{V}[n]) \\ &= \boldsymbol{D}(z)\widetilde{\boldsymbol{A}}[n] + \boldsymbol{F}(z)\boldsymbol{V}[n] \end{aligned} \tag{5.11}$$

A good approximation of the inverse is:

$$\begin{aligned} \boldsymbol{D}(z)^{-1} &= (\boldsymbol{I} + \overline{\boldsymbol{D}}(z))^{-1} \\ &\approx \boldsymbol{I} - \overline{\boldsymbol{D}}(z) \\ &\approx 2\boldsymbol{I} - \boldsymbol{D}(z) \end{aligned} \tag{5.12}$$

The first order symbol estimation for user of interest is then:

$$\begin{aligned} \widehat{\boldsymbol{a}}_1^1[n] &= [\boldsymbol{c}_1^{1\,H}\boldsymbol{S}_1^H[n]\ \ 0](2\boldsymbol{I} - \boldsymbol{D}(z))\boldsymbol{Z}[n] \\ &= [\boldsymbol{c}_1^{1\,H}\boldsymbol{S}_1^H[n]\ \ 0](2\boldsymbol{I} - \boldsymbol{F}(z)\boldsymbol{G}(z))\boldsymbol{Z}[n] \\ &= \boldsymbol{c}_1^{1\,H}\boldsymbol{S}_1^H[n]\boldsymbol{F}_1(z)(2\boldsymbol{Y}[n] - \boldsymbol{G}(z)\boldsymbol{F}(z)\boldsymbol{Y}[n]) \end{aligned} \tag{5.13}$$

The implementation of this receiver corresponds to Fig. 5.16 but without the projection and (de)scrambling operations.

5.1.2.3 Soft Handover Reception

In the case of soft handover, the signal of interest (assume user 1) is transmitted by (e.g.) two BS. The proper modification of the end part of the receivers, which so far consisted of a filter-correlator part for BS 1 and user 1, becomes the sum of two such branches, as indicated in Fig. 5.17.

5.1.2.4 Numerical Examples

We assume here the same set of parameters of section 5.1.1.1 and one receive antenna ($q = 1$). The filters $\boldsymbol{G}$ play the role of filters $\boldsymbol{F}$ i section 5.1.1.

In Fig. 5.18 to Fig. 5.20, “MMSE-PE” in the legend refers to the first order symbol rate polynomial expansion structure which uses (chip rate) MMSE equalizers, and “RAKE-PE” refers to the use of matched filters as equalizers.

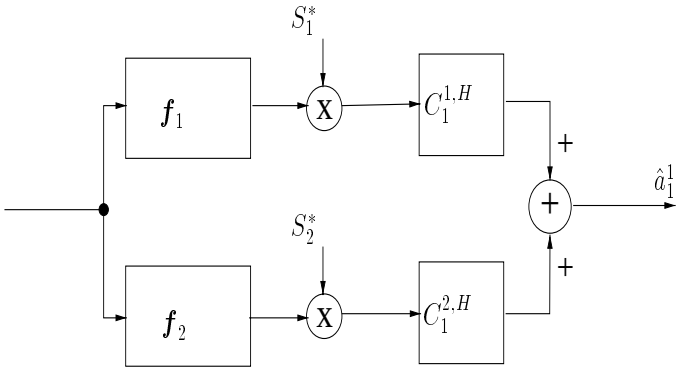

Figure 5.17: Soft handover receiver end.

Fig. 5.18 shows that the "MMSE-PE" structure performs better than hybrid structure 3, and hence is the best of all the structures studied, despite being less complex because it does not need optimization of the "re-channelling" filter.

Fig. 5.19 and Fig. 5.20 show that the first order (symbol rate) polynomial expansion structure (using either channel matched filters of MMSE equalizers for the $\boldsymbol{f}_j$) are sensitive to the number of users in the system, but this sensitivity appears to be acceptable in the case of the "MMSE-PE" since its performance remains the best for reasonable E_b/N_0. We believe that inserting a scaling factor in the subtraction branch, that is optimized for MMSE of the subtraction error, should eliminate the performance degradation at low E_b/N_0.

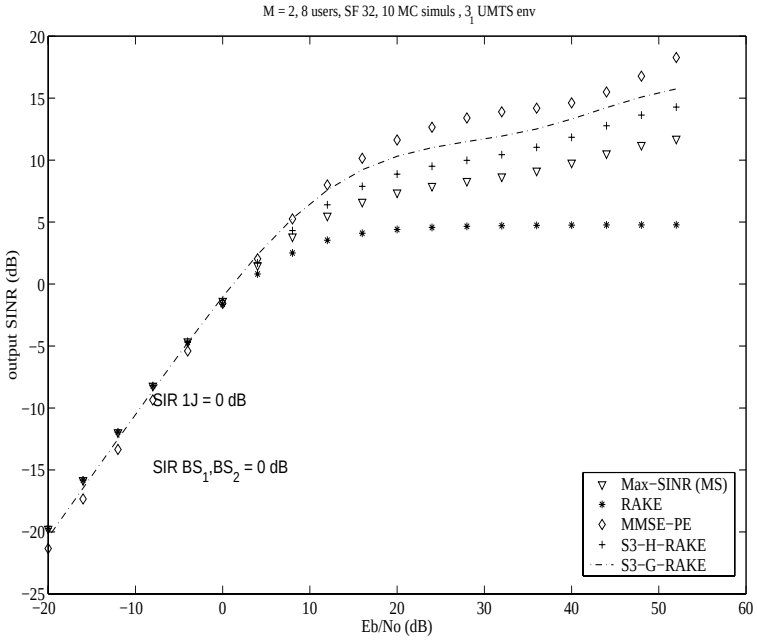

Figure 5.18: Output SINR versus E_b/N_0, PE structures, 25% loaded BSs, spreading factor 32 and equal power distribution, aperiodic scrambling, MMSE equalizers

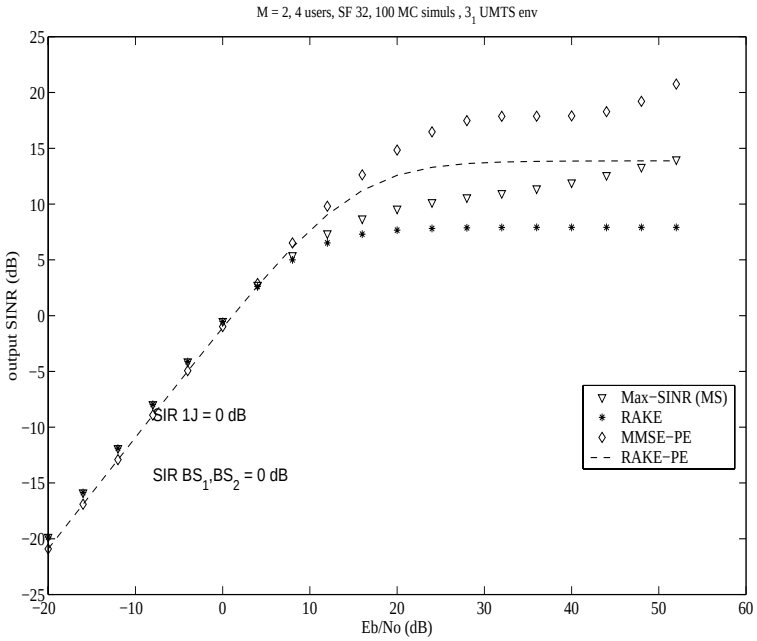

Figure 5.19: Output SINR versus E_b/N_0, PE structures, 12.5% loaded BSs, spreading factor 32 and equal power distribution, aperiodic scrambling, MMSE equalizers

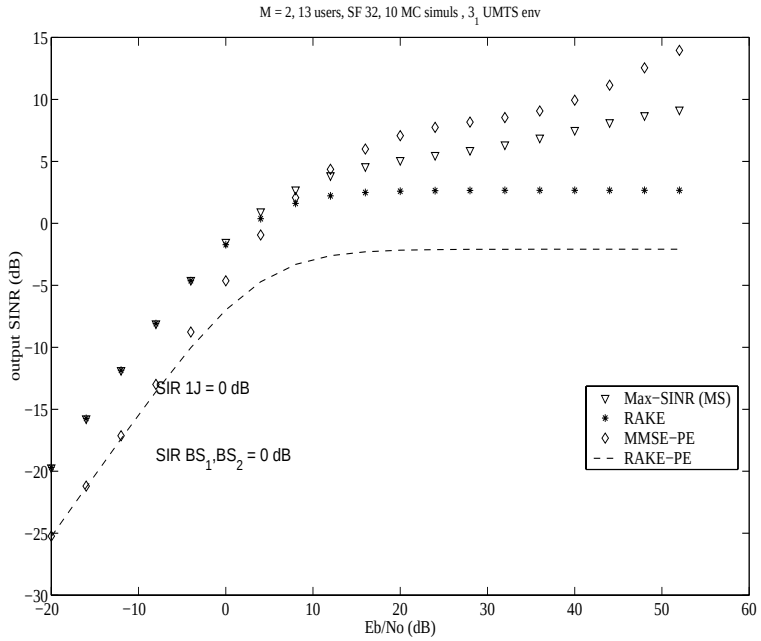

Figure 5.20: Output SINR versus E_b/N_0, PE structures, 40.6% loaded BSs, spreading factor 32 and equal power distribution, aperiodic scrambling, MMSE equalizers

5.2 Base Station TD Schemes

Multiple transmitting antennas at the base station can improve performances due to increase in diversity and some schemes have been proposed for open loop systems (no knowledge of the downlink channel at the transmitter). Basically, 4 kinds of Transmission Diversity (TD) schemes have been proposed for a base station: Orthogonal TD (OTD, see [37]), Space-Time TD (STTD, see [38]), Time-Switched TD (TSTD, see [37]) and Delay TD (DTD, see [39]). The UMTS norm for 3rd generation wireless systems specifies, for the FDD downlink, that the use of Transmission Diversity techniques is optional at the base station, while it is mandatory for the mobile station.

5.2.1 Orthogonal TD, Space-Time TD and Delay TD

Fig. 5.1 in section 5.1.1 shows the downlink signal model in baseband. $j = 2$ indicates here the second antenna of the transmitting base station and not an interfering base station.

OTD SCHEME

For each user k, this TD scheme generates, from a pair of symbols to transmit $a_{k,2P}$ and $a_{k,2P+1}$, where $2P$ stays for even symbol periods, the two pairs of symbols to be sent through the two antennas as following:

$$\begin{array}{ll} a^1_{k,2P} = a_{k,2P} & a^1_{k,2P+1} = a_{k,2P} \\ a^2_{k,2P} = a_{k,2P+1} & a^2_{k,2P+1} = -a_{k,2P+1} \end{array} \tag{5.14}$$

STTD SCHEME

Similarly to OTD, this technique produces two pairs of symbols, but now

$$\begin{array}{ll} a^1_{k,2P} = a_{k,2P} & a^1_{k,2P+1} = a_{k,2P+1} \\ a^2_{k,2P} = -a^*_{k,2P+1} & a^2_{k,2P+1} = a^*_{k,2P} \end{array} \tag{5.15}$$

where $*$ denotes the complex conjugate operation.

DTD SCHEME

This scheme operates differently from the previous two, because it sends the same symbol sequence on the two antennas, but it introduces a delay of D chip periods on the transmission on the second antenna. So it works as if there is just one antenna, but

the channel is the sum of $h^1(t)$ and $h^2(t - D \cdot T_c)$:

$$\begin{aligned} a^1_{k,n} &= a^2_{k,n} = a_{k,n}\ ,\ b^1_l = b^2_l = b_l \\ h(z) &= h^1(z) + z^{-D} \cdot h^2(z) \end{aligned} \tag{5.16}$$

where $h(z)$ represent the channel in the *z*-domain.

5.2.2 Linear Receivers Structures: RAKE and Max-SINR

DTD RECEIVER

The structure in section 2.4.2 is valid also in the case of Delay Transmission Diversity. Eq. 4.1 to Eq. 4.13 are also applicable for this TD scheme, when the channel $\boldsymbol{h}$ is as in the Eq. (5.16). The same results and conclusions are then valid, in particular, in the noiseless case, the max-SINR receiver becomes the ZF equalizer.

OTD RECEIVER

When other schemes of Transmission Diversity are used, other structures are needed. The received signal in this case can be expressed as

$$\boldsymbol{Y}_n = \boldsymbol{Y}^1_n + \boldsymbol{Y}^2_n + \boldsymbol{V}_n \tag{5.17}$$

where

$$\begin{aligned} \boldsymbol{Y}^1_n &= \mathcal{T}(\boldsymbol{h}^{1'})\boldsymbol{S}_n \sum_{k=1}^{K} \boldsymbol{C}_k \boldsymbol{A}^1_{k,n} \\ \boldsymbol{Y}^2_n &= \mathcal{T}(\boldsymbol{h}^{2'})\boldsymbol{S}_n \sum_{k=1}^{K} \boldsymbol{C}_k \boldsymbol{A}^2_{k,n} \end{aligned} \tag{5.18}$$

where superscripts 1,2 refer to base station transmitting antennas 1,2.

Fig. 5.21 shows the linear processing needed in an OTD receiver, which distinguishes even ($2P$) and odd ($2P+1$) symbol periods within the received signal $\boldsymbol{Y}_n$. The receiver processes the two signals separately with two chip rate filters $\boldsymbol{f}_1$ and $\boldsymbol{f}_2$, whose outputs are then despreaded, by applying a (total) despreader similarly to what is shown in the figure of section 2.4.2. When this scheme is implemented, the two soft outputs (at half of the symbol rate) are the estimators for even symbol period (z^1) and odd symbol period (z^2) where $\alpha^{j\bar{j}}_d$ is defined as in Eq. 4.3 for filter $\boldsymbol{f}_j$ and channel $\boldsymbol{h}^{\bar{j}}$:

$$\alpha^{j\bar{j}}_d = \boldsymbol{f}_j \boldsymbol{h}^{\bar{j}}\ . \tag{5.19}$$

We can write the two soft outputs z^j as

$$\begin{aligned} z^1 &= \boldsymbol{c}^H_1\ \boldsymbol{S}^H_{2P} \mathcal{T}(\boldsymbol{f}_1)\boldsymbol{Y}_{2P} + \boldsymbol{c}^H_1\ \boldsymbol{S}^H_{2P+1} \mathcal{T}(\boldsymbol{f}_1)\boldsymbol{Y}_{2P+1} \\ z^2 &= \boldsymbol{c}^H_1\ \boldsymbol{S}^H_{2P} \mathcal{T}(\boldsymbol{f}_2)\boldsymbol{Y}_{2P} - \boldsymbol{c}^H_1\ \boldsymbol{S}^H_{2P+1} \mathcal{T}(\boldsymbol{f}_2)\boldsymbol{Y}_{2P+1} \end{aligned} \tag{5.20}$$

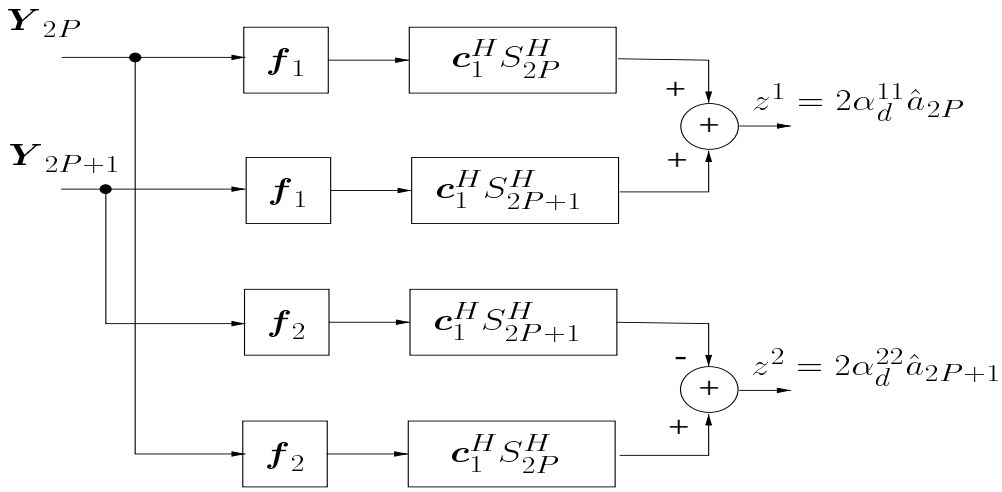

Figure 5.21: The downlink receiver OTD structure

When a RAKE implementation is wanted, then $\boldsymbol{f}_1 = \boldsymbol{h}^{1^H}$ and $\boldsymbol{f}_2 = \boldsymbol{h}^{2^H}$, $\alpha_d^{11} = \|\boldsymbol{h}^1\|^2$ and $\alpha_d^{22} = \|\boldsymbol{h}^2\|^2$. The SINR for the soft output z_j is

$$\Gamma_j = \frac{2 \cdot \sigma_1^2 |\alpha_d^{jj}|^2}{\boldsymbol{f}_j \boldsymbol{A}_1 \boldsymbol{f}_j^H} \tag{5.21}$$

where

$$\boldsymbol{A}_1 = \boldsymbol{R}_{VV} + \sigma_{tot}^2[\mathfrak{T}(\boldsymbol{h}^{1'})\mathfrak{T}^H(\boldsymbol{h}^{1'}) + \mathfrak{T}(\boldsymbol{h}^{2'})\mathfrak{T}^H(\boldsymbol{h}^{2'}) - \left(\boldsymbol{h}^1\boldsymbol{h}^{1^H} + \boldsymbol{h}^2\boldsymbol{h}^{2^H}\right)] \tag{5.22}$$

see the proof in Appendix 5.A. From the OTD receiver structure is clear that the maximization of Γ_1 and Γ_2 is independent (z_1 depends only on $\boldsymbol{f}_1$ and z_2 only on $\boldsymbol{f}_2$). The expression for the filters turns out to be the solution of

$$\boldsymbol{f}_{j,MAX} = \arg \max_{\boldsymbol{f}_{j:2}\boldsymbol{f}_j\boldsymbol{h}=1} \Gamma_j = \arg \min_{\boldsymbol{f}_{j:2}\boldsymbol{f}_j\boldsymbol{h}^j=1} \boldsymbol{f}_j \boldsymbol{A}_1 \boldsymbol{f}_j^H \tag{5.23}$$

that is

$$\boldsymbol{f}_{j,MAX} = \frac{1}{2}\left(\boldsymbol{h}^{j^H}\boldsymbol{A}_1^{-1}\boldsymbol{h}^j\right)^{-1}\boldsymbol{h}^{j^H}\boldsymbol{A}_1^{-1} \ . \tag{5.24}$$

In this case the maximum SINR for soft output z_j becomes

$$\Gamma_{j,MAX} = 2 \cdot \sigma_1^2 \cdot \boldsymbol{h}^{j^H}\boldsymbol{A}_1^{-1}\boldsymbol{h}^j \ . \tag{5.25}$$

$\Gamma_{1,MAX}$ and $\Gamma_{2,MAX}$ are not equal so the transmission quality of the two equivalent channels is different. The total SINR for OTD is then defined as $\Gamma_{MAX,OTD} = 2\left(\frac{1}{\Gamma_{1,MAX}} + \frac{1}{\Gamma_{2,MAX}}\right)^{-1}$ which corresponds to take the MSE as the average of the MSEs for the two soft outputs.

STTD RECEIVER

Fig. 5.22 shows the STTD receiver structure; now each of the two soft output depends on both $\boldsymbol{f}_j$ and the two input signals $\boldsymbol{Y}_{2P}$ and $\boldsymbol{Y}_{2P+1}$ are complex conjugated before being filtered by $\boldsymbol{f}_2$. We can write the two STTD soft outputs z^j as

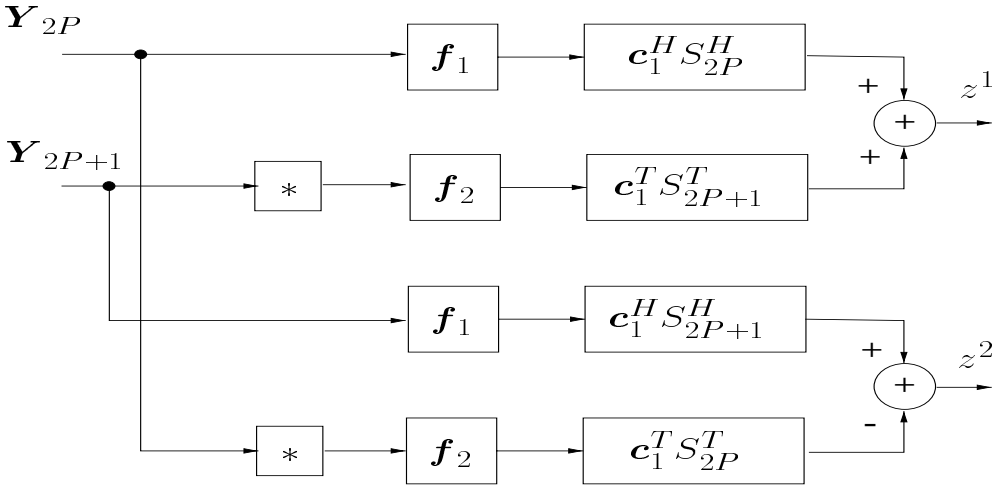

Figure 5.22: The downlink receiver STTD structure

$$\begin{aligned} z^1 &= \boldsymbol{c}_1^H\, \boldsymbol{S}_{2P}^H \mathcal{T}(\boldsymbol{f}_1)\boldsymbol{Y}_{2P} + \boldsymbol{c}_1^T\, \boldsymbol{S}_{2P+1}^T \mathcal{T}(\boldsymbol{f}_2)\boldsymbol{Y}_{2P+1}^* \\ z^2 &= \boldsymbol{c}_1^H\, \boldsymbol{S}_{2P+1}^H \mathcal{T}(\boldsymbol{f}_1)\boldsymbol{Y}_{2P+1} - \boldsymbol{c}_1^T\, \boldsymbol{S}_{2P}^T \mathcal{T}(\boldsymbol{f}_2)\boldsymbol{Y}_{2P}^* \end{aligned} \tag{5.26}$$

By defining $\boldsymbol{F} = [\boldsymbol{f}_1, \boldsymbol{f}_2]$, $\boldsymbol{H}_1 = \left[\boldsymbol{h}^{1^T}, \boldsymbol{h}^{2^H}\right]^T$ and $\boldsymbol{H}_2 = \left[-\boldsymbol{h}^{2^T}, \boldsymbol{h}^{1^H}\right]^T$ and by taking the expectation over the despreading/descrambling, we can restate the two soft outputs estimates z^1 and z^2 as

$$\begin{aligned} z^1 &= \boldsymbol{F}\boldsymbol{H}_1 \hat{a}_{2P} + \boldsymbol{F}\boldsymbol{H}_2 \hat{a}_{2P+1}^* \\ z^2 &= \boldsymbol{F}\boldsymbol{H}_1 \hat{a}_{2P+1} - \boldsymbol{F}\boldsymbol{H}_2 \hat{a}_{2P}^* \end{aligned} \tag{5.27}$$

and the SINR for the z^j soft output becomes

$$\Gamma_j = \frac{\sigma_1^2 \left(|\boldsymbol{F}\boldsymbol{H}_1|^2 + |\boldsymbol{F}\boldsymbol{H}_2|^2\right)}{\boldsymbol{F}\boldsymbol{A}\boldsymbol{F}^H + R_j} \tag{5.28}$$

where $\boldsymbol{A} = \begin{pmatrix} \boldsymbol{A}_1 & 0 \\ 0 & \boldsymbol{A}_1^* \end{pmatrix}$ and $\boldsymbol{A}_1$ is defined in Eq. (5.22). The term R_j in the denominator depends mainly on the used spreading codes (so the mobile receiver should know them), but we will see in the numerical examples below that it is negligible with respect to the other term, so that, from Eq. (5.28), $\Gamma_1 = \Gamma_2$ and

$$\Gamma_{STTD} = \frac{\sigma_1^2 \left(|\boldsymbol{F}\boldsymbol{H}_1|^2 + |\boldsymbol{F}\boldsymbol{H}_2|^2\right)}{\boldsymbol{F}\boldsymbol{A}\boldsymbol{F}^H} \tag{5.29}$$

Since we want z^1 to be the estimator for a_{2P} and z^2 the one for a_{2P+1}, the filter $\boldsymbol{F}_{MAX}$ that maximize Γ_{STTD} comes from the problem

$$\arg \max_{\substack{\boldsymbol{F}:\, \boldsymbol{F}\boldsymbol{H}_1 = 1 \\ \boldsymbol{F}\boldsymbol{H}_2 = 0}} \Gamma_{STTD} = \arg \min_{\substack{\boldsymbol{F}:\, \boldsymbol{F}\boldsymbol{H}_1 = 1 \\ \boldsymbol{F}\boldsymbol{H}_2 = 0}} \boldsymbol{F}\boldsymbol{A}\boldsymbol{F}^H \tag{5.30}$$

that is, solving by Lagrange multipliers,

$$\boldsymbol{F}_{MAX} = \left(\boldsymbol{H}_1^H \boldsymbol{A}^{-1} \boldsymbol{H}_1\right)^{-1} \boldsymbol{H}_1^H \boldsymbol{A}^{-1} \,. \tag{5.31}$$

In this case the maximum SINR becomes

$$\Gamma_{MAX,STTD} = \sigma_1^2 \left(\boldsymbol{h}^{1^H} \boldsymbol{A}_1^{-1} \boldsymbol{h}^1 + \boldsymbol{h}^{2^H} \boldsymbol{A}_1^{-1} \boldsymbol{h}^2\right) \,. \tag{5.32}$$

For a RAKE receiver: $\boldsymbol{F} = \left[\boldsymbol{h}^{1^H}, \boldsymbol{h}^{2^T}\right]$, $\boldsymbol{F}\boldsymbol{H}_1 = \left(\|\boldsymbol{h}^1\|^2 + \|\boldsymbol{h}^2\|^2\right)$ and $\boldsymbol{F}\boldsymbol{H}_2 = 0$.

5.2.2.1 Numerical Examples

Fig. 5.23 to Fig. 5.27 present some of the simulations that we have performed to evaluate the various schemes and receivers. In the legends of these figures, R and MS refer to RAKE and max-SINR receiver respectively. The K users are considered synchronous, with the same spreading factor $L = 32$ and using the same downlink channels $\boldsymbol{h}^1$ and $\boldsymbol{h}^2$ which are FIR filters, convolution of a sparse Vehicular A UMTS channel and a pulse shape (root-raised cosine with roll-off factor of 0.22). The channel(s) length is $N = 19$ chips, due to the UMTS chip rate of 3.84 Mchips/sec. An oversampling factor of $M = 2$ is assumed. Two possible user power distributions are simulated: all interferers have the same power and the user of interest has either the same power also or 15dB less power (near-far situation). The performances of the different receiver instances are shown in terms of the output SINR versus the SNR at the receiver. The length of all the filters in the simulations is equal for all the TD schemes and is either the channel length N or the channel length of the DTD channel ($N + D$).

Due to the interference between the two channels (see Eq. (5.22)) and to the presence of the scrambler, it is clear that a ZF equalization for OTD and STTD can not exist; this is confirmed by the simulations in Fig. 5.23 to Fig. 5.26, where there is always SINR saturation for OTD and STTD structures, while DTD is saturating for shorter FIR filters because their length does not permit zero forcing. In this set of figures the delay D for DTD is equal to the channel length N.

We can notice how the DTD max-SINR receiver performs much better than the other structures for both user power distributions when the filter lengths coincide with

the DTD channel length ($2N$); see Fig. 5.23 and Fig. 5.24. The DTD RAKE implementation is also the best one in these cases.

When, instead, the filter lengths are taken equal to the channel length N, but maintaining $D = N$, the DTD receivers clearly suffer. In this case STTD performs better in the RAKE implementation (see Fig. 5.25 and Fig. 5.26) and besides the DTD complexity is here half of the STTD complexity. Their max-SINR performances are similar.

Fig. 5.27 shows the case when the delay D is taken as half the channel length N and the filter lengths are equal to $N + D$ (so the complexity is reduced by one quarter). The performances are very similar to those in Fig. 5.23.
The last figure, Fig. 5.28, is shown to confirm that the terms R_j in Eq. (5.28) are negligible. We can see that when they are taken into account (x's and sparse dots), the performance/results are identical, on the average, to the case when they are dropped (dashed and solid lines respectively).

5.3 Conclusions

We presented in this chapter our work on Intercell Interference Cancellation and on base station Transmit Diversity schemes.

In the case of aperiodic scrambling, the classical RAKE receiver exhibits significant limitations when a strong interfering base station is present. The Max-SINR receiver, which is a MMSE equalizer-correlator cascade, allows improved performance. Still better performance can be achieved when more knowledge about the signal structure gets exploited. We proposed two receiver structures that exploit the existence of excess (unused) codes. One type of structure, called hybrid structure, was developed based on intuitive ideas about noise cancellation in the direction of unused codes. The other structure is based on the more formal polynomial expansion approach. We have observed that the two approaches yield very similar structures. In the case of polynomial expansion, we also introduced a chip rate approach, in which only the scrambling sequences of the base stations are exploited (and not the excess codes). The proposed structures have a reasonable complexity and allow important performance gains. In particular, the structures exhibit no SINR saturation at high SNR (in contrast to the RAKE receiver) which means that all interference can be forced to zero.
On the contrary, in the case of periodic scrambling, the max-SINR linear receiver outperforms all the other (linear and non-linear) structures. This is due to the fact that the excess codes (codes not used by a base station) give rise to time-invariant noise subspaces which are used to cancel the interfering base station. In the case of aperiodic scrambling, these noise subspaces are time-variant and the only way to exploit them

for IC with time-invariant filters is with hybrid structures.

Concerning the Base Station Transmission Diversity schemes, the RAKE performs best with the DTD scheme, regardless of how much delay is introduced between the two channels (hence even if only partial diversity). Nevertheless, lesser temporal overlap between the two channels in DTD leads to better performance. When a max-SINR receiver is employed, performance still gets improved significantly for DTD, compared to a RAKE receiver. The good performance of the DTD scheme can be explained by the fact that it is the only TD scheme that allows zero-forcing equalization. STTD schemes often perform significantly worse than DTD schemes, though they may occasionally outperform DTD schemes a bit. We can also conclude that the OTD scheme leads to the worst performance in all receiver cases.

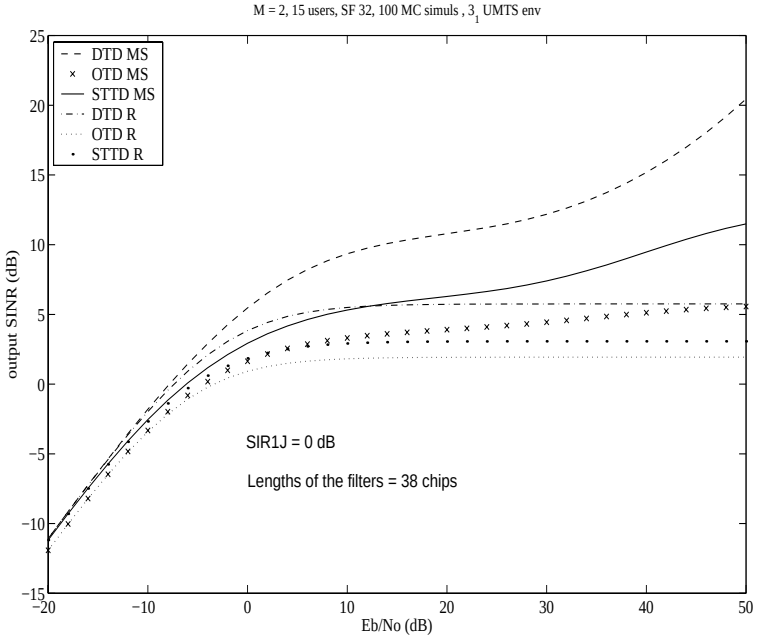

Figure 5.23: Output SINR versus E_b/N_0, TD structures, 50% loaded system, spreading factor 32 and equal power distribution

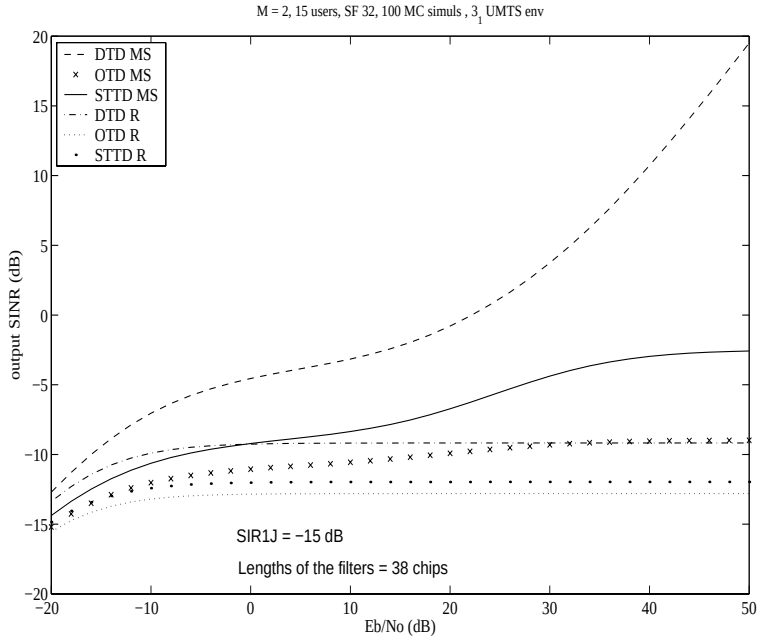

Figure 5.24: Output SINR versus E_b/N_0, TD structures, 50% loaded system, spreading factor 32 and near-far situation

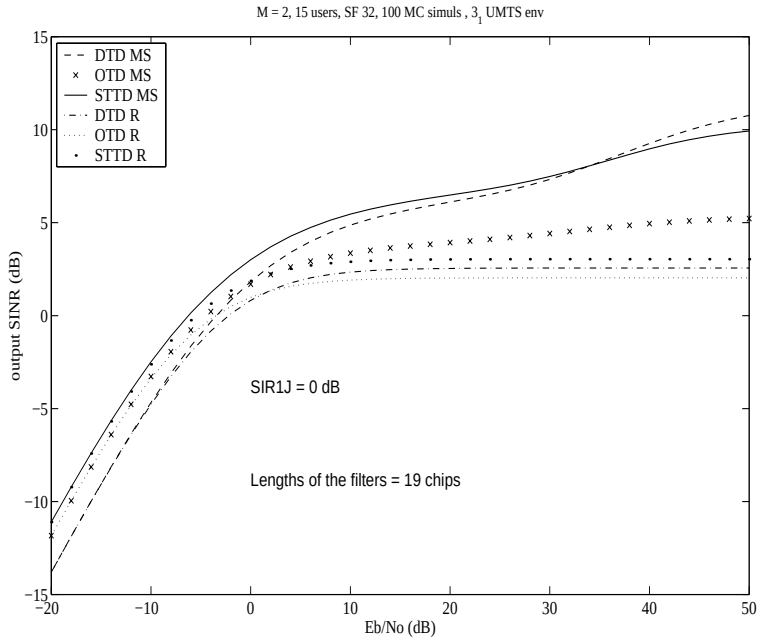

Figure 5.25: Output SINR versus E_b/N_0, TD structures, 50% loaded system, spreading factor 32 and equal power distribution

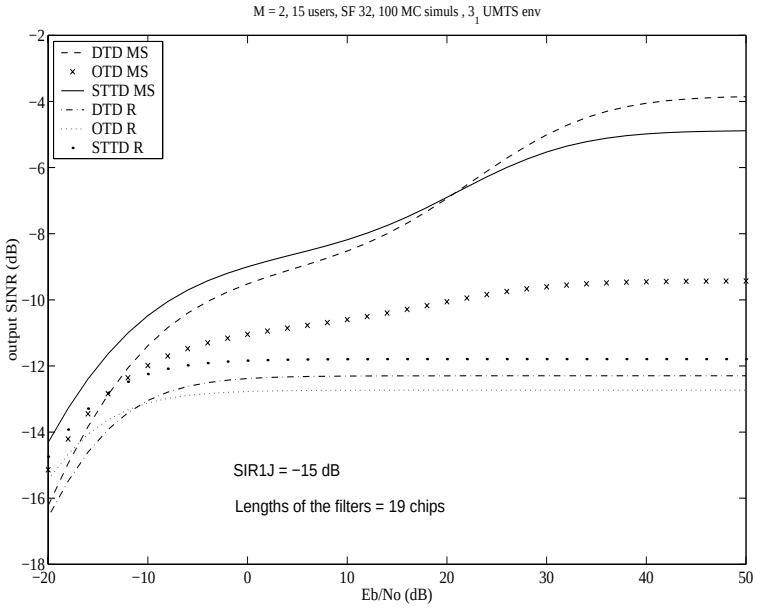

Figure 5.26: Output SINR versus E_b/N_0, TD structures, 50% loaded system, spreading factor 32 and near-far situation

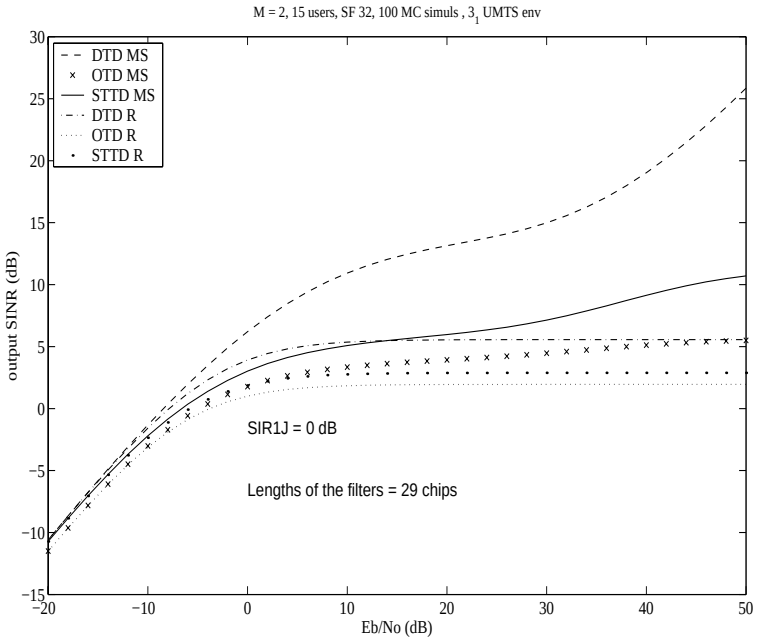

Figure 5.27: Output SINR versus E_b/N_0, TD structures, 50% loaded system, spreading factor 32 and equal power distribution

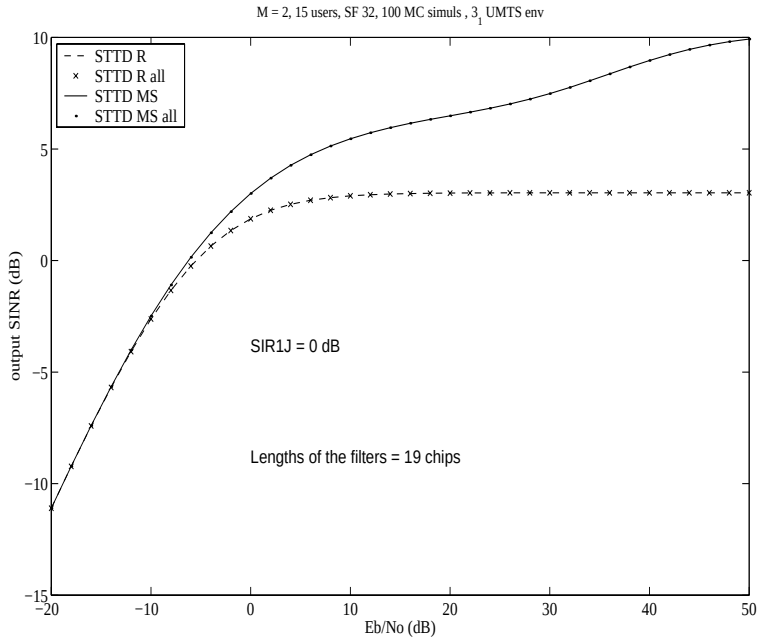

Figure 5.28: Output SINR versus E_b/N_0, TD structures, 50% loaded system, spreading factor 32 and equal power distribution, STTD case only

5.A Proof of Equations 5.21 and 5.22

By defining $\Im(\boldsymbol{f}_j)\Im(\boldsymbol{h}^{\vec{j'}}) = \Im(\boldsymbol{\alpha}^{j\vec{j}}) = \Im(\boldsymbol{\alpha}_d^{j\vec{j}}) + \Im(\overline{\boldsymbol{\alpha}}^{j\vec{j}})$, from equations 5.14, 5.18 and 5.20 we get, when averaging over scrambling sequences,

$$\begin{aligned} E[z_1] &= \sum_{k=1}^{K} \boldsymbol{c}_1^H \left(\alpha_d^{11}\boldsymbol{c}_k\left(a_{k,2P}^1 + a_{k,2P+1}^1\right) + \alpha_d^{12}\boldsymbol{c}_k\left(a_{k,2P}^2 + a_{k,2P+1}^2\right)\right) \\ &= \sum_{k=1}^{K} \delta_{1,k} 2a_{k,2P}^1 = 2\alpha_d^{11} a_{1,2P}^1 \end{aligned}$$

The $MSE = E|z^1 - \hat{z}^1|^2$ for the soft output z^1 is given by

$$E|\sum_{k=1}^{K} \boldsymbol{c}_1^H \boldsymbol{S}_{2P}^H \left[\Im(\overline{\boldsymbol{\alpha}}_d^{11})\boldsymbol{S}_{2P}\boldsymbol{C}_k\boldsymbol{A}_{k,2P}^1 + \Im(\overline{\boldsymbol{\alpha}}_d^{12})\boldsymbol{S}_{2P}\boldsymbol{C}_k\boldsymbol{A}_{k,2P}^2 + \Im(\boldsymbol{f}_1)\boldsymbol{V}_{2P}\right] +$$
$$\boldsymbol{c}_1^H \boldsymbol{S}_{2P+1}^H \left[\Im(\overline{\boldsymbol{\alpha}}_d^{11})\boldsymbol{S}_{2P+1}\boldsymbol{C}_k\boldsymbol{A}_{k,2P+1}^1 + \Im(\overline{\boldsymbol{\alpha}}_d^{12})\boldsymbol{S}_{2P+1}\boldsymbol{C}_k\boldsymbol{A}_{k,2P+1}^2 + \Im(\boldsymbol{f}_1)\boldsymbol{V}_{2P+1}\right]|^2$$

Expectations of the crossterms within the sum are zero because of the scrambling symbol aperiodicity and of the symbol transmission definitions. So we get

$$MSE(z^1) = 2\sigma_{tot}^2\left[\|\overline{\boldsymbol{\alpha}}_d^{11}\|^2 + \|\overline{\boldsymbol{\alpha}}_d^{12}\|^2\right] + \boldsymbol{f}_1\boldsymbol{R}_{V_{2P}V_{2P}}\boldsymbol{f}_1^H + \boldsymbol{f}_1\boldsymbol{R}_{V_{2P+1}V_{2P+1}}\boldsymbol{f}_1^H$$

With the same reasoning we have

$$MSE(z^2) = 2\sigma_{tot}^2\left[\|\overline{\boldsymbol{\alpha}}_d^{21}\|^2 + \|\overline{\boldsymbol{\alpha}}_d^{22}\|^2\right] + \boldsymbol{f}_2\boldsymbol{R}_{VV}\boldsymbol{f}_2^H$$

because $\boldsymbol{R}_{V_{2P}V_{2P}} = \boldsymbol{R}_{V_{2P+1}V_{2P+1}} = \boldsymbol{R}_{VV}$. But, due to the fact that

$$\boldsymbol{R}_{Y_{2P}Y_{2P}} = \boldsymbol{R}_{Y_{2P+1}Y_{2P+1}} = \boldsymbol{R}_{VV} + \sigma_{tot}^2\left[\Im(\boldsymbol{h}^{1'})\Im(\boldsymbol{h}^{1'})^H + \Im(\boldsymbol{h}^{2'})\Im(\boldsymbol{h}^{2'})^H\right] = \boldsymbol{R}_{YY}$$

we can also write

$$\begin{aligned} MSE(z^1) &= 2\boldsymbol{f}_1\boldsymbol{R}_{YY}\boldsymbol{f}_1^H - 2\sigma_{tot}^2\left[|\alpha_d^{11}|^2 + |\alpha_d^{12}|^2\right] \\ &= 2\boldsymbol{f}_1\boldsymbol{R}_{YY}\boldsymbol{f}_1^H - 2\sigma_{tot}^2\left[\boldsymbol{f}_1\boldsymbol{h}_1\boldsymbol{h}_1^H\boldsymbol{f}_1^H + \boldsymbol{f}_1\boldsymbol{h}_2\boldsymbol{h}_2^H\boldsymbol{f}_1^H\right] \\ &= 2\boldsymbol{f}_1\boldsymbol{A}_1\boldsymbol{f}_1^H \end{aligned}$$

with

$$\begin{aligned} \boldsymbol{A}_1 &= \boldsymbol{R}_{YY} - \sigma_{tot}^2\left[\boldsymbol{h}_1\boldsymbol{h}_1^H + \boldsymbol{h}_2\boldsymbol{h}_2^H\right] \\ &= \boldsymbol{R}_{VV} + \sigma_{tot}^2\left[\Im(\boldsymbol{h}_1')\Im(\boldsymbol{h}_1')^H + \Im(\boldsymbol{h}_2')\Im(\boldsymbol{h}_2')^H - \left(\boldsymbol{h}_1\boldsymbol{h}_1^H + \boldsymbol{h}_2\boldsymbol{h}_2^H\right)\right] \end{aligned} .$$

The SINR for the soft output z^1 is then defined as (similar for z^2)

$$\Gamma_1 = \frac{E[z_1]^2}{2\boldsymbol{f}_1\boldsymbol{A}_1\boldsymbol{f}_1^H} = \frac{\sigma_1^H|2\boldsymbol{f}_1\boldsymbol{h}_1|^2}{2\boldsymbol{f}_1\boldsymbol{A}_1\boldsymbol{f}_1^H} = \frac{2\sigma_1^H|\boldsymbol{f}_1\boldsymbol{h}_1|^2}{\boldsymbol{f}_1\boldsymbol{A}_1\boldsymbol{f}_1^H}$$

5.B Proof of Equation 5.28

The same reasoning of appendix 5.A applied to equation 5.26 brings us to equation 5.27. The $MSE = E|z^1 - \hat{z}^1|^2$ for soft output z^1 is here defined as

$$E|\sum_{k=1}^{K} \boldsymbol{c}_1^H \boldsymbol{S}_{2P}^H \left[\mathcal{T}(\overline{\boldsymbol{\alpha}}_d^{11})\boldsymbol{S}_{2P}\boldsymbol{C}_k\boldsymbol{A}_{k,2P}^1 + \mathcal{T}(\overline{\boldsymbol{\alpha}}_d^{12})\boldsymbol{S}_{2P}\boldsymbol{C}_k\boldsymbol{A}_{k,2P}^2 + \mathcal{T}(\boldsymbol{f}_1)\boldsymbol{V}_{2P}\right] +$$
$$\boldsymbol{c}_1^T \boldsymbol{S}_{2P+1}^T \left[\mathcal{T}(\overline{\boldsymbol{\alpha}}_d^{21^*})\boldsymbol{S}_{2P+1}^*\boldsymbol{C}_k^*\boldsymbol{A}_{k,2P+1}^{1^*} + \mathcal{T}(\overline{\boldsymbol{\alpha}}_d^{22^*})\boldsymbol{S}_{2P+1}^*\boldsymbol{C}_k^*\boldsymbol{A}_{k,2P+1}^{2^*} + \mathcal{T}(\boldsymbol{f}_2)\boldsymbol{V}_{2P+1}^*\right]|^2$$

Expectations of the crossterms within the sum are zero because of the scrambling symbol aperiodicity and of the symbol transmission definitions. So we get

$$MSE(z^1) = \boldsymbol{f}_1\boldsymbol{R}_{V_{2P}V_{2P}}\boldsymbol{f}_1^H + \boldsymbol{f}_2\boldsymbol{R}_{V_{2P+1^*}V_{2P+1^*}}\boldsymbol{f}_2^H +$$
$$\sigma_{tot}^2\left[\|\overline{\boldsymbol{\alpha}}_d^{11}\|^2 + \|\overline{\boldsymbol{\alpha}}_d^{12} + \overline{\boldsymbol{\alpha}}_d^{21^*}\|^2 + \|\overline{\boldsymbol{\alpha}}_d^{22^*}\|^2\right] + 2Re\left[-\boldsymbol{E}_{auto} + \boldsymbol{E}_{cross}\right]$$

where $\boldsymbol{E}_{auto}$ and $\boldsymbol{E}_{cross}$ are of the form

$$\boldsymbol{E}_{xx} = \sum_{k=1}^{K}\sigma_k^2\sum_{s=0}^{N-2}\sum_{r=0}^{s}\mathcal{T}^1(\overline{\boldsymbol{\alpha}}_d^{xx})_{r,s}\mathcal{T}^{-1^*}(\overline{\boldsymbol{\alpha}}_d^{\overline{xx}})_{s+L-N+1,r}\times$$
$$\boldsymbol{c}_1^*(L-1-r)\boldsymbol{c}_k(N-s-2)\boldsymbol{c}_k(L-1-r)\boldsymbol{c}_1^*(N-s-2)$$

where $auto = 11$, $\overline{auto} = 22^*$, $cross = 12$ and $\overline{cross} = 21^*$, N is the delay spread of the overall channel in chip periods, L is the spreading factor and $\boldsymbol{c}_k$ is the spreading sequence of user k. $\mathcal{T}^1(\bullet)$ and $\mathcal{T}^{-1}(\bullet)$ are the $L \times N - 1$ most left and most right parts, respectively, of $\mathcal{T}(\bullet)$. We showed by simulations that the term $2Re\left[\boldsymbol{E}_{auto} + \boldsymbol{E}_{cross}\right]$ is negligible w.r.t. all the other addendums in the MSE.

If we define $\mathbf{Y} = \left[\boldsymbol{Y}_{2P}\boldsymbol{Y}_{2P+1}^*\right]^T$ then we have

$$\boldsymbol{R}_{\mathbf{YY}} = \begin{bmatrix} \boldsymbol{R}_{\boldsymbol{Y}_{2P}\boldsymbol{Y}_{2P}} & \boldsymbol{R}_{\boldsymbol{Y}_{2P}\boldsymbol{Y}_{2P+1}^*} \\ \boldsymbol{R}_{\boldsymbol{Y}_{2P+1}^*\boldsymbol{Y}_{2P}} & \boldsymbol{R}_{\boldsymbol{Y}_{2P+1}^*\boldsymbol{Y}_{2P+1}^*} \end{bmatrix}$$

The off-diagonal terms in the matrix are zero because of STTD definitions in 5.15 and of the scrambling aperiodicity. The diagonal terms, due the STTD definitions and the noise i.i.d. nature w.r.t. the signals, are equal to

$$\begin{aligned} \boldsymbol{R}_{\boldsymbol{Y}_{2P}\boldsymbol{Y}_{2P}} &= \boldsymbol{R}_{VV} + \sigma_{tot}^2\left[\mathcal{T}(\boldsymbol{h}_1')\mathcal{T}^H(\boldsymbol{h}_1') + \mathcal{T}(\boldsymbol{h}_2')\mathcal{T}^H(\boldsymbol{h}_2')\right] \\ \boldsymbol{R}_{\boldsymbol{Y}_{2P+1}^*\boldsymbol{Y}_{2P+1}^*} &= \boldsymbol{R}_{\boldsymbol{Y}_{2P}\boldsymbol{Y}_{2P}}^* \end{aligned}$$

Therefore, by defining

$$\mathcal{T} = \mathcal{T}(\boldsymbol{h}_1')\mathcal{T}^H(\boldsymbol{h}_1') + \mathcal{T}(\boldsymbol{h}_2')\mathcal{T}^H(\boldsymbol{h}_2')$$

we can rewrite $\boldsymbol{R}_{\mathbf{YY}}$ as ($\boldsymbol{R}_{VV}$ with appropriate dimensions)

$$\boldsymbol{R}_{\mathbf{YY}} = \boldsymbol{R}_{VV} + \sigma_{tot}^2\begin{bmatrix} \mathcal{T} & \mathbf{0} \\ \mathbf{0} & \mathcal{T}^* \end{bmatrix}$$

and

$$\boldsymbol{F}\boldsymbol{R}_{\mathbf{YY}}\boldsymbol{F}^H = \sigma_v^2\left(\boldsymbol{f}_1\boldsymbol{f}_1^H + \boldsymbol{f}_2\boldsymbol{f}_2^H\right) + \sigma_{tot}^2\left[\|\boldsymbol{\alpha}_d^{11}\|^2 + \|\boldsymbol{\alpha}_d^{12}\|^2 + \|\boldsymbol{\alpha}_d^{21^*}\|^2 + \|\boldsymbol{\alpha}_d^{22^*}\|^2\right] .$$

So, neglecting $2Re\left[\boldsymbol{E}_{auto} + \boldsymbol{E}_{cross}\right]$ in the denominator of the MSE, we get

$$\begin{aligned}
MSE &= \boldsymbol{F}\boldsymbol{R}_{\mathbf{YY}}\boldsymbol{F}^H - \sigma_{tot}^2\left[\boldsymbol{f}_1\boldsymbol{h}_1\boldsymbol{h}_1^H\boldsymbol{f}_1^H + \boldsymbol{f}_1\boldsymbol{h}_2\boldsymbol{h}_2^H\boldsymbol{f}_1^H + \boldsymbol{f}_2\boldsymbol{h}_1^*\boldsymbol{h}_1^T\boldsymbol{f}_2^H + \boldsymbol{f}_2\boldsymbol{h}_2^*\boldsymbol{h}_2^T\boldsymbol{f}_2^H\right] \\
&= \boldsymbol{F}\left(\boldsymbol{R}_{\mathbf{YY}} - \sigma_{tot}^2\begin{bmatrix} \left(\boldsymbol{h}_1\boldsymbol{h}_1^H + \boldsymbol{h}_2\boldsymbol{h}_2^H\right) & \mathbf{0} \\ \mathbf{0} & \left(\boldsymbol{h}_1^*\boldsymbol{h}_1^T + \boldsymbol{h}_2^*\boldsymbol{h}_2^T\right) \end{bmatrix}\right)\boldsymbol{F}^H \\
&= \boldsymbol{F}\left(\boldsymbol{R}_{\mathbf{YY}} - \sigma_{tot}^2\begin{bmatrix} \boldsymbol{H} & \mathbf{0} \\ \mathbf{0} & \boldsymbol{H}^* \end{bmatrix}\right)\boldsymbol{F}^H \\
&= \boldsymbol{F}\begin{bmatrix} \boldsymbol{R}_{VV} + \sigma_{tot}^2\left(\mathcal{T} - \boldsymbol{H}\right) & \mathbf{0} \\ \mathbf{0} & \left(\boldsymbol{R}_{VV} + \sigma_{tot}^2\left(\mathcal{T} - \boldsymbol{H}\right)\right)^* \end{bmatrix}\boldsymbol{F}^H \\
&= \boldsymbol{F}\boldsymbol{A}\boldsymbol{F}^H
\end{aligned}$$

with

$$\begin{aligned}
\boldsymbol{R}_{VV} + \sigma_{tot}^2\left(\mathcal{T} - \boldsymbol{H}\right) &= \boldsymbol{A}_1 \\
&= \boldsymbol{R}_{VV} + \sigma_{tot}^2\left[\mathcal{T}(\boldsymbol{h}_1')\mathcal{T}^H(\boldsymbol{h}_1') + \mathcal{T}(\boldsymbol{h}_2')\mathcal{T}^H(\boldsymbol{h}_2') - \left(\boldsymbol{h}_1\boldsymbol{h}_1^H + \boldsymbol{h}_2\boldsymbol{h}_2^H\right)\right] .
\end{aligned}$$

Chapter 6

Downlink Channel Estimation

This chapter focuses on the overall channel estimation and on the (sparse) radio propagation channel approximation. First we present the general pilot-symbols based FIR channel estimation approach stated by the UMTS-FDD norm and some channel approximation algorithms along the lines of Matching Pursuit that exploit the limited bandwidth of the pulse-shape. Secondly we consider adaptive Wiener filtering for estimation of mobile (overall) channels that are modelled as autoregressive processes with a bandwidth commensurate with the Doppler spread. "Sparsification" of these refined channel estimates shows better performance w.r.t. its application to the brute FIR estimates. To conclude, we analyse the effect of channel estimation on the RAKE output SINR and we present a possible practical architecture of a RAKE receiver.

6.1 Channel Estimation and Approximation Strategies

In the discrete-time RAKE, the estimation of the path delays becomes an issue of detecting at which sampling instants a finger should be put (which may be simpler than finding continuously valued delays). A different advantage of the discrete time RAKE over the continuous-delay RAKE is that if the channel is diffuse, then the RAKE may have a problem in concentrating many paths around the same time instant. In the discrete-time RAKE, only resolvable paths will be considered (the temporal resolution is inversely proportional to the bandwidth, hence to the sampling rate). Note that

for any RAKE to give a good sparse model, the positioning of fingers should be approached as an approximation problem (much like multipulse excitation modelling in speech coding) instead of putting fingers at all positions where the output of the pulse shaping MF plus correlator give non-zero contributions.

The estimation of the channel parameters in the discrete-time RAKE has to be carried out in a different fashion compared to the classical RAKE. Indeed, to have a sparse channel representation, one should not estimate the channel at the output of the (path-wise) correlators, but apply an approximation strategy in which the convolution of the sparse channel model with the sampled pulse shape tries to approximate the sampled version of the convolution of the true channel and the pulse shape ("matching pursuit" technique). However, such an approximation approach may be more complex. The complexity just referred to is the complexity of the channel estimation. All this in an attempt to sparsify the channel model, with the goal of reducing the complexity of the matched filtering (RAKE).

In the classical channel estimation approach, a pilot sequence is correlated with the received (pilot) signal. To estimate the path delays of the sparse channel, this approach looks for the positions of the maxima in this correlation (Early-Late technique). But due to oversampling and pulse-shape filtering, spurious maxima appear in the correlation, corresponding to the sidelobes of the pulse shape. The optimal approach considers a basis decomposition of the channel impulse response with the basis functions being delayed versions of the pulse shape. The basis decomposition gets estimated by an analysis-by-synthesis technique. However, the optimal approach leads to an exhaustive search, so suboptimal approaches are needed.

6.2 Pilot Symbols Based FIR Channel Estimation

We concentrate on the downlink Dedicated Physical Channel (DPCH) of the UMTS norm, which contains some pilot symbols (postamble) for channel estimation. The general slot format of the channel is shown in Fig. 2.2. It should be noted that the number of pilot symbols can change, depending on the operational mode of the system. For the sake of (simulation) simplicity, we will consider a fixed amount of pilot chips in a slot equal to 20% of the slot itself, i.e. 512 chips out of 2560 in a slot. This percentage seems to be the average within a range varying from 1.25% to 40% of the slot (see Table 11 of [17]).

We assume that training chips are sent in every user's slot during transmission. Let's define $\boldsymbol{B}_1 = \mathsf{B}_1 \otimes \boldsymbol{I}_M$ as the block Hankel matrix containing the training chip sequence of user 1 (the user of interest here); and $\boldsymbol{Y}$ is the received signal during the

training sequence, vectors $\boldsymbol{g}_{M_p} = \left[g_1 g_2 \cdots g_{M_p}\right]^T$ and $\boldsymbol{\tau}_{M_p} = \left[\tau_1 \cdots \tau_{M_p}\right]$ contain the (complex) path amplitudes and delays ($\tau_i \in [\tau_{min}, \tau_{max}]$, the τ_i are integers here, denoting a delay in units of sampling period) of the M_p paths of the radio propagation channel; finally $\boldsymbol{P}_i(\boldsymbol{\tau}_i)$ is the matrix of the delayed pulse shape matched filters

$$\boldsymbol{P}_i\left(\boldsymbol{\tau}_i\right) = \begin{bmatrix} \vdots & & \vdots \\ p_{k-\tau_1} & \cdots & p_{k-\tau_i} \\ \vdots & & \vdots \end{bmatrix} \tag{6.1}$$

$$\boldsymbol{\tau}_i = [\tau_1 \cdots \tau_i] \qquad \boldsymbol{g}_i = [g_1 \cdots g_i]^T$$

where p_k is the oversampled root raised cosine with roll-off 0.22. The columns of $\boldsymbol{P}_i\left(\boldsymbol{\tau}_i\right)$ contain in fact samples of $p_{k-\tau}$. Then we can write the column vector containing the samples of the overall channel as $\boldsymbol{h} = \boldsymbol{P}_{M_p}\left(\boldsymbol{\tau}_{M_p}\right)\boldsymbol{g}_{M_p}$.

Due to the whiteness of the training chips, the least-squares fitting problem for the sparse channel parameters becomes

$$\begin{aligned} &\arg \min_{\boldsymbol{\tau}_{M_p}, \boldsymbol{g}_{M_p}} \left\|\boldsymbol{Y} - \boldsymbol{B}_1 \overline{\boldsymbol{P}}_{M_p}\left(\boldsymbol{\tau}_{M_p}\right)\boldsymbol{g}_{M_p}\right\|^2 \quad \approx \\ &\arg \min_{\boldsymbol{\tau}_{M_p}, \boldsymbol{g}_{M_p}} \left\|\widehat{\boldsymbol{h}} - \overline{\boldsymbol{P}}_{M_p}\left(\boldsymbol{\tau}_{M_p}\right)\boldsymbol{g}_{M_p}\right\|^2 \end{aligned} \tag{6.2}$$

where

$$\widehat{\boldsymbol{h}} = \left(\boldsymbol{B}_1^H \boldsymbol{B}_1\right)^{-1} \boldsymbol{B}_1^H \boldsymbol{Y} \approx \frac{1}{\beta} \boldsymbol{B}_1^H \boldsymbol{Y} \tag{6.3}$$

represents the brute FIR overall channel pilot-symbols based estimation, β is the training chip sequence energy and $\overline{\boldsymbol{P}}_{M_p}$ is similar to $\boldsymbol{P}_{M_p}$, but contains delayed truncated RRC. Note that the sparse channel estimation problem is separable: it becomes a two step process in which an FIR channel gets estimated in the first step and the FIR channel estimate gets approximated by a sparse model in a second step. The second step becomes Least-Squares fitting problem between the FIR estimate $\widehat{\boldsymbol{h}}$ of the overall channel and a sparse model $\boldsymbol{h} = \overline{\boldsymbol{P}}_{M_p}\boldsymbol{g}_{M_p}$ of it. The sampling rate discrete-time channel impulse response can be written as $h_k = \sum_{i=1}^{M_p} g_i p_{k-\tau_i}$. For the sake of simple notation, take anyway $\overline{\boldsymbol{P}} = \boldsymbol{P}$ in the following.

6.2.1 Recursive Least-Squares-Fitting Techniques (RLSF)

This class of techniques minimizes with respect to the path delays and amplitudes the error between the FIR estimate of the overall channel and its theoretical expression. At

each iteration (path to be added), we can reoptimize the amplitudes found in the previous steps or not (Matching Pursuit). The optimal approach would be to exhaustively search over all possible sets of M_p delays in $[\tau_{min}, \tau_{max}]$ with optimized amplitudes; in other words,

1. exhaustive search

$$\widehat{\boldsymbol{\tau}} = \arg \min_{\boldsymbol{\tau} \in [\tau_{min}, \tau_{max}]^{M_p}} \left\{ \min_{\boldsymbol{g}_{M_p}} \| \widehat{\boldsymbol{h}} - \boldsymbol{P}_{M_p} \left(\boldsymbol{\tau}_{M_p} \right) \boldsymbol{g}_{M_p} \|^2 \right\} \tag{6.4}$$

but three suboptimal recursive (iterative) techniques are envisaged:

2. Without amplitude reoptimization ("matching pursuit")

   for $i = 1, \cdots, M_p$

$$\widehat{\tau}_i = \arg \min_{\tau_i \in [\tau_{min}, \tau_{max}]} \left\{ \underbrace{\min_{g_i} \| \widehat{\boldsymbol{h}} - \widehat{\boldsymbol{P}}_i \widehat{\boldsymbol{g}}_i \|^2}_{\rightarrow \widehat{g}_i^{(i)}} \right\} \tag{6.5}$$

   end

   where $\widehat{\boldsymbol{P}}_i = \boldsymbol{P}_i \left(\widehat{\tau}_1, \cdots, \widehat{\tau}_{i-1}, \tau_i \right)$ and $\widehat{\boldsymbol{g}}_i = \left[\widehat{g}_1^{(1)}, \cdots, \widehat{g}_{i-1}^{(i-1)}, g_i \right]^T$

3. With only final amplitude reoptimization

   for $i = 1, \cdots, M_p$

$$\widehat{\tau}_i = \arg \min_{\tau_i \in [\tau_{min}, \tau_{max}]} \left\{ \min_{g_i} \| \widehat{\boldsymbol{h}} - \widehat{\boldsymbol{P}}_i \widehat{\boldsymbol{g}}_i \|^2 \right\} \tag{6.6}$$

   end
   $\widehat{\boldsymbol{g}}_{M_p} = \arg \min_{\boldsymbol{g}_{M_p}} \| \widehat{\boldsymbol{h}} - \widehat{\boldsymbol{P}}_{M_p}^H \widehat{\boldsymbol{g}}_{M_p}^H \|^2$

4. With intermediate amplitude reoptimization

   for $i = 1, \cdots, M_p$

$$\widehat{\tau}_i = \arg \min_{\tau_i \in [\tau_{min}, \tau_{max}], \boldsymbol{g}_i} \| \widehat{\boldsymbol{h}} - \widehat{\boldsymbol{P}}_i \boldsymbol{g}_i \|^2 \tag{6.7}$$

   end

These three suboptimal recursive techniques are put in order of increasing performance, so algorithm 6.7 gives the best suboptimal technique.

6.2.2 Recursive Early-Late (REL)

This technique derives from the basic Early-Late approach, which maximizes, with respect to the path delays, the correlation between the received signal and the training sequence convolved with the pulse shape. In other words, Early-Late finds the M_p largest peaks in the correlation sequence. Recursive Early-Late (REL) corresponds to applying the Matching Pursuit technique to the convolution between the FIR estimate of the overall channel $\widehat{h}_k$ and the pulse-shape matched filter (p^*_{-k}). In matrix notation (when reoptimizing jointly by LS the amplitudes):

$\boldsymbol{P}_0 = 0 \quad \widehat{\boldsymbol{g}}_0 = 0$

for $i = 1, \cdots, M_p$

$$\begin{aligned} \widehat{\tau}_i &= \arg\max_{\tau} |\boldsymbol{P}_1^H(\tau) \left(\widehat{\boldsymbol{h}} - \boldsymbol{P}_{i-1}(\widehat{\boldsymbol{\tau}}_{i-1}) \widehat{\boldsymbol{g}}_{i-1} \right)|^2 \\ \widehat{\boldsymbol{g}}_i &= \left(\boldsymbol{P}_i^H(\widehat{\boldsymbol{\tau}}_i) \boldsymbol{P}_i(\widehat{\boldsymbol{\tau}}_i) \right)^{-1} \boldsymbol{P}_i^H(\widehat{\boldsymbol{\tau}}_i) \widehat{\boldsymbol{h}} \end{aligned} \tag{6.8}$$

end

where multiplying with $\boldsymbol{P}_1^H(\tau)$ for all τ corresponds to convolving with p^*_{-k}. At each iteration the algorithm subtracts the contributions of previously found delayed pulse shapes, so that the corresponding spurious maxima don't interfere in the delay searching.

The reoptimization could be done only for the amplitude of the current iteration, in which case we have: $\widehat{g}_i = \left(\boldsymbol{P}_1^H(\widehat{\tau}_i) \boldsymbol{P}_1(\widehat{\tau}_i) \right)^{-1} \boldsymbol{P}_1^H(\widehat{\tau}_i) \widehat{\boldsymbol{h}}$. In this last case, if $f_k^0 = f_k = \widehat{h}_k * p^*_{-k}$ and $q_k = p_k * p^*_{-k}$, the loop is:

for $i = 1, \cdots, M_p$ *or until* $\dfrac{||\boldsymbol{f}^i||^2}{||\boldsymbol{f}||^2} < \mu$

$$\begin{aligned} \tau_i &= \arg\max_k |f_k^{i-1}|^2 \\ g_i &= f_{\tau_i} / q_0 \\ f_k^i &= f_k - \sum_{l=1}^{i} g_l \, q_{k-\tau_l} \quad = f_k^{i-1} - g_i \, q_{k-\tau_i} \end{aligned} \tag{6.9}$$

end

where, for example, $\mu = 0.1$.

6.2.3 SINR Degradation

We assume a specular channel model and we assume that the number of paths for the estimated channel equals the number of paths in the true channel, M_p. We shall analyse

the SINR degradation due to channel estimation for a fictitious estimator that somehow knows how to put the discrete-time delays optimally. The performance results thus obtained will represent a bound for the actual performance of the algorithms considered in the previous section. We will also specialize here in a first instance the results to the case in which the true channel delays happen to fall at discrete-time instants. In that case it is immediate to define the optimal discrete-time delays.

Assume N is the channel length in chip periods and the FIR filter $\boldsymbol{f}$ is an estimate of the overall channel (pulse-shape plus radio propagation channel) matched filter, that is $\boldsymbol{f}^H = \widehat{\boldsymbol{h}} = \boldsymbol{h} + \widetilde{\boldsymbol{h}}$ ($\widetilde{\boldsymbol{h}}$ is the channel estimation error - we take here $\boldsymbol{f}$ to have the same length and position as the channel matched filter). Let's define N_P as the number of training chips, $\sigma^2_{k,P}$ as the variance of training symbols for user k and $\mathsf{P} = \widehat{\boldsymbol{P}}_{M_p}\left(\widehat{\boldsymbol{P}}^H_{M_p}\widehat{\boldsymbol{P}}_{M_p}\right)^{-1}\widehat{\boldsymbol{P}}^H_{M_p}$ as the projection on the subspace spanned by the columns of $\widehat{\boldsymbol{P}}^H_{M_p}$, then we can rewrite the (numerator and denominator) averaged SINR as

$$\begin{aligned} SINR &= \frac{\sigma_1^2 E|\widehat{\boldsymbol{h}}^H\boldsymbol{h}|^2}{E\left\{\widehat{\boldsymbol{h}}^H\boldsymbol{R}_{YY}\widehat{\boldsymbol{h}} - \frac{\sigma^2_{tot}}{L}|\widehat{\boldsymbol{h}}^H\boldsymbol{h}|^2\right\}} \\ &= \frac{\sigma_1^2 E|\widehat{\boldsymbol{h}}^H\boldsymbol{h}|^2}{\boldsymbol{h}^H\mathsf{P}\boldsymbol{R}_{YY}\mathsf{P}\boldsymbol{h} + Tr\left\{\boldsymbol{R}_{YY}\boldsymbol{C}_{\widetilde{h}\widetilde{h}}\right\} - \frac{\sigma^2_{tot}}{L}E|\widehat{\boldsymbol{h}}^H\boldsymbol{h}|^2} \end{aligned} \tag{6.10}$$

where E denotes expectation, $Tr\{\boldsymbol{A}\}$ trace of matrix $\boldsymbol{A}$ and $\boldsymbol{C}_{\widetilde{h}\widetilde{h}}$ the covariance matrix of the channel estimation error, whose expression is given at the end of this section. In the case of "no delay approximation" ($\widehat{\boldsymbol{P}}_{M_p} = \boldsymbol{P}_{M_p} \Rightarrow \mathsf{P}\boldsymbol{h} = \boldsymbol{h}$) and $\frac{N_P}{N} \to \infty$ it is possible to show (see appendix 6.A) that the averaged SINR becomes approximately:

$$SINR = \frac{\sigma_1^2\, a}{\sigma_v^2\|\boldsymbol{h}\|^2 + \frac{\sigma^2_{tot}}{L}\left(\|\boldsymbol{\alpha}_h\|^2 - a\right) + b} \tag{6.11}$$

where

$$\begin{aligned} a &= \|\boldsymbol{h}\|^4 + \frac{\sigma_v^2 L}{\sigma^2_{1,P}N_P}\|\boldsymbol{h}\|^2 + \frac{\sigma^2_{tot,P} - \sigma^2_{1,P}}{\sigma^2_{1,P}N_P}\|\boldsymbol{\alpha}_h\|^2 \\ b &= \frac{1}{\sigma^2_{1,P}N_P}\left(L\sigma_v^4 M_p + \sigma_v^2\left(\sigma^2_{tot} + \sigma^2_{tot,P} - \sigma^2_{1,P}\right)Tr\{\boldsymbol{C}\}\right) + \\ &\quad + \frac{1}{\sigma^2_{1,P}N_P}\left(\frac{\sigma^2_{tot}}{L}\left(\sigma^2_{tot,P} - \sigma^2_{1,P}\right)Tr\{\boldsymbol{C}^2\}\right) \\ \boldsymbol{C} &= \mathsf{P}\mathcal{T}(\boldsymbol{h}')\mathcal{T}^H(\boldsymbol{h}')\mathsf{P}\,. \end{aligned}$$

The power $\sigma^2_{tot,P}$ denotes the total training symbol power, $\sigma^2_{tot,P} = \sum_{k=1}^K \sigma^2_{k,P}$ and $\boldsymbol{\alpha}_h$ is the channel-channel matched filter cascade impulse response, i.e. $\boldsymbol{\alpha}_h =$

$\boldsymbol{h}^H \mathcal{T}(\boldsymbol{h}')$, so that $\alpha_N = \boldsymbol{h}^H \boldsymbol{h} = \|\boldsymbol{h}\|^2$. $\mathcal{T}(\boldsymbol{h}')$ is a block Toeplitz filtering matrix with the zero padded $\boldsymbol{h}' = [\boldsymbol{h}_0 \cdots \boldsymbol{h}_{N-1}]$ as first block row.

The Normalized Mean Square channel estimation Error (NMSE) is given by

$$\begin{aligned} NMSE &= \frac{Tr\{\boldsymbol{C}_{\widetilde{h}\widetilde{h}}\}}{\|\boldsymbol{h}\|^2} \\ \text{with} \quad \boldsymbol{C}_{\widetilde{h}\widetilde{h}} &= \frac{L\sigma_v^2}{\sigma_{1,P}^2 N_p}\mathsf{P} + \frac{\sigma_{tot,P}^2 - \sigma_{1,P}^2}{\sigma_{1,P}^2 N_p}\mathsf{P}\mathcal{T}(\boldsymbol{h}')\mathcal{T}^H(\boldsymbol{h}')\mathsf{P} \end{aligned} \tag{6.12}$$

These SINR expressions for the downlink RAKE allow us to make the following observations. First, in the absence of channel estimation error, the SINR is not the same when the (intracell) interference gets replaced by white noise of the same power. Second, the effect of channel estimation error is not quite the same as when one treats the channel estimation error as an increase in additive noise.

6.2.4 Numerical example

In figures 6.1 and 6.2, "G estim" refers to a RAKE RX that knows the true delays but estimates the amplitudes of every path by LS fitting, "EL-LS estim" refers to a RAKE RX that estimates the propagation channel by the basic Early-late approach (puts the delays at the largest samples of $\hat{h}_k * p^*_{-k}$ and performs LS optimization of the amplitudes), "LS-OPT estim" refers to a RAKE RX that approximates the propagation channel by the best suboptimal RLSF technique of equation 6.7, "rec EL-LS estim" refers to a RAKE RX that approximates the propagation channel by REL (section 6.2.2) and "Analysis" to the theoretical performance when the true delays are integer multiples of the sampling period (see section 6.2.3).

In Fig. 6.1, the environment is UMTS Indoor, which has 2 paths, delay spread of about 1 μs, -10 dB average power of the second path w.r.t. the first, spreading factor is $L = 8$ with $K = 2$ users transmitting with the same power and 20% of the slot symbols are considered training symbols. In Fig. 6.2 we have the same other parameters, but $K = 4$ and the second path has the same average power of the first, giving more temporal diversity to compensate the greater number of users (increased MAI).

We can note how the NMSE performance of the REL approach is closer to the performance of a RAKE that knows the true delay ("G estim" curve) than the RLSF techniques performance and much closer than the basic EL performance.

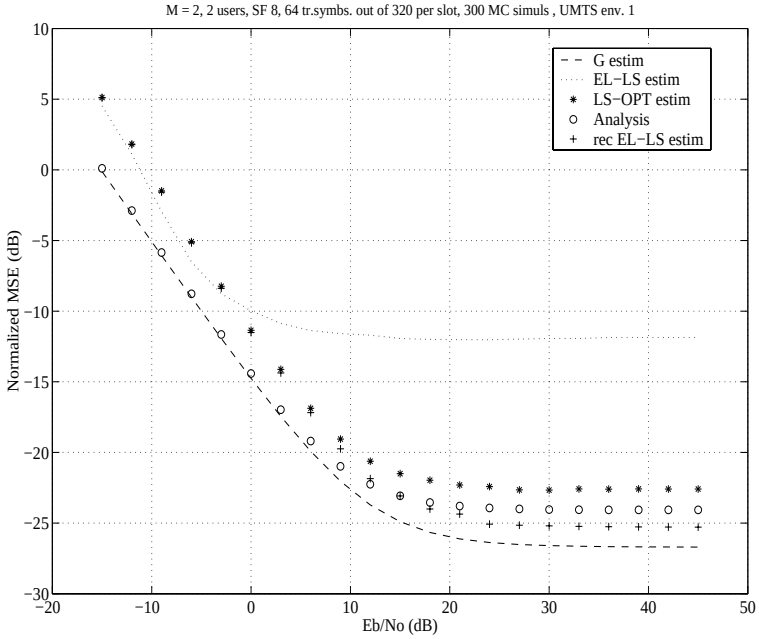

Figure 6.1: Channel Approximation NMSE versus E_b/N_0, UMTS env. 1

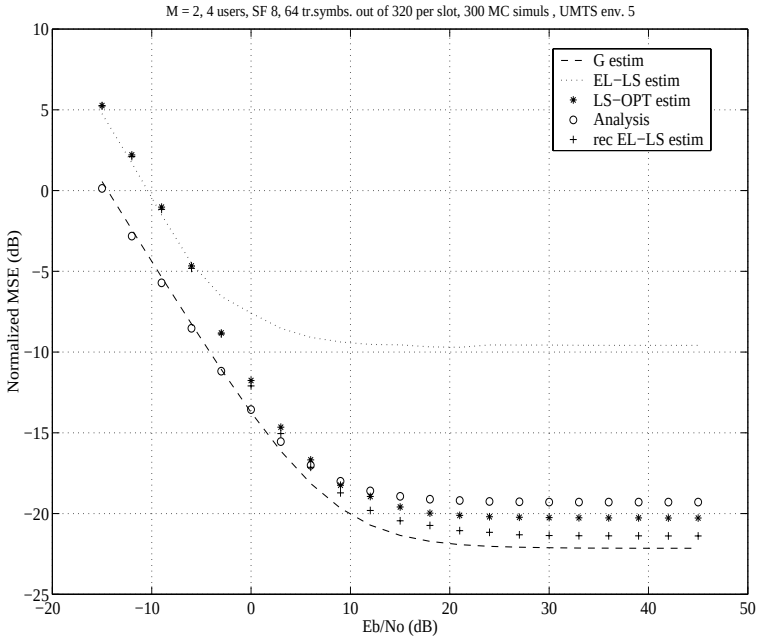

Figure 6.2: Channel Approximation NMSE versus E_b/N_0, UMTS env. 5

6.3 Autoregressive Channel Estimation

We consider the estimation of mobile channels that are modelled as autoregressive processes with a bandwidth commensurate with the Doppler spread. Pilot based estimation leads to brute FIR channel estimates on a slot by slot basis. These estimates are then refined by Wiener filtering across slots that performs the optimal compromise between temporal decorrelation due to Doppler spread and slot-wise estimation error. The sparse channel representation is done via an approximation strategy in which the convolution of the discrete-time sparse channel model $\widehat{h}_k^{pr}$ with the sampled pulse-shape p_k approximates the sampled version of the convolution $p(t) * h_{pr}(t)$ of the true channel and the pulse-shape.

The user codes considered are aperiodic, due to fact that a cell-dependent scrambling gets superposed to the user-dependent spreading; scrambling does not destroy the orthogonality between the intracell users, but it destroys the symbol-interval cyclostationarity of the CDMA signals, making the techniques derived for periodic (short) codes non applicable, e.g. [41].

Previous results in the context of channel estimation in aperiodic-code downlink systems either have computational complexity not suited for MS real-time implementation or they need knowledge of the propagation delays, e.g. [42], [43]. In [44], a multi-rate pilot-aided Least-Squares approach is presented for both the uplink and the downlink, with the possibility of recursive implementation. They assume, however, the use of rectangular pulse-shape filter. They use a Least-Squares-based procedure on the received signal (symbol) samples, which can still lead to high computational complexity for low-rate users.

Pilot-assisted channel estimation operates generally on a slot-by-slot basis, without exploiting the temporal correlation of the channel coefficients of adjacent slots. In [45], an average of the FIR estimate over slots is performed on the basis of a Karhunen-Loéve decomposition of the channel tap autocorrelation function. By applying optimal Wiener filtering across slots, we can provide an alternative approach to refine the brute FIR pilot-based estimates, optimally compromising between temporal decorrelation (Doppler spread) and slot-wise estimation error. We furthermore propose adaptive filtering techniques to implement the optimal filtering.

In the context of the 3G UMTS W-CDMA FDD downlink system, we consider the impulse response (at sampling rate) of the radio channel from the base station BS to a mobile station MS as $h(t,\tau) = \sum_{i=1}^{M_p} g_i(t)p(\tau - \tau_i(t))$, the convolution of a sparse multipath propagation channel containing M_p paths with a pulse-shape filter (transmitter filter).

The receiver samples M times per chip the lowpass filtered received signal. Stacking the M samples per chip period in vectors, we get the discrete-time representation of the mobile channel at chip rate $\boldsymbol{h}_l = [h_{1,l} \cdots h_{M,l}]^T$, which represents the vectorized samples of the overall channel, including pulse shape, propagation channel and receiver filter. The overall channel is assumed to have a delay spread of N chips, so in matrix notation, we have $\boldsymbol{h}(n) = \boldsymbol{P}\boldsymbol{g}(n)$ where $\boldsymbol{h} = [\boldsymbol{h}_1 \cdots \boldsymbol{h}_N]^T \in \mathcal{C}^{MN\times 1}$, $\boldsymbol{g} = \left[g_1 \cdots g_{M_p}\right] \in \mathcal{C}^{M_p\times 1}$ are the complex path amplitudes and the temporal index n is related to the transmission of slot n from the BS to the MS. We consider the channel constant over a slot. If we consider the delays $\tau_i(t)$ constant in a particular environment (we can assume this even in the case of relatively high mobile speed), the pulse-shape convolution matrix $\boldsymbol{P} = \boldsymbol{P}_{M_p} \in \mathcal{R}^{MN\times M_p}$ (see equation 6.1) of the delayed pulse shape responses is constant.

In order to have a simple model for the evolution of the complex path amplitudes over slots and to have low complexity associated optimal filtering algorithms, we can model their variation with an autoregressive (AR) process of order sufficiently high to characterize the Doppler spectrum. If we want to match only the channel bandwidth with the Doppler spread, the resulting first-order AR(1) model is

$$\begin{aligned}
&\boldsymbol{g}(n) = \rho\,\boldsymbol{g}(n-1) + \sqrt{1-\rho^2}\Delta\boldsymbol{g}(n) \qquad \text{where} \\
&\rho \;=\; \text{channel temporal correlation factor} \\
&\quad =\; 2 - \cos 2\pi f_{3dB} - \sqrt{\left(2-\cos 2\pi f_{3dB}\right)^2 - 1} \\
&f_{3dB} = \frac{v}{c} f_c\, SP \qquad \text{where} \quad \text{SP = slot period,} \\
&v, c = \text{mobile,light speed} \qquad f_c = \text{carrier frequency} \\
&\sigma^2_{g_k} = \sigma^2_{\Delta g_k}
\end{aligned} \tag{6.13}$$

Therefore, because of $\boldsymbol{P}$ being constant, we have

$$\begin{aligned}
\boldsymbol{h}(n) &= \rho\boldsymbol{h}(n-1) + \sqrt{1-\rho^2}\Delta\boldsymbol{h}(n) \\
&= \frac{\sqrt{1-\rho^2}}{1-\rho q^{-1}}\Delta\boldsymbol{h}(n)\,.
\end{aligned} \tag{6.14}$$

q^{-1} denotes the delay operator: $q^{-1}y(n) = y(n-1)$. Variance of $h_k(n)$ (component k of $\boldsymbol{h}(n)$): $\sigma^2_{h_k} = \sigma^2_{\Delta h_k} = \boldsymbol{P}_k\boldsymbol{D}\boldsymbol{P}_k^H$ where $\boldsymbol{P}_k = k^{th}$ line of $\boldsymbol{P}$ and $\boldsymbol{D} = \text{diag}\,\{\sigma^2_{\Delta g_1}, \sigma^2_{\Delta g_2}, \ldots\}$.

6.3.1 Optimal Wiener Filtering and its RLS Adaptation

If at the receiver we get/have an estimate of the overall channel, $\widehat{\boldsymbol{h}}(n)$, a channel estimation error $\widetilde{\boldsymbol{h}}$ has to be considered, $\widehat{\boldsymbol{h}}(n) = \boldsymbol{h}(n) + \widetilde{\boldsymbol{h}}(n)$, where $\boldsymbol{h}$ and $\widetilde{\boldsymbol{h}}$ are mutually

uncorrelated, the components of $\widetilde{\boldsymbol{h}}$ are uncorrelated and their variance depends on the training symbol power, on the mobile speed and on the SINR, and is independent of position k.

To refine the estimate of the overall channel $\widehat{\boldsymbol{h}}(n)$, we propose to process it over slots with the optimal causal Wiener filter. The refined estimate $\widehat{\widehat{\boldsymbol{h}}}(n)$ is of the form $\widehat{\widehat{\boldsymbol{h}}}(n) = H(q)\widehat{\boldsymbol{h}}(n)$ where $H(q)$ represents the optimal Wiener filter (of unlimited order).

For every component of the channel estimate we can then write

$$\begin{aligned} \widehat{\widehat{h}}_k(n) &= H_k(q)\widehat{h}_k(n) \\ H_k(q) &= \frac{1}{S^+_{\widehat{h}_k\widehat{h}_k}(q)} \left\{ \frac{S_{h_k h_k}(q)}{S^-_{\widehat{h}_k\widehat{h}_k}(q)} \right\}^+ \end{aligned} \tag{6.15}$$

where $S_{xx}(q)$ is the power spectral density (PSD) of x, $\{\bullet\}^+$ means "take the causal part of" and $S_{xx}(q) = S^+_{xx}(q)S^-_{xx}(q)$ is the spectral factorisation of $S_{xx}(q)$ in its causal minimum-phase factor and in its anti-causal maximum-phase counterpart. It turns out that, for an AR(1) model for the channel amplitudes given in (6.14), the PSD of $\widehat{h}_k(n)$ is

$$\begin{aligned} S_{\widehat{h}_k\widehat{h}_k}(q) &= S_{h_k h_k}(q) \; + \sigma^2_{\widetilde{h}_k} \\ &= \frac{\left(1-\rho^2\right)\sigma^2_{h_k}}{\left(1-\rho q^{-1}\right)\left(1-\rho q\right)} \; + \sigma^2_{\widetilde{h}_k} \\ &= \sigma^2_{\widetilde{h}_k} \frac{a_k\left(1-b_k q^{-1}\right)\left(1-b_k q\right)}{\left(1-\rho q^{-1}\right)\left(1-\rho q\right)} \end{aligned}$$

where

$$\begin{aligned} b_k &= \left(\overline{J}_k - \sqrt{\left(\overline{J}_k\right)^2 - 4\rho^2}\right)(2\rho)^{-1} \\ a_k = \frac{\rho}{b_k} &= \frac{2\rho^2}{\overline{J}_k - \sqrt{\left(\overline{J}_k\right)^2 - 4\rho^2}} \\ \overline{J}_k &= 1 + \rho^2 + \left(1-\rho^2\right)J_k \\ J_k &= \frac{\sigma^2_{h_k}}{\sigma^2_{\widetilde{h}_k}} \quad \text{channel estimation SNR} \end{aligned} \tag{6.16}$$

Hence

$$\begin{aligned} S^{+}_{\widehat{h}_k\widehat{h}_k}(q) &= \sigma_{\widetilde{h}_k}\sqrt{a_k}\frac{1-b_kq^{-1}}{1-\rho q^{-1}} \\ S^{-}_{\widehat{h}_k\widehat{h}_k}(q) &= \sigma_{\widetilde{h}_k}\sqrt{a_k}\frac{1-b_kq}{1-\rho q} \\ \left\{\frac{S_{h_kh_k}(q)}{S^{-}_{\widehat{h}_k\widehat{h}_k}}\right\}^{+} &= \left\{\frac{\gamma_k q}{1-b_kq}+\frac{\beta_k}{1-\rho q^{-1}}\right\}^{+} \\ &= \frac{\beta_k}{1-\rho q^{-1}} \end{aligned} \tag{6.17}$$

where

$$\begin{aligned} \beta_k &= \frac{\left(1-\rho^2\right)\sigma^2_{h_k}}{\sigma_{\widetilde{h}_k}\sqrt{a_k}\left(1-b_k\rho\right)} \\ \gamma_k &= \beta_k b_k \end{aligned}$$

Substituting (6.17) in (6.15), we have

$$\begin{aligned} H_k(q) &= \frac{\beta_k}{\sigma_{\widetilde{h}_k}\sqrt{a_k}\left(1-b_kq^{-1}\right)} \\ \Rightarrow \quad \widehat{\widehat{h}}_{k,n} &= b_k\,\widehat{\widehat{h}}_{k,n-1}+\alpha_k\,\widehat{h}_{k,n} \end{aligned} \tag{6.18}$$

where b_k is given in (6.16) and

$$\alpha_k = \frac{\beta_k}{\sigma_{\widetilde{h}_k}\sqrt{a_k}} = \frac{\sigma^2_{h_k}}{\sigma^2_{\widetilde{h}_k}}\frac{\left(1-\rho^2\right)}{\rho\left(1-b_k\rho\right)}b_k\ . \tag{6.19}$$

When there is no time correlation ($\rho = 0$) over slots, we have $b_k = 0$ and $\alpha_k = \frac{\sigma^2_{h_k}}{\sigma^2_{h_k}+\sigma^2_{v_k}}$, that is the filtering weights every component taking into account a priori variance information and channel estimation error.

Having in mind the optimal Wiener filtering of (6.18), we would like to minimize the squared error between the true overall channel delay $h_k(n)$ and its refined estimate $\widehat{\widehat{h}}_k(n)$, by adapting the two coefficients b_k and α_k to adapt to the Doppler speed of the overall channel taps. We can show that this minimization is equivalent to the minimization of the mean square difference between $\widehat{h}_k(n)$ and $\widehat{\widehat{h}}_k(n)$ (realizable practically) when corrected with a factor dependent only on α_k and $\sigma^2_{\widetilde{h}_k}$. Indeed

$$\begin{aligned} & E|\widehat{\widehat{h}}_k(n)-h_k(n)|^2 \\ &= E|b_k\widehat{\widehat{h}}_k(n-1)+\alpha_k\widehat{h}_k(n)-h_k(n)|^2 \\ &= E|b_k\widehat{\widehat{h}}_k(n-1)+(\alpha_k-1)h_k(n)|^2+\alpha_k^2\sigma^2_{\widetilde{h}_k} \end{aligned}$$

and

$$\begin{aligned}
&E|\widehat{\widehat{h}}_k(n) - \widehat{h}_k(n)|^2 \\
&= E|b_k\widehat{\widehat{h}}_k(n-1) + (\alpha_k - 1)\widehat{h}_k(n)|^2 \\
&= E|b_k\widehat{\widehat{h}}_k(n-1) + (\alpha_k - 1)h_k(n)|^2 + (\alpha_k - 1)^2\sigma^2_{\tilde{h}_k}
\end{aligned}$$

Therefore $E|\widehat{\widehat{h}}_k(n) - \widehat{h}_k(n)|^2 + \delta_k$ behaves like $E|\widehat{\widehat{h}}_k(n) - h_k(n)|^2$ (where $\delta_k = (\alpha_k^2 - (\alpha_k - 1)^2)\sigma^2_{\tilde{h}_k} = (2\alpha_k - 1)\sigma^2_{\tilde{h}_k}$).

Introducing temporal averaging over slots, with exponential weighting, we formulate now the RLS adaptation algorithm for the minimization problem stated above. Derivatives with respect to b_k and α_k of (here slot timing is indicated by the second subscript)

$$\sum_{i=0}^{n} \lambda^{n-i} \left(\left| b_k \widehat{\widehat{h}}_{k,n-i-1} + (\alpha_k - 1)\widehat{h}_{k,n-i} \right|^2 + (2\alpha_k - 1)\sigma^2_{\tilde{h}_k} \right)$$

are forced to zero to give the recursive solution for each component k of the overall channel at each slot n

$$\left\{ \begin{array}{lcl}
\boldsymbol{R}_n &=& \lambda \boldsymbol{R}_{n-1} + Re\left\{ \begin{bmatrix} \widehat{\widehat{h}}_{k,n-1} \\ \widehat{h}_{k,n} \end{bmatrix} \begin{bmatrix} \widehat{\widehat{h}}_{k,n-1} \\ \widehat{h}_{k,n} \end{bmatrix}^H \right\} \\
\boldsymbol{P}_n &=& \lambda \boldsymbol{P}_{n-1} - \begin{bmatrix} 0 \\ \sigma^2_{\tilde{h}_k} \end{bmatrix} \\
\boldsymbol{\theta}_n &=& \begin{bmatrix} b_k \\ \alpha_k - 1 \end{bmatrix} = \boldsymbol{R}_n^{-1}\boldsymbol{P}_n
\end{array} \right. \tag{6.20}$$

where $Re\{\bullet\}$ means "take real part of". Since the number of coupled parameters is only two, one may as well invert the 2×2 matrix rather than using true RLS. Initialisation of the algorithm requires only R_0 to be different from zero, so we can set it to $R_0 = 10^{-3}\boldsymbol{I}$; furthermore, $\widehat{\widehat{\boldsymbol{h}}}_{k,0} = \widehat{\boldsymbol{h}}_{k,1}$.

6.3.1.1 Channel Estimation Error Variance Estimation

$\sigma^2_{\tilde{h}} = \sigma^2_{\tilde{h}_k} = \sigma^2_{\tilde{h}_k}$ for impulse response samples k at which $h_k(n) \approx 0$. Hence $\sigma^2_{\tilde{h}}$ can be estimated from $\widehat{h}_k$ at delays k where we don't expect the channel to contain any energy. For example by overestimating the delay spread, we can use the tail of the channel estimate to obtain an unbiased estimate of $\sigma^2_{\tilde{h}}$ (averaging across slots and across delays k for which $\widehat{h}_k \equiv 0$ can be performed.

Alternatively, in order not to increase the length of the channel impulse response to be estimated, we can estimate $\sigma^2_{\tilde{h}}$ from the $\widehat{h}_k$ with smallest variance. Consider the

variance estimates $\sigma^2_{\widehat{h}_k}(n) = \xi\sigma^2_{\widehat{h}_k}(n-1) + (1-\xi)|\widehat{h}_k(n)|^2$. Note that $\sigma^2_{\widehat{h}}$ is averaged over channel realizations, and hence will only change with changes in channel fading statistics and user powers. Therefore, a long time constant $\frac{1}{1-\xi}$ can be used here, leading to accurate estimates. Assume that the impulse response h_k contains I samples $\{h_{k_i}, i = 1, \ldots, I\}$ such that $\sigma^2_{h_{k_i}} = 0$ or is sufficiently small (tails of the pulse shape). Let $\{k_i\}$ represent a reordering of the variance estimates $\sigma^2_{\widehat{h}_k}(n)$ such that $\sigma^2_{\widehat{h}_{k_1}} \leq \sigma^2_{\widehat{h}_{k_2}} \leq \cdots \leq \sigma^2_{\widehat{h}_{k_{MN}}}$. Then we can estimate $\sigma^2_{\widehat{h}}(n) = \frac{1}{I}\sum_{i=1}^{I}\sigma^2_{\widehat{h}_{k_i}}(n)$. This gives in principle a slightly underestimated and hence a biased estimate of $\sigma^2_{\widehat{h}}$. However, this bias will in practice tend to be offset by an energy increase because of leakage from the pulse shape tails.

6.3.1.2 Numerical examples

We apply the REL algorithm of section 6.2.2 to the refined FIR overall channel estimate $\widehat{\widehat{\boldsymbol{h}}}(n)$ instead of to the slotwise estimate $\widehat{\boldsymbol{h}}(n)$ in 6.3.

From equations 4.7 and 4.14, we have that the SINR at RAKE output, Γ_R, is

$$\Gamma_R = \frac{E\left\{\sigma_1^2|\boldsymbol{f}(n)\boldsymbol{h}(n)|^2\right\}}{E\left\{\boldsymbol{f}(n)R_{YY}\boldsymbol{f}^H(n) - \frac{\sigma^2_{tot}}{SF}|\boldsymbol{f}(n)\boldsymbol{h}(n)|^2\right\}}$$

where $\boldsymbol{f}$ is the overall channel MF built with the estimated channel from the REL approach (e.g. in the true channel case, we have $\boldsymbol{f} = \boldsymbol{h}^H(n)$), $\sigma_k^2 = \mathrm{E}\,|a_{k,n}|^2$ (a being the symbols sent by the BS), $\sigma^2_{tot} = \sum_{k=1}^{K}\sigma_k^2$ and
$R_{YY} = \sigma_v^2 I + \frac{\sigma^2_{tot}}{SF}\mathcal{T}(\boldsymbol{h}(n))\mathcal{T}^H(\boldsymbol{h}(n))$ is the covariance matrix of the received signal, where $\mathcal{T}(\boldsymbol{h}(n))$ is the (block) Toeplitz convolution matrix with the impulse response $\boldsymbol{h}(n)$ and $R_{VV} = \sigma_v^2 I$ is the noise model (which can be extended to a banded block Toeplitz matrix model).

In figures 6.3 to 6.10, "true ch" refers to a RAKE receiver that has complete knowledge of the channel, "REL FIR" refers to a RAKE that estimates the overall channel via REL on the FIR brute estimate $\hat{h}(n)$, "REL OPT" refers to a RAKE with REL on $\hat{\hat{h}}_{n,k}$ of (6.18) that uses the optimal b_k of (6.16) and α_k of (6.19), "REL EST" refers to a RAKE with REL on $\hat{\hat{h}}_{n,k}$ with filtering parameters b_k and α_k determined by adaptive filtering (6.20),"REL FIX" refers to a RAKE with REL on the estimate $\hat{\hat{h}}_{n,k}$ where the two coefficients b_k and α_k are fixed (for every component of the overall channel) to ρ and $(1-\rho)$ respectively (the ρ of the AR(1) channel model).

In Fig. 6.3 to Fig. 6.6, the environment is UMTS Pedestrian (Ped: 3 km/h, 2 paths, delay spread of about 1 μs, equal average power of the two paths); in Fig. 6.7 to Fig. 6.10, the environment is UMTS Vehicular (Veh: 120 km/h, 4 paths, delay spread

of 4 chip periods, exponentially decaying average power of the paths); spreading factor is always $SF = 64$ with 5 or 32 users transmitting with equal power and 20% of the slot symbols are considered training symbols; the forgetting factor λ of the RLS algorithm is always 0.99.

We can notice how the SINRs of the various REL implementations are very close to each other, in the SNR range of interest, when few users are active in the system. On the other hand, multi user interference (MUI) degrades channel estimation and hence further degrades SINR, more for non optimal refining as "REL FIR" or "REL FIX". We can also notice how the NMSE of the "REL EST" channel estimate is always close to the NMSE of the optimal "REL OPT" channel estimate, even in high MUI situation.

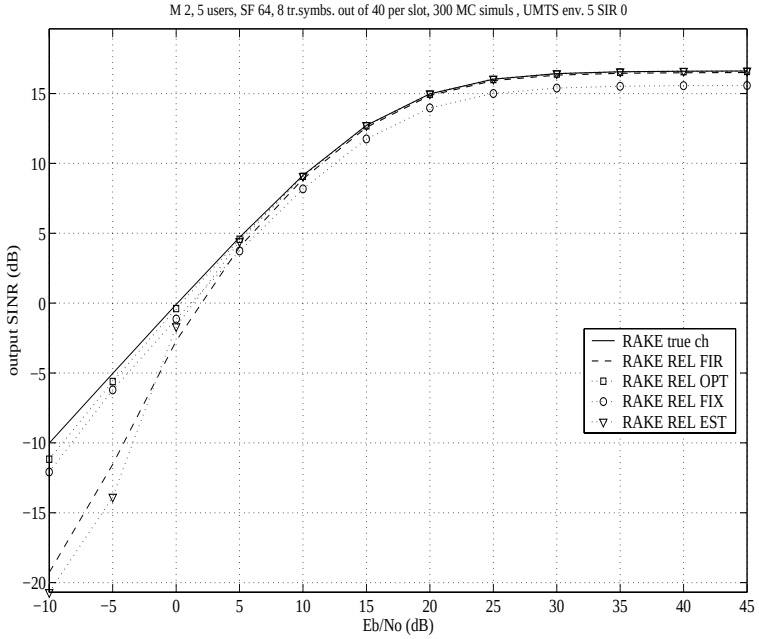

Figure 6.3: Pedestrian, 3 Km/h, $\lambda = 0.99$, 5 users: SINR vs. E_b/N_0

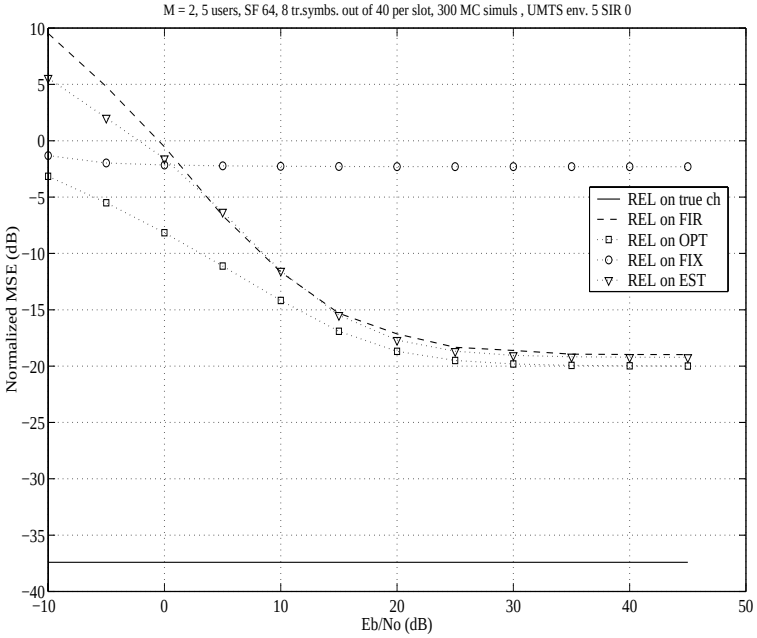

Figure 6.4: Pedestrian, 3 Km/h, $\lambda = 0.99$, 5 users: NMSE vs. E_b/N_0

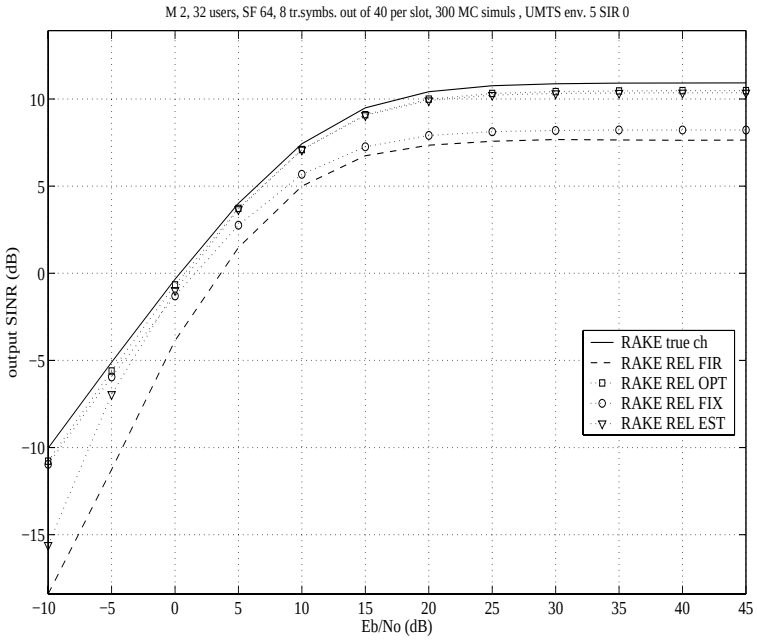

Figure 6.5: Pedestrian, 3 Km/h, $\lambda = 0.99$, 32 users: SINR vs. E_b/N_0

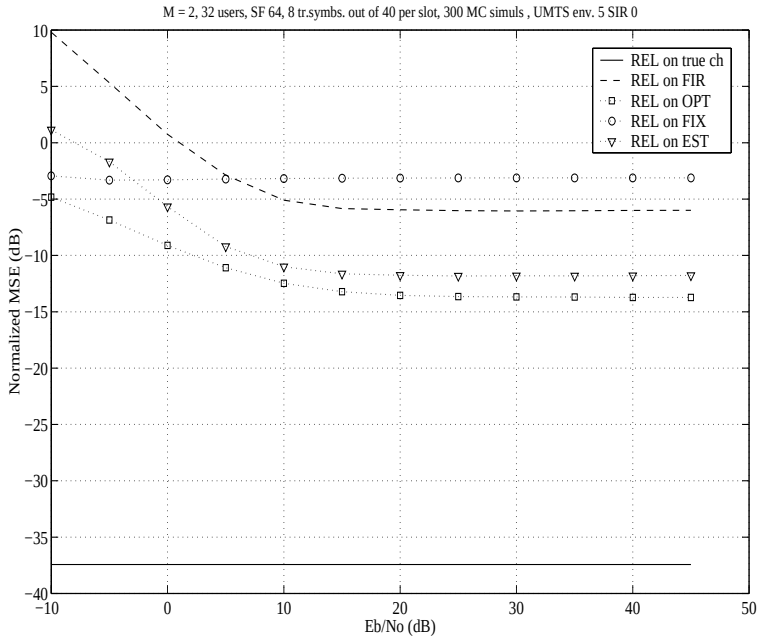

Figure 6.6: Pedestrian, 3 Km/h, $\lambda = 0.99$, 32 users: NMSE vs. E_b/N_0

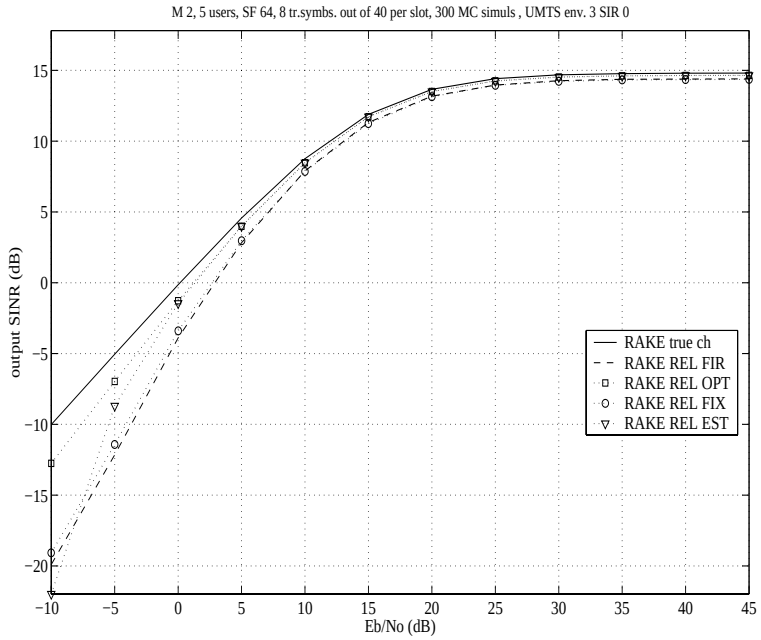

Figure 6.7: Vehicular, 120 Km/h, $\lambda = 0.99$, 5 users: SINR vs. E_b/N_0

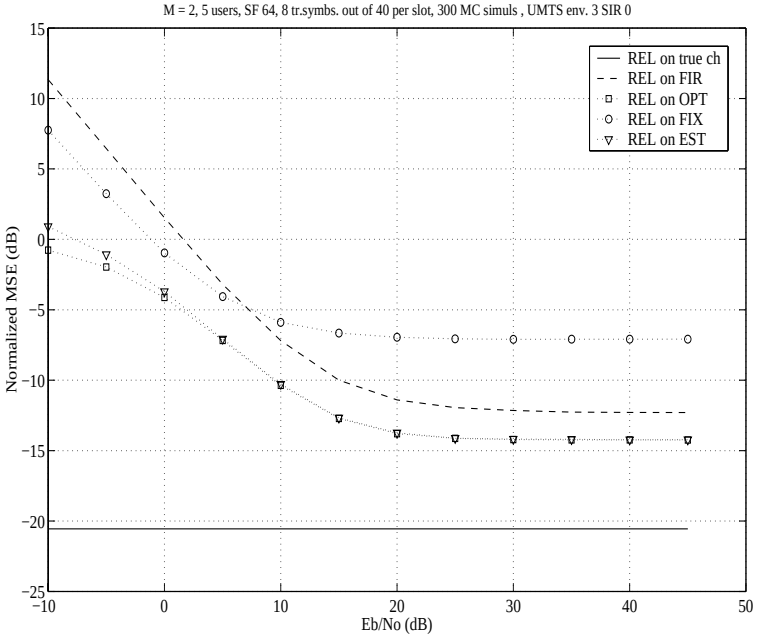

Figure 6.8: Vehicular, 120 Km/h, $\lambda = 0.99$, 5 users: NMSE vs. E_b/N_0

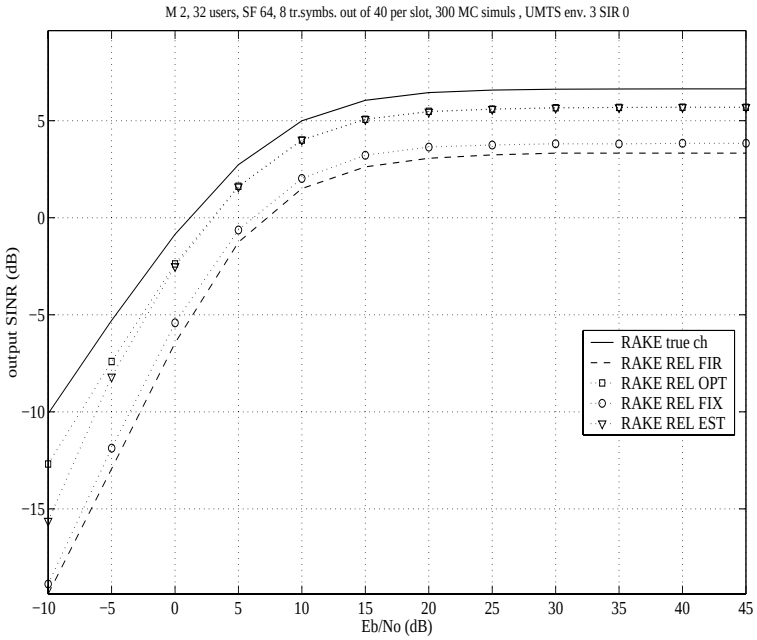

Figure 6.9: Vehicular, 120 Km/h, $\lambda = 0.99$, 32 users: SINR vs. E_b/N_0

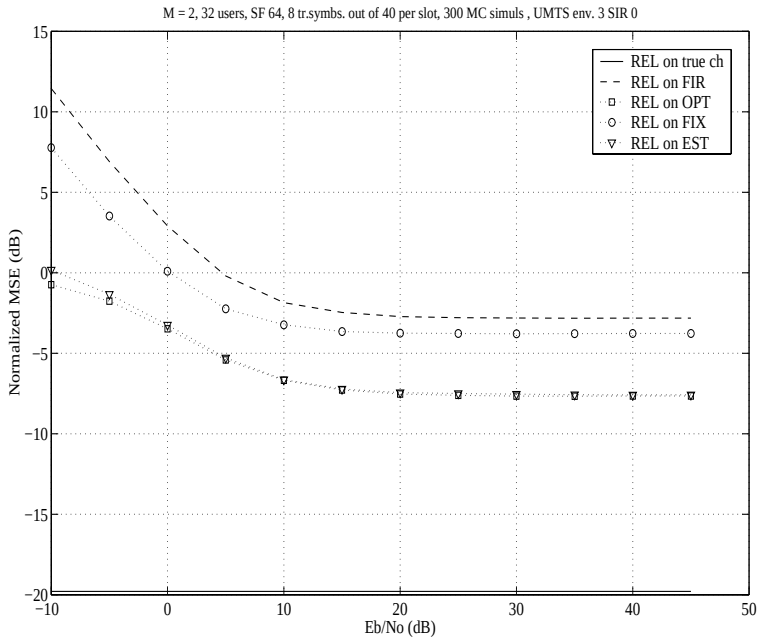

Figure 6.10: Vehicular, 120 Km/h, $\lambda = 0.99$, 32 users: NMSE vs. E_b/N_0

6.3.2 Application to the UMTS-FDD WCDMA Downlink Multi-sensor Receivers

In section 4.4 we studied lower-complexity implementations of the equalizer, including a cascade of a pulse shape matched filter and a sparse filter, whose coefficients were optimized to maximize the output SINR. In section 4.5 the case of a mobile terminal equipped with multiple sensors, has been studied. The equalizer simply becomes a spatio-temporal MMSE equaliser. Here we introduce the application of polynomial expansion, see [36], to the reduced complexity versions of this max-SINR receiver and their adaptation. The Linearly Constrained Minimum Variance (LCMV) adaptation can be done in a semi-blind fashion at symbol rate using all symbol periods, while requiring the same information (channel estimate, which can be obtained using pilot information) as the RAKE receiver. The mobile channel is modelled as in previous section 6.3 and channel approximation is performed by Recursive Early-late, on a pilot-based channel estimate, refined by adaptive optimal Wiener filtering across slots.

The multiuser downlink signal model is the one presented in 4.5. Let's remind here that the overall channel is assumed to have a delay spread of N chips due to contributions from M_p paths and that the multipath description of the channel for oversampling phase m at antenna j ($j = 1 \cdots J$) and during chip period l is

$$h^j_{m,l} = \sum_{p=1}^{M_p} \alpha^j_p \; p(lT_c + \frac{(m-1)T_c}{M} - \tau_p)$$

For antenna j, $\{\alpha^j_p\}$ is the complex amplitude of path p with corresponding delay $\{\tau_p\}$ (the delays for a given path are equal for all J MS antennas).

Furthermore, within the structured equalizer receivers presented in section 4.5, we keep for simulations the GRAKE, for which the pulse-shape equalizer F (see Fig. 4.10) is simply the Root-Raised-Cosine (RRC) matched filter (as in the RAKE) and the sparse filter coefficients are optimized for max-SINR, and we keep the JIEQRAKE, which optimizes, alternatingly, both filters, but F has in this case just different temporal filters for each antenna (not full spatiotemporal). We will compare these two equalizers with the unstructured FIR max-SINR equalizer (4.12) and with the RAKE.

Channel estimation and approximation is carried out as in previous section 6.3, with adaptive optimal Wiener filtering applied on the brute FIR pilot-based channel estimate and Recursive Early-Late channel approximation. The sampling rate discrete-time channel impulse response during transmission of slot n can be written as $h_{k,n} = \sum_{i=1}^{M_p} g_{i,n} p_{k-\tau_{i,n}}$. When reoptimization is done only for the amplitude of the current iteration, we can reformulate the REL algorithm as following (define $f^0_k = f_k =$

$\widehat{\widehat{h}}_{k,n} * p^*_{-k}$ and $q_k = p_k * p^*_{-k}$):

$$\textit{for } i = 1, \cdots, M_p \quad \textit{or until } \frac{||\boldsymbol{f}_n^i||^2}{||\boldsymbol{f}_n||^2} < \beta$$

$$\begin{aligned} \tau_{i,n} &= \arg\max_k |f_k^{i-1}|^2 \\ g_{i,n} &= f_{\tau_{i,n}}/q_0 \\ f_k^i &= f_k - \sum_{l=1}^{i} g_{l,n}\, q_{k-\tau_{l,n}} = f_k^{i-1} - g_{i,n}\, q_{k-\tau_{i,n}} \end{aligned} \tag{6.21}$$

end

where, for example, $\beta = 0.1$

6.3.2.1 Covariance Matrices Estimation

With the estimated $g_{i,n}$ and $\tau_{i,n}$ we finally obtain the estimated channel

$$h_{k,n}^{est} = \sum_{i=1}^{M_p} g_{i,n} p_{k-\tau_{i,n}}$$

and we can build the estimated received signal covariance matrix

$$\widehat{\boldsymbol{R}}_{YY,n} = \widehat{\sigma}_{v,n}^2\, \boldsymbol{I} + \widehat{\sigma}_{tot,n}^2 \mathcal{T}(\boldsymbol{h}_n^{est}) \mathcal{T}^H(\boldsymbol{h}_n^{est})$$

needed for max SINR equalizers construction. $\widehat{\sigma}_{v,n}^2$, $\widehat{\sigma}_{tot,n}^2$ can be obtained by covariance matching between the $\widehat{\boldsymbol{R}}_{YY}$ above and a sample covariance estimate. The covariance matching can be limited to a small fraction of R_{YY} (since we expect this estimation to work well, true σ_v^2, σ_{tot}^2 are used in simulations). The noise model $R_{VV} = \sigma_v^2 I$ can be extended to a more elaborate parsimonious model (e.g. banded block Toeplitz) [46]. The slot-wise periodicity can be replaced by another period.

6.3.2.2 Polynomial Expansion Extensions

We have seen in section 5.1.2 (see also [36] for background) how we can apply the chip-rate Polynomial Expansion (PE) theory to the path-wise receiver structures. We can write the received chip-rate signal $\boldsymbol{y}_l = \boldsymbol{H}(z) b_l + \boldsymbol{v}_l$, where $\boldsymbol{H}(z)$ is the channel transfer function at chip rate. The equalizer output $\boldsymbol{x}_l = \boldsymbol{F}(z)\boldsymbol{x}_l$ can be rewritten as $\boldsymbol{x}_l = \boldsymbol{D}(z) b_l + \boldsymbol{F}(z)\boldsymbol{v}_l$, where $\boldsymbol{D}(z) = \boldsymbol{F}(z)\boldsymbol{H}(z)$, and an estimate of the user of interest (user 1) symbol can be obtained by $\hat{a}_1(n) = \boldsymbol{c}_1^H \boldsymbol{S}_n^H \boldsymbol{D}^{-1}(z) \boldsymbol{X}_n$, being $\boldsymbol{X}_n$ a concatenation of $\boldsymbol{x}_l$ over a symbol period. Computation of the exact inverse of $\boldsymbol{D}(z)$ would lead to high complexity, so we can approximate it by polynomial expansion,

assuming that the main tap ($\alpha_d = \alpha_0 = 1$) of $\boldsymbol{D}(z)$ is dominant in magnitude over all the other taps (close to zero forcing), $\boldsymbol{D}^{-1}(z) = \sum_{i=0}^{\infty} (\boldsymbol{I} - \boldsymbol{D}(z))^i$. As a result, an estimate of the user of interest symbols, at first order polynomial expansion, can be rewritten as $\hat{a}_1(n) = \boldsymbol{c}_1^H \boldsymbol{S}_n^H \bar{\boldsymbol{F}}(z) \boldsymbol{Y}_n$ with $\bar{\boldsymbol{F}}(z) = \boldsymbol{F}(z)\,(2\boldsymbol{I} - \boldsymbol{H}(z)\boldsymbol{F}(z))$. The corresponding implementation is depicted in Fig. 6.11. Both filters $\boldsymbol{f}$'s can be structured and optimized jointly for max SINR. Matrix $\Pi = \boldsymbol{I}$ for chip-rate PE, while for symbol-rate PE $\Pi = \boldsymbol{S}_l^H \boldsymbol{P} \boldsymbol{S}_l$, where $\boldsymbol{S}$ is the scrambler and $\boldsymbol{P}$ projects on the used codes subspace.

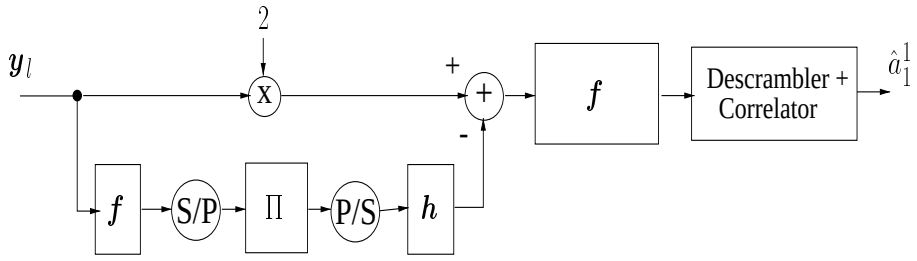

Figure 6.11: Chip Rate Polynomial Expansion structure

6.3.2.3 Numerical examples

We present results for 3 different scenarios: indoor with 2 propagation paths of equal average power (strong reflection) at low speed (3km/h) and 20% of training symbols, and 2 vehicular scenarios, both with 4 propagation paths of exponentially-decaying intensity profile at high speed (120km/h), but one with 20% of training symbols, while the other with 100% (training plus data). In the figures 6.12 to 6.17, "REL" refers to channels estimated with the procedure in section 6.21, "max-SINR" refers to an unstructured FIR equalizer of section 4.22, and "mSINR ALT" refers to a structured equalizer with alternating optimization (section 4.5.1.4).

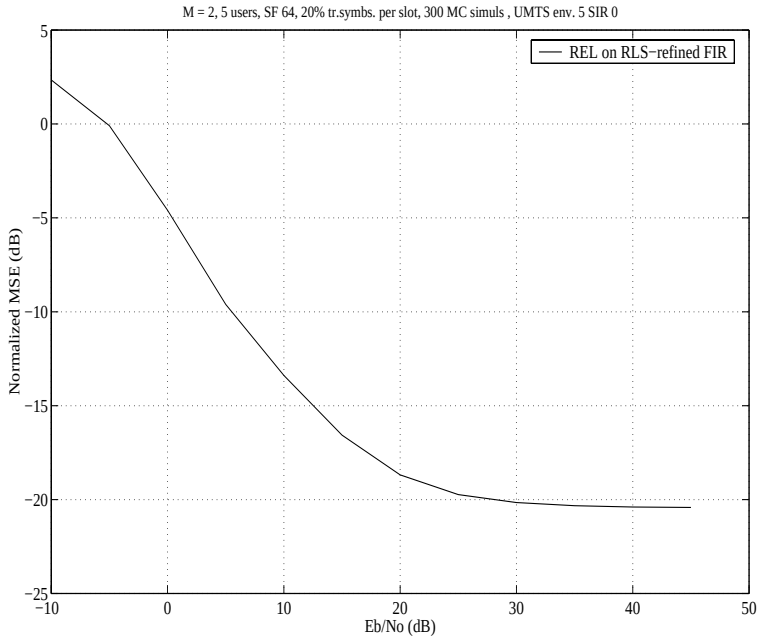

Figure 6.12: Indoor, 5 users, 20% slot of training: NMSE vs. E_b/N_0

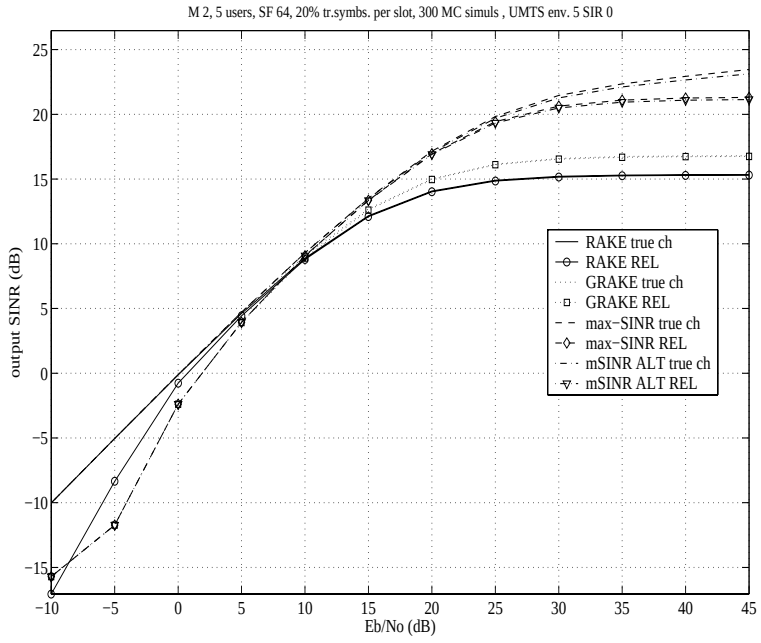

Figure 6.13: Indoor, 5 users, 20% slot of training: output SINR vs. E_b/N_0

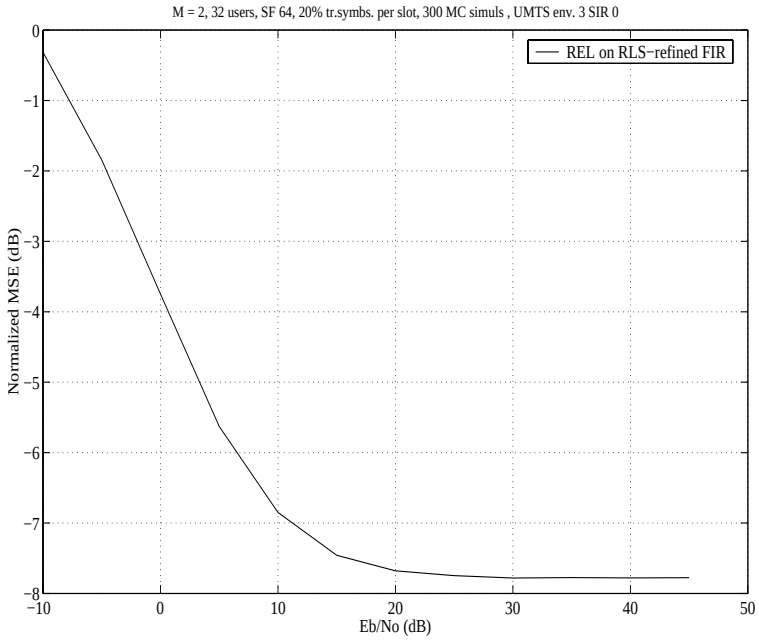

Figure 6.14: Vehicular, 32 users, 20% slot of training: NMSE vs. E_b/N_0

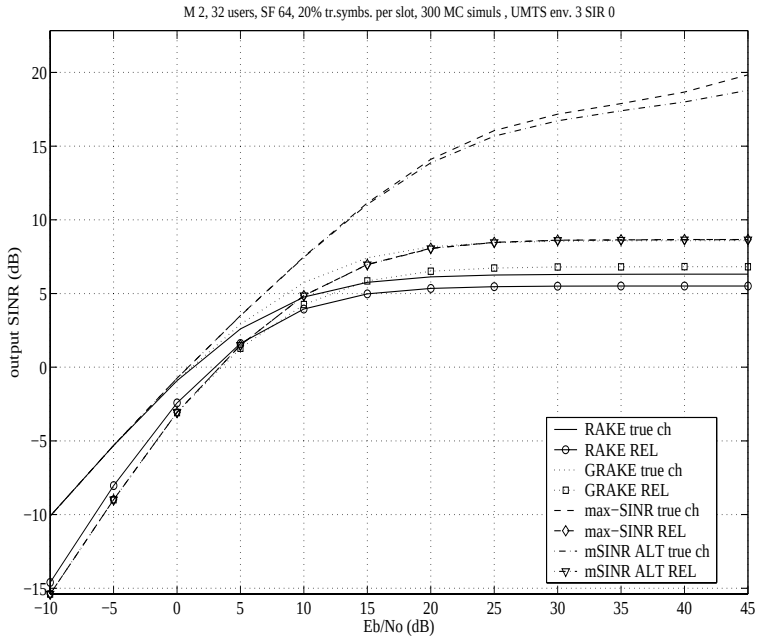

Figure 6.15: Vehicular, 32 users, 20% slot of training: output SINR vs. E_b/N_0

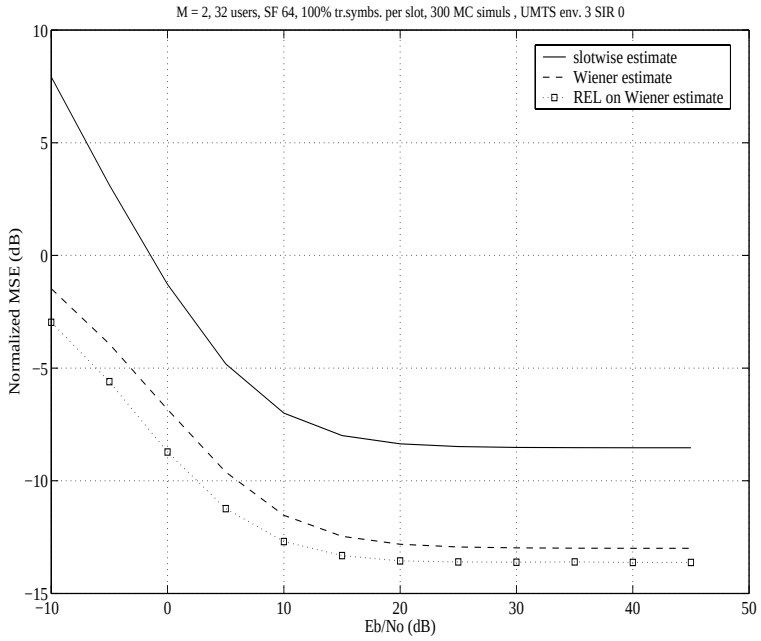

Figure 6.16: Vehicular, 32 users, 100% slot of training: NMSE vs. E_b/N_0

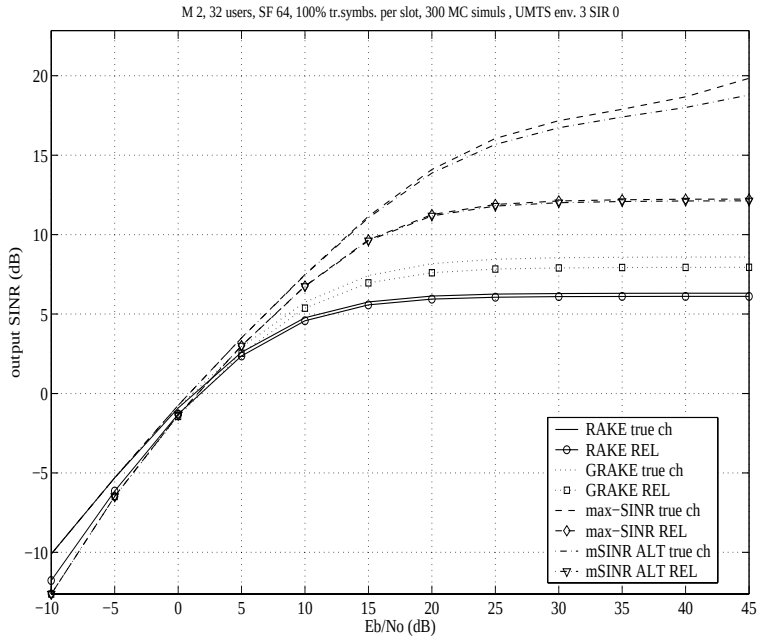

Figure 6.17: Vehicular, 32 users, 100% slot of training: output SINR vs. E_b/N_0

6.4 RAKE Architecture: fingers, searcher and REL channel approximation

We can see in Fig. 6.19 how we can imagine the discrete-time RAKE architecture. Every branch (finger) of the RAKE has the same structure, i.e. a delay followed by a downsampling operation to recover the chip rate, by a descrambler, by a correlator with the user of interest code and by a multiplication with a constant (delay and constant are given by the channel estimation block). Maximal Ratio Combining is applied to sum up contributions of every path.

The Searcher structure is the same of a RAKE branch, but the constant corresponds to the training symbols and the delay is variable (one sampling at each slot). The Searcher adds contributions of every training symbol in a slot. When having one only correlator dedicated to the construction of the "Delay Power Profile" (DPP), we can use it differently in time, due to the fact that paths that appear more frequently are normally concentrated in the beginning of the delay spread. In Fig. 6.18 we can follow how DPP evaluation can be done. First every delay position in the range R_0 are evaluated, then those in R_0+R_1, then those in $R_0+R_1+R_2$, etc. In every range $\sum_{i=0}^{I} R_i$, the number

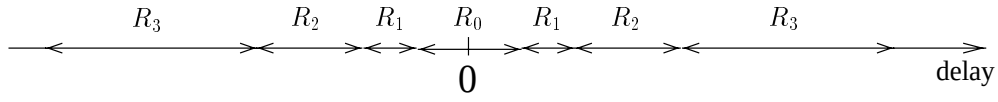

Figure 6.18: Delay Sets

of evaluated positions are doubled with respect to the previous range $\sum_{i=0}^{I-1} R_i$, so the delays in R_0 are evaluated more frequently then those in R_I. Correlations are then incoherently and exponentially averaged over more channel realizations. The estimator selects a sub-set of "active" delays, $\{\widehat{\tau}_i\}_{i=1}^{M_a}$, using some thresholds calculated from the mean and the variance of the samples in every R_i.

As we said in the previous section, REL is the best approach for channel approximation; it corresponds to apply Matching Pursuit to $\widehat{h}_n * p^*_{-n}$, the convolution of the FIR channel estimation, $\widehat{h}_n = r_n * b^*_{-n}$ (b_n being the training sequence), and the pulse-shape matched filter, p^*_{-n} ($p^*_{-n} = p_n$ for the Root Raised Cosine). To estimate $\widehat{h}_n$ we have as many branches as the "active" delays, M_a, with every branch having again the same structure of a RAKE branch, but with delays $\{\widehat{\tau}_i\}_{i=1}^{M_a}$. Moreover, at the end of every branch exponential averaging is performed, due to channel variation over slots; its constant λ is related with the mobile speed and with the carrier frequency, but also with the estimation error of the FIR channel estimation.

6.5 Conclusions

This chapter was devoted to the downlink channel estimation. By exploiting the fact that all active user signals in the system are synchronously passing through the same radio propagation channel, some Least-Square approaches, based on pilot symbols of the user of interest, can be developped. The traditional Early-Late scheme is overperformed by techniques that exploit the sparse nature of the radio propagation channel and consider a basis decomposition of the overall channel impulse response (being the basis functions delayed versions of the pulse shape). Exaustive search is too complex and we studied different suboptimal recursive Least-Squares-Fitting (LSF) approaches. Initially, by exploting the whiteness of the training chips, we simplify the LSF problem for the sparse channel parameters into a less costly LSF problem that works on the brute FIR pilot based channel estimate instead of on the received training signal. We propose as well a Recursive Early-Late approach that corresponds to apply the Matching Pursuit technique to the convolution of the brute FIR pilot based channel estimate and the pulse shape matched filter. It is a pretty simple technique that performs very close to the best suboptimal recursive Least-Squares-Fitting technique. We studied also the effect of the Least-Square channel estimation on the RAKE output SINR.

Secondly, we considered the estimation of mobile channel that are modelled as autoregressive processes across slots and we introduced optimal causal Wiener filtering, adapted to the Doppler spread of the channel, to improve the brute FIR pilot-based channel estimation accuracy. The adaptive version of this filtering, via RLS, has a slot as time unit, so its complexity is affordable. Optimal causal Wiener filtering allows optimal compromising between temporal decorrelation and slot-wise estimation error and not only temporal decorrelation like filtering on the basis of a Karhunen-Loéve decomposition of the channel tap autocorrelation function. We then apply recursive path extraction in every slot. Along this work, we made some suggestions for channel-based covariance estimation (covariance matching) and channel estimation error variance estimation.

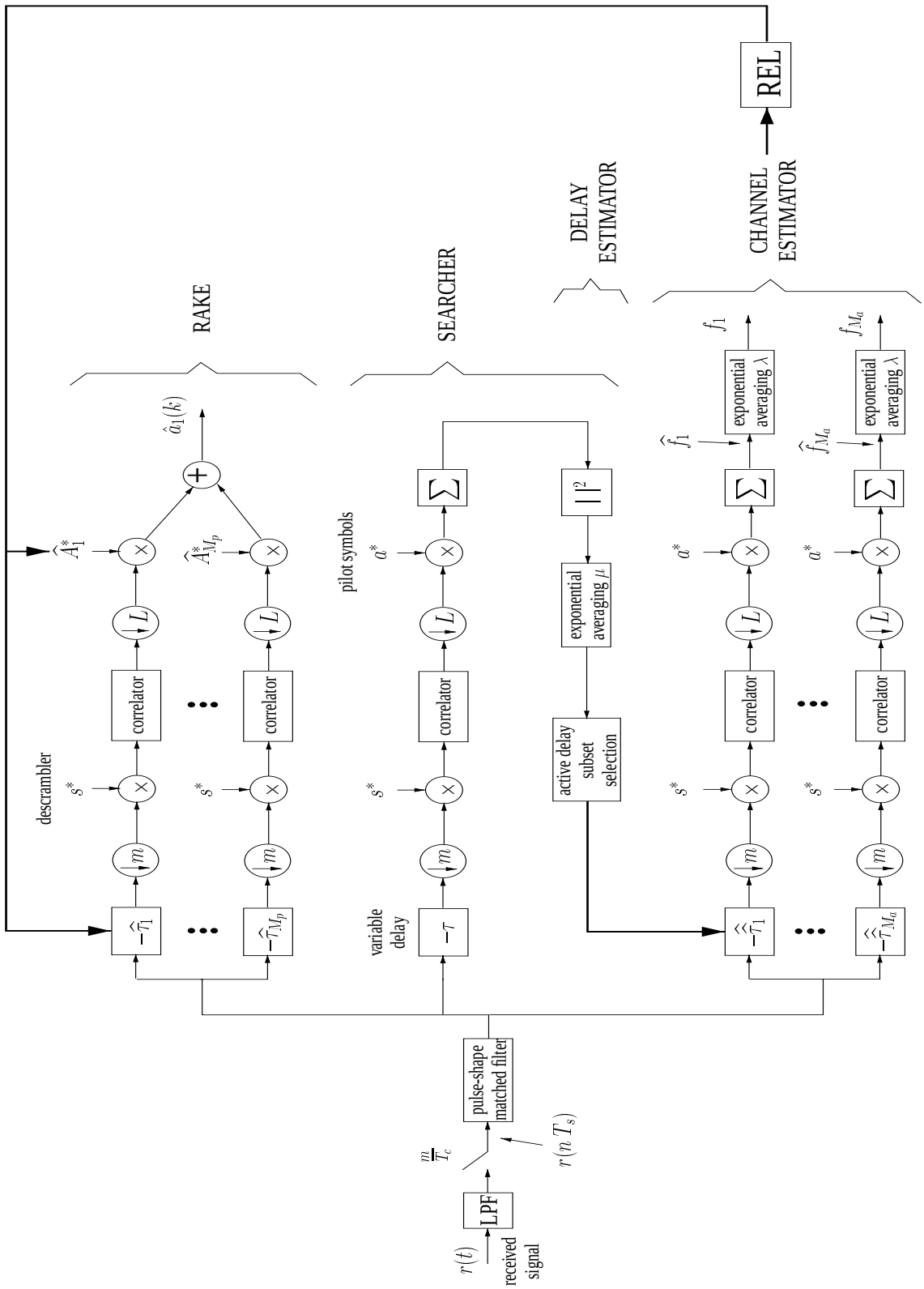

Figure 6.19: RAKE Architecture

6.A Proof of equations 6.11 and 6.12

We assume channel estimation is done via Least Squares on training chip sequence. Since we model our overall channel as the convolution of the transmitter pulse shape, of the radio propagation channel and of the receiver antialiasing filter (limiting the bandwidth to the bandwidth of the pulse shape filter itself), we can write the channel estimate as $\widehat{h} = \boldsymbol{P}\widehat{\boldsymbol{g}} = \boldsymbol{h} + \widetilde{\boldsymbol{h}}$ where

$$\widehat{\boldsymbol{g}} = \arg\min_{\boldsymbol{g}} \|\boldsymbol{Y} - \boldsymbol{B}_1\boldsymbol{P}\boldsymbol{g}\|^2$$

and $\boldsymbol{Y} = \left(\sum_{k=1}^{K} \boldsymbol{B}_k\right)\boldsymbol{P}\boldsymbol{g} + \boldsymbol{V}$ ($R_{VV} \approx \sigma_v^2\boldsymbol{I}$ and individual training chip sequences variances $\frac{\sigma_{k,P}^2}{L}$). The solution is

$$\begin{aligned}\widehat{\boldsymbol{g}} &= \left(\boldsymbol{P}^H\boldsymbol{B}_1^H\boldsymbol{B}_1\boldsymbol{P}\right)^{-1}\boldsymbol{P}^H\boldsymbol{B}_1^H\boldsymbol{Y} \\ &\approx \frac{L}{\sigma_{1,P}^2 N_p}\left(\boldsymbol{P}^H\boldsymbol{P}\right)^{-1}\boldsymbol{P}^H\boldsymbol{B}_1^H\boldsymbol{Y}\end{aligned}$$

where the approximation is due to the high autocorrelation of the training chips, which let close to multiple of identity the product $\boldsymbol{B}_1^H\boldsymbol{B}_1$. Therefore, we have

$$\begin{aligned}\widehat{\boldsymbol{h}} &\approx \frac{L}{\sigma_{1,P}^2 N_p}\mathsf{P}\boldsymbol{B}_1^H\left[\boldsymbol{B}_1\boldsymbol{h} + \sum_{k=2}^{K}\boldsymbol{B}_k\boldsymbol{h} + \boldsymbol{V}\right] \\ &= \underbrace{\mathsf{P}\boldsymbol{h}}_{E\{\widehat{\boldsymbol{h}}\}} + \underbrace{\frac{L}{\sigma_{1,P}^2 N_p}\mathsf{P}\boldsymbol{B}_1^H\left[\sum_{k=2}^{K}\boldsymbol{B}_k\boldsymbol{h} + \boldsymbol{V}\right]}_{\widetilde{\boldsymbol{h}}} = E\{\widehat{\boldsymbol{h}}\} + \widetilde{\boldsymbol{h}}\end{aligned}$$

where $\mathsf{P} = \boldsymbol{P}\left(\boldsymbol{P}^H\boldsymbol{P}\right)^{-1}\boldsymbol{P}^H = \mathsf{P}^H$ is the projection matrix on the space spanned by the columns of $\boldsymbol{P}^H$.

We have to see what numerator and denominator of equation 6.10 become now. The term in the numerator can be written as $E|\widehat{\boldsymbol{h}}^H\boldsymbol{h}|^2 = |\left(E\{\widehat{\boldsymbol{h}}\}\right)^H\boldsymbol{h}|^2 + \boldsymbol{h}^H\boldsymbol{C}_{\widetilde{h}\widetilde{h}}\boldsymbol{h}$ where $\boldsymbol{C}_{\widetilde{h}\widetilde{h}}$ is the covariance matrix of the channel estimation error $\widetilde{\boldsymbol{h}}$, which can be expressed like

$$\boldsymbol{C}_{\widetilde{h}\widetilde{h}} = \left(\frac{L}{\sigma_{1,P}^2 N_p}\right)^2\mathsf{P}\,E\left\{\boldsymbol{B}_1^H\left(\sum_{k=2}^{K}\boldsymbol{B}_k\right)\boldsymbol{h}\boldsymbol{h}^H\left(\sum_{k=2}^{K}\boldsymbol{B}_k^H\right)\boldsymbol{B}_1\right\}\mathsf{P} + \left(\frac{L}{\sigma_{1,P}^2 N_p}\right)\sigma_v^2\mathsf{P}$$

where the expectation can be rewritten as

$$\begin{aligned}E\{\bullet\} &= \sum_{k=2}^{K} E\left\{\boldsymbol{B}_1^H\boldsymbol{B}_k\boldsymbol{h}\boldsymbol{h}^H\boldsymbol{B}_k^H\boldsymbol{B}_1\right\} \\ &= \sum_{k=2}^{K} E\left\{\boldsymbol{B}_1^H E\left\{\boldsymbol{B}_k\boldsymbol{h}\boldsymbol{h}^H\boldsymbol{B}_k^H\right\}\boldsymbol{B}_1\right\} + \sum_{k=2}^{K} E\left\{\boldsymbol{B}_1^H\boldsymbol{B}_k\right\}\boldsymbol{h}\boldsymbol{h}^H E\left\{\boldsymbol{B}_k^H\boldsymbol{B}_1\right\}\,.\end{aligned}$$

The second addendum is zero because $E\{\boldsymbol{B}_1^H \boldsymbol{B}_k\} = 0$ since the off-diagonal elements are zero due to the whiteness of the scrambler and the diagonal elements are zero because of the (spreading) orthogonality between users. So we have to analyse the first addendum. We have

$$\begin{aligned} E\left\{\boldsymbol{B}_k \boldsymbol{h}\boldsymbol{h}^H \boldsymbol{B}_k^H\right\} &= \frac{\sigma_{k,P}^2}{L} \begin{bmatrix} \sum \boldsymbol{h}_i \boldsymbol{h}_i^H & \sum \boldsymbol{h}_{i+1} \boldsymbol{h}_i^H & \cdots & \mathbf{0} \\ \sum \boldsymbol{h}_i \boldsymbol{h}_{i+1}^H & \ddots & \ddots & \\ \vdots & \ddots & \ddots & \\ \mathbf{0} & \ddots & \ddots & \ddots \end{bmatrix} \\ &= \frac{\sigma_{k,P}^2}{L} \mathfrak{T}(\boldsymbol{h}) \mathfrak{T}^H(\boldsymbol{h}) \end{aligned}$$

and thus we have as well that, for example, element $(1,1)$ of $E\left\{\boldsymbol{B}_1^H E\left\{\boldsymbol{B}_k \boldsymbol{h}\boldsymbol{h}^H \boldsymbol{B}_k^H\right\} \boldsymbol{B}_1\right\}$ becomes

$$\begin{aligned} &= E\left\{ \left[b_{k-M+1}^* b_{k-M}^* \cdots\right] \frac{\sigma_{k,P}^2}{L} \mathfrak{T}(\boldsymbol{h}) \mathfrak{T}^H(\boldsymbol{h}) \begin{bmatrix} b_{k-M+1} \\ b_{k-M} \\ \vdots \end{bmatrix} \right\} \\ &= \frac{\sigma_{k,P}^2 \sigma_{1,P}^2}{L^2} \underbrace{\begin{bmatrix} N_p \sum \boldsymbol{h}_i \boldsymbol{h}_i^H & \cdots & (N_p - M + 1) \sum \boldsymbol{h}_{M-1} \boldsymbol{h}_0^H \\ (N_p - M) \sum \boldsymbol{h}_i \boldsymbol{h}_{i+1}^H & \ddots & \vdots \\ \vdots & \ddots & \vdots \end{bmatrix}}_{= N_p \boldsymbol{R}_{\boldsymbol{h}} \;\rightarrow\; N_p \mathfrak{T}(\boldsymbol{h}) \mathfrak{T}^H(\boldsymbol{h})} \end{aligned}$$

when $\frac{N_p}{M} \rightarrow \infty$.

In the case of no delay approximation ($\mathsf{P}\boldsymbol{h} = \boldsymbol{h}$), since $\boldsymbol{h}^H \mathfrak{T}(\boldsymbol{h}) \mathfrak{T}^H(\boldsymbol{h}) \boldsymbol{h} = \|\boldsymbol{\alpha}_h\|^2$ and $\left(E\widehat{\boldsymbol{h}}\right)^H \boldsymbol{h} = \boldsymbol{h}^H \mathsf{P} \boldsymbol{h} = \|\boldsymbol{h}\|^2$ we get

$$E|\widehat{\boldsymbol{h}}^H \boldsymbol{h}|^2 = \|\boldsymbol{h}\|^4 + \frac{\sigma_v^2 L}{\sigma_{1,P}^2 N_p} \|\boldsymbol{h}\|^2 + \frac{\sigma_{tot,P}^2 - \sigma_{1,P}^2}{\sigma_{1,P}^2 N_p} \|\boldsymbol{\alpha}_h\|^2 = const\ a\ .$$

Looking at the denominator terms, we have for $Tr\left\{\boldsymbol{R}_{YY}\boldsymbol{C}_{\widetilde{h}\widetilde{h}}\right\}$

$$
\begin{aligned}
&= Tr\left\{\left(\sigma_v^2\boldsymbol{I}+\frac{\sigma_{tot}^2}{L}\mathcal{T}(\boldsymbol{h})\mathcal{T}^H(\boldsymbol{h})\right)\left(\frac{\sigma_v^2 L}{\sigma_{1,P}^2 N_p}\mathsf{P}+\frac{\sigma_{tot,P}^2-\sigma_{1,P}^2}{\sigma_{1,P}^2 N_p}\mathsf{P}\mathcal{T}(\boldsymbol{h})\mathcal{T}^H(\boldsymbol{h})\mathsf{P}\right)\right\}\\
&= \frac{\sigma_v^4 L}{\sigma_{1,P}^2 N_p}M_p+\frac{\sigma_v^2\left(\sigma_{tot,P}^2-\sigma_{1,P}^2\right)}{\sigma_{1,P}^2 N_p}Tr\left\{\boldsymbol{C}\right\}+\\
&\qquad +\frac{\sigma_v^2\sigma_{tot}^2}{\sigma_{1,P}^2 N_p}Tr\left\{\boldsymbol{C}\right\}+\frac{\sigma_{tot}^2\left(\sigma_{tot,P}^2-\sigma_{1,P}^2\right)}{\sigma_{1,P}^2 N_p L}Tr\left\{\boldsymbol{C}^2\right\}\\
&= \frac{1}{\sigma_{1,P}^2 N_p}\left(L\sigma_v^4 M_p+\sigma_v^2\left(\sigma_{tot}^2+\sigma_{tot,P}^2-\sigma_{1,p}^2\right)Tr\left\{\boldsymbol{C}\right\}\right)+\\
&\qquad \frac{1}{\sigma_{1,P}^2 N_p}\left(\frac{\sigma_{tot}^2}{L}\left(\sigma_{tot,P}^2-\sigma_{1,p}^2\right)Tr\left\{\boldsymbol{C}^2\right\}\right)\\
&= const\, b\,.
\end{aligned}
$$

where M_p is the number of paths in the radio propagation channel and $\boldsymbol{C}=\mathsf{P}\mathcal{T}(\boldsymbol{h})\mathcal{T}^H(\boldsymbol{h})\mathsf{P}\,(=\mathcal{T}(\boldsymbol{h})\mathcal{T}^H(\boldsymbol{h})\mathsf{P})$.

Chapter 7

General Conclusions

This Thesis focused on channel estimation and on linear interference rejection for improving physical layer performance in the context of UMTS-FDD WCDMA downlink systems. Basing our studies and simulations on the 3GPP UMTS standard, in a collaborative framework of Eurécom and the RNRT "AUBE" project, we developed algorithms for the mobile receiver that take into account the characteristics of the transmitted signal, the interference caused by the multiple access to the system and the sparse nature of the radio propagation channel.

RAKE receivers suffer important performance degradation in multiuser systems and multipath environments and alternative receivers that improve RAKE performance need to be devised. By introducing temporal and spatial oversampling, we presented a class of discrete-time linear receivers that maximize the output SINR by minimizing the interference-plus-noise contribution to the received signal. We found that such receivers are in fact the unbiased MMSE receiver for user-of-interest chip sequence, which in the noiseless case become the Zero-Forcing equalizer. This unstructured max-SINR equalizer replaces the overall channel matched filter and greatly outperforms the RAKE SINR performance at the cost of higher computational complexity. Thus we studied lower-complexity max-SINR solutions that exploit the sparse nature of the radio channel. The equalizer gets factored into a cascade of a short FIR filter (the pulse shape matched filter in the RAKE) and a short sparse equalizer (the propagation channel matched filter), whose coefficients are optimized, separately, jointly

or alternatingly, for maximum output SINR. The case of multiple sensors at the mobile receiver has been included too, leading to spatiotemporal filters. The following conclusions arise from these investigations:

- The Linearly Constrained Minimum Variance (LCMV) criterion gives the maximum output SINR, or unbiased MMSE, equalizer solution.
- The proposed max-SINR receiver outperforms the standard RAKE receiver, even in the case of a structured implementation that exploits the sparseness of the radio channel.
- The use of multiple sensors at the receiver allows more diversity and consequently better interference cancellation, in particular for similarly structured intercell interference.

For Intercell Interference Cancellation, based on intuitive ideas and on (chip- or symbol-rate) polynomial expansion techniques, we presented, still in the case of aperiodic scrambling sequences (FDD mode), two hybrid structures that exploit the unused (excess) spreading codes in the system or just the scrambling sequences of the base stations involved. The two approaches lead to similar receiver structures, in which an Intercell Interference Cancellation branch preceeds a normal RAKE or max-SINR linear receiver. In the case of chip-rate polynomial expansion, only the scrambling sequencies are exploited. We can deduce the following conclusions:

- The max-SINR receiver itself improves RAKE performance also in the presence of interfering base stations.
- Hybrid structures or polynomial expansion techniques achieve even better performance because they exploit more knowledge about the signal structure.
- When the scrambling sequences are periodic (TDD mode), the normal max-SINR receiver outperforms all the other linear and non-linear structures due to the time-invariant noise subspaces created by the unused codes that are used to cancel the intercell interference.

We also presented receiver structures in the context of Base Station Transmit Diversity schemes, in particular the structures that use max-SINR receivers are new. We studied implementations of three different TD schemes, DTD, STTD and OTD. The Delay TD scheme performs almost always better than the other schemes, expecially when RAKE receivers are used. In the case of max-SINR solutions, DTD can be generally seen as the best scheme, but in particular situations (too short filters) Spatio

Temporal TD schemes perform similarly to DTD schemes. We can also state that the Orthogonal TD scheme is always the worst scheme.

We addressed the channel impulse response time discretization problem too. By working at a higher sampling rate (w.r.t. the chip rate), we proposed dicrete-time channel matched filters, so that a study was needed to understand how large the channel approximation error gets. Our approach to approximate an entire overall channel was to iteratively add one approximating tap at the delay that minimizes the approximation error (Matching Pursuit technique) and to reestimate the channel amplitudes by Least-Squares. The best technique between the suboptimal Recursive Least-Squares-Fitting techniques is the one that reoptimizes all the amplitudes at each delay position before chosing the delay for the newpath to be added. Traditionally, in continuous-time signal processing, the channel delays are estimated via the Early-Late approach and this motivated us for introducing a discrete-time Recursive Early-Late (REL) technique that corresponds to applying Matching Pursuit to the convolution of a FIR estimate of the channel and the pulse shape matched filter. But at each iteration previously found delayed pulse shapes are subtracted, so that spurious maxima (pulse shape sidelobes) don't interfere anymore. We analysed also the SINR degradation due to channel estimation via Least-Squares. Some conclusions can be drawn:

- The mean SNR (considering the approximation error as noise) is much better than what the SINR of the received signal can be expected to be, so this approximation error is negligible.
- Of course, the approximation error can be further reduced by assigning more discrete-time taps per continuous-time path.
- The Recursive Early-Late approach is quite simple, not too complex to be implemented and has performance close to the performance of an estimator that knows in advance the true channel delays.

We considered also the estimation of time-varying radio channels modeled as autoregressive processes with bandwidth commensurate with the Doppler spread. By using optimal causal Wiener filtering and its RLS adaptation, we are able to refine the brute FIR pilot-based channel estimates, so that recursive path extraction via REL gets improved. Optimal Wiener filtering across slots is a good compromise between temporal decorrelation and slot-wise estimation error. We suggested as well some techniques for channel-based covariance estimation (covariance matching) and "channel estimation error variance" estimation.

Some important open issues for further studies are:

- Optimal placement and number of taps in the sparse channel equalizer for max-SINR structured equalizers.
- Combining chip- and symbol-level equalization for low spreading factors, since in this case ISI is present. It is preferable to perform the symbol-level eqaulization with a more optimal technique such as Viterbi algorithm, and only leave the chip-level equalization (between symbols) equalization to a linear equalizer.
- (Semi)Blind downlink channel estimation and receiver adaptation.
- In the case of tracking time-varying sparse channels, interchange the order of the operations of Wiener filtering refinement and "sparsification", and verify that this optimal filtering is suitable for the case of specular channels.

Bibliography

[1] M. Lenardi and D. T. M. Slock, "A RAKE Receiver with Intracell Interference Cancellation for a DS-CDMA Synchronous Downlink with Orthogonal Codes," in *Proc. VTC 2000 Spring*, (Tokyo, Japan), May 2000.

[2] M. Lenardi, A. Medles, and D. T. M. Slock, "Comparison of Downlink Transmit Diversity Schemes for RAKE and SINR MAximizing Receivers," in *Proc. ICC 2001*, (Helsinki, Finland), June 2001.

[3] M. Lenardi and D. T. M. Slock, "SINR Maximizing Equalizer Receiver for DS-CDMA," in *Proc. EUSIPCO 2000*, (Tampere, Finland), September 2000.

[4] M. Lenardi, A. Medles, and D. T. M. Slock, "A SINR Maximizing RAKE Receiver for DS-CDMA Downlinks," in *Proc. ASILOMAR 2000*, (Pacific Grove, California - USA), Oct.-Nov. 2000.

[5] M. Lenardi, A. Medles, and D. T. M. Slock, "A SINR Maximizing 2D RAKE Receiver for Multi-Sensor WCDMA Mobile Terminals ," in *Proc. VTC 2001 Spring*, (Rhodes, Greece), May 2001.

[6] M. Lenardi, A. Medles, and D. T. M. Slock, "Downlink Intercell Interference Cancellation in WCDMA by Exploiting Excess Codes," in *Proc. SAM 2000*, (Boston, Massachusset - USA), March 2000.

[7] M. Lenardi, A. Medles, and D. T. M. Slock, "Intercell Interference Cancellation at a WCDMA Mobile Terminal by Exploiting Excess Codes," in *Proc. VTC 2001 Spring*, (Rhodes, Greece), May 2001.

[8] M. Lenardi and D. T. M. Slock, "Channel Estimation for a Discrete-Time RAKE Receiver in a WCDMA Downlink: Algorithms and Repercussions on SINR," in *Proc. VTC 2001 Fall*, (Atlantic City, NJ), October 2001.

[9] M. Lenardi and D. T. M. Slock, "Estimation of Time-Varying Wireless Channels and Application to the UMTS W-CDMA FDD Downlink," in *submitted to European Wireless 2002*, (Florence - Italy), February 2002.

[10] M. Lenardi and D. T. M. Slock, "A RAKE Structured SINR Maximizing Mobile Receiver for the WCDMA Downlink," in *Proc. ASILOMAR 2001*, (Pacific Grove, California - USA), November 2001.

[11] G. Jourdain and F. Baldit, "Rapport final pour le projet AUBE," tech. rep., LIS Grenoble, 2001. RNRT AUBE Project.

[12] Various, "Special issue on signal synchronization for digital transmission systems," *IEEE Journal of Selected Areas in Communications*, vol. 19, December 2001.

[13] H. Holma and A. Toskala, *WCDMA for UMTS (Radio Access for Third Generation Mobile Communications*. Wiley, 2000.

[14] K. Pajukoski and J. Savusalo, "WCDMA Test System," in *Proc. IEEE Int. Conf. on Personal Indoor and Mobile Radio Communications*, September 1-4 1997. PIMRC'97, Helsinki - Finland.

[15] E. Nikula, A. Toskala, E. Dahlman, L. Girard, and A. Klein, "Frames multiple access for umts and imt-2000," *IEEE Personal Communications Magazine*, pp. 16–24, April 1998.

[16] 3GPP TSG, "http://www.3gpp.org," tech. rep., 3GPP. UMTS Standardization.

[17] 3GPP TSG RAN # 5 (99)587, "TS 25.211 v3.0.0 (1999-10): Physical Channels and Mapping of Transport Channels onto Physical Channels (FDD)," tech. rep., 3GPP, October 1999. UMTS Standardization.

[18] 3GPP TSG RAN # 5 (99)587, "TS 25.213 v3.0.0 (1999-10): Spreading and Modulation (FDD)," tech. rep., 3GPP, October 1999. UMTS Standardization.

[19] W. C. Jakes, *Microwave Mobile Communications*. New York: Wiley, 1974.

[20] W. C. Y. Lee, *Mobile Communications Engineering Theory and Applications (II edition)*. McGraw-Hill Telecommunications, 1998.

[21] G. Stüber, *Principles of Mobile Communications*. Kluwer Academic Press, 1996.

[22] T. S. Rappaport, *Wireless Communications - Principles & Practice*. Upper Saddle River, NJ: Prentice Hall, 1996.

[23] R. L. Peterson, Ziemer, R. E., Borth, and D. E., *Introduction to spread-spectrum communications*. Englewood Cliffs, NJ: Prentice Hall, 1995.

[24] COST 207, "Digital Land Mobile Radio Communications," tech. rep., Office for Official Publications of the European Communities, 1989. Luxembourg, final report.

[25] 3GPP TSG RAN # 5 (99)587, "TS 25.101 v3.0.0 (1999-10): Radio Propagation Conditions," tech. rep., 3GPP, October 1999. UMTS Standardization.

[26] J. G. Proakis, *Digital Communications*. New York, NY: McGraw-Hill, 3rd. ed., 1995.

[27] H. Oppenheim and R. Shafer, *Discrete-Time Signal Processing*. Prentice-Hall, 1989.

[28] G. Golub and C. Loan, *Matrix Computation*. The John Hopkins University Press, 3rd. ed., 1996.

[29] S. Verdú, *Multiuser Detection*. Cambridge University Press, 1998.

[30] B. Ng, M. Cedervall, and A. Paulraj, "A structured channel estimator for maximum likelihood sequence detection in multipath fading channels." submitted to IEEE Transactions on Vehicular Technology, Jan. 1997.

[31] I. Ghauri and D. T. M. Slock, "Linear receivers for the DS-CDMA downlink exploiting orthogonality of spreading sequences," in *Proc. 32nd Asilomar Conf. on Signals, Systems & Computers*, (Pacific Grove, CA), November 1998.

[32] A. Klein, "Data detection algorithms specially designed for the downlink of CDMA mobile radio systems," in *Proc. VTC*, (Phoenix, AZ), pp. 203–207, May 1997.

[33] C. D. Frank and E. Visotsky, "Adaptive interference suppression for direct-sequence CDMA systems with long spreading codes," in *Proc. 36th Annual Allerton Conference on Communication, Control, and Computing*, (Urbana-Champaign, IL), September 1998.

[34] D. T. M. Slock and I. Ghauri, "Blind Maximum SINR for the DS-CDMA Downlink," in *Proc. ICASSP 2000*, (Istambul, Turkey), May 2000.

[35] T. O. G. Bottomley and Y. Wang, "A generalized rake receiver for interference suppression," *IEEE Journal Selected Areas Communications*, vol. 18, pp. 1536–1545, August 2000.

[36] S. Moshavi, E. Kanterakis, and D. Shilling, "Multistage linear receivers for ds-cdma systems," *Int. J. of Wireless Information Networks*, vol. 3, no. 1, 1996.

[37] "Space Time Block Coded Transmit Antenna Diversity for WCDMA," tech. rep., Texas Instruments, November 1998. Contribution to 3GPP standardization.

[38] S. M. Alamouti, "A simple transmit diversity technique for wireless communications," *IEEE JSAC*, vol. 16, pp. 1451–1458, October 1998.

[39] A. Wittneben, "A new bandwidth efficient transmit antenna modulation diversity scheme for linear digital modulation," in *Proc. IEEE International Conf. Communications (ICC'93)*, (Atlanta, GA), pp. 1630–1634, May 1993.

[40] G. Caire and U. Mitra, "Structured multiuser channel estimation for block-synchronous DS/CDMA." Submitted to IEEE Trans. on Communications, July 1999.

[41] S. Bensley and B. Aazhang, "Subspace-based channel estimation for code-division multiple access communication systems," *IEEE Transactions on Communications*, vol. 44, pp. 1009–1020, August 1996.

[42] A. J. Weiss and B. Friedlander, "Channel estimation for DS-CDMA downlink with aperiodic spreading codes," *IEEE Transactions on Communications*, vol. 47, pp. 1561–1569, October 1999.

[43] Z. Xu and K. Tsatsanis, "Blind channel stimation for long code multiuser cdma systems," *IEEE Transactions on Signal Processing*, vol. 48, pp. 988–1001, April 2000.

[44] S. Buzzi and H. V. Poor, "Channel estimation and multiuser detection in long-code ds/cdma systems," *IEEE Journal of Selected Areas in Communications*, vol. 19, pp. 1476–1487, August 2001.

[45] H. Boujemâa and M. Siala, "On a Maximum Likelihood Delay Acquisition Algorithm," in *Proc. ICC 2001*, (Helsinki, Finland), June 2001.

[46] M. Jansson and B. Ottersten, "Structured Covariance Matrix Estimation: A Parametric Approach," in *Proceedings IEEE International Conference on Acoustics, Speech, and Signal Processing*, (Istanbul, Turkey), pp. 3172–3175, June 2000.

[47] M. D. Zoltowski and J. S. Goldstein, "Structured MMSE Equalization for Synchronous CDMA with Sparse Multipath Channels," in *Proc. ICASSP 2001*, (Salt Lake City, UT), May 2001.

[48] B. Ottersten, P. Stoica, and R. Roy, "Covariance Matrix Estimation Techniques for Array Signal Processing Applications," in *In Digital Signal Processing, a Review Journal*, (Stockholm, Sweden), pp. 8:185–210, 1998.

[49] K. Insung, M. Fitz, and S. Gelfand, "Blind estimation of multipath channel parameters: a modal analysis approach," *IEEE Transactions on Communications*, vol. 47, pp. 1140–1150, August 1999.

[50] R. R. G. Bottomley, E. Sourour and S. Chennakeshu, "Optimizing the performance of limited complexity rake receivers," in *Proc. VTC'98 Fall Conference*, 1998.

Curriculum Vitae